

# Electric Dipole Moments in the MSSM Reloaded

John Ellis<sup>a</sup>, Jae Sik Lee<sup>b,c,d</sup> and Apostolos Pilaftsis<sup>e</sup>

<sup>a</sup>*Theory Division, CERN, CH-1211 Geneva 23, Switzerland*

<sup>b</sup>*Physics Division, National Center for Theoretical Sciences, Hsinchu, Taiwan*

<sup>c</sup>*Department of Physics and Center for Mathematics and Theoretical Physics,  
National Central University, Chung-Li, Taiwan*

<sup>d</sup>*Institute of Physics, Academia Sinica, Taipei, Taiwan*

<sup>e</sup>*School of Physics and Astronomy, University of Manchester,  
Manchester M13 9PL, United Kingdom*

## ABSTRACT

We present a detailed study of the Thallium, neutron, Mercury and deuteron electric dipole moments (EDMs) in the CP-violating Minimal Supersymmetric extension of the Standard Model (MSSM). We take into account the complete set of one-loop graphs, the dominant Higgs-mediated two-loop diagrams, the complete CP-odd dimension-six Weinberg operator and the Higgs-mediated four-fermion operators. We improve upon earlier calculations by including the resummation effects due to CP-violating Higgs-boson mixing and to threshold corrections to the Yukawa couplings of all up- and down-type quarks and charged leptons. As an application of our study, we analyse the EDM constraints on the CPX, trimixing and Maximally CP- and Minimally Flavour-Violating (MCPMFV) scenarios. Cancellations may occur among the CP-violating contributions to the three measured EDMs arising from the 6 CP-violating phases in the MCPMFV scenario, leaving open the possibility of relatively large contributions to other CP-violating observables. The analytic expressions for the EDMs are implemented in an updated version of the code CPsuperH2.0.

# 1 Introduction

With the imminent advent of the LHC, we are entering an exciting era for probing new physics at the TeV scale. If new physics is indeed observed at this scale, the questions of its flavour and CP structure will immediately become very critical. The non-observation of the Thallium ( $^{205}\text{Tl}$ ) [1], neutron ( $n$ ) [2], and Mercury ( $^{199}\text{Hg}$ ) [3] electric-dipole moments (EDMs) already provide remarkably tight bounds on possible new CP-violating phases beyond the Cabibbo–Kobayashi–Maskawa (CKM) one of the Standard Model (SM). Complementary to the direct explorations at the LHC, a new generation of precision low-energy experiments is also expected to play an important role. The new precision experiments will place much stronger indirect constraints on the possible CP and flavour structure of models of TeV-scale physics. In particular, if the proposed experiment searching for a deuteron ( $^2\text{H}^+$ ) EDM achieves the projected sensitivity [4, 5], this will improve the existing bounds on possible CP-violating chromoelectric operators by several orders of magnitude [6].

One of the theoretically best-motivated scenarios of new physics is Supersymmetry (SUSY) [7]. Its minimal realization, the Minimal Supersymmetric extension of the Standard Model (MSSM), with SUSY broken softly at the TeV scale, addresses the naturalness of the gauge hierarchy, predicts gauge-coupling unification, provides a viable candidate for Cold Dark Matter (CDM) and may help explain the baryon asymmetry in the Universe (BAU) via a first-order electroweak phase transition [8]. An essential role in the generation of the BAU could be played by the new CP-odd phases that appear in the MSSM [8]. However, the non-observation of EDMs severely constrains these CP-violating phases [9].

The aim of this paper is to present a detailed study of the  $^{205}\text{Tl}$ ,  $n$ ,  $^{199}\text{Hg}$  and  $^2\text{H}^+$  EDMs in the CP-violating MSSM. We include in our study the complete set of one-loop graphs [10, 11], the dominant Higgs-mediated two-loop diagrams [12–14] of the Barr–Zee type [15] and the Higgs-mediated four-fermion operators [13, 16, 17], originally studied by Barr [18] within a two-Higgs doublet model\*. We improve upon earlier calculations [19, 20] by calculating the complete CP-odd dimension-six Weinberg operator [21] and by including resummation effects due to CP-violating Higgs-boson mixing [22] and to threshold corrections to the Yukawa couplings of the up- and down-type quarks and charged leptons [23]. We then use this compendium to derive representative constraints on the CP-violating parameters of phenomenologically relevant benchmarks in the MSSM, such as the CPX scenario [24], the trimixing scenario [14, 25] and the general Maximally CP- and Minimally Flavour-Violating (MCPMFV) framework [26], for selected sets of values of the CP-conserving parameters. Clearly, sufficiently small values of the CP-violating parameters must be compatible with the experimental upper limits on the EDMs but, as we shall illustrate with explicit examples, larger values may also be allowed by non-trivial

---

\*However, we do not include here the contributions of a possible non-zero CP-violating QCD vacuum parameter  $\theta$ .

cancellations.

For the presentation of our analytic results, we follow the conventions and notations of `CPsuperH` [27], especially for the masses and mixing matrices of the neutral Higgs bosons and SUSY particles. We note parenthetically that the new version of `CPsuperH`, `CPsuperH2.0`, includes an improved treatment of Higgs-boson propagators and Higgs couplings, and enables numerical predictions for a number of flavour-changing-neutral-current (FCNC)  $B$ -meson observables, including CP-violating effects. On the basis of the results in this work, we further improve the code `CPsuperH2.0` by implementing the computation of the Thallium, neutron, Mercury and deuteron EDMs in the CP-violating MSSM.

The layout of the paper is as follows. Section 2 presents all formulae relevant to the one-loop contributions to the electric and chromoelectric dipole moments of the charged leptons and quarks that result from chargino-, neutralino-, and gluino-mediated diagrams. Non-holomorphic threshold effects on the light-quark Yukawa couplings have been appropriately resummed, as these are the dominant source of higher-order corrections. In Section 3, we calculate the CP-odd dimension-six three-gluon Weinberg operator, taking into account loop diagrams involving  $t$  and  $b$  quarks and Higgs bosons, in addition to the previously known loop effects due to  $t$  and  $b$  squarks and gluinos. In addition, we present analytic results for the Higgs-mediated four-fermion operators and the dominant Higgs-mediated two-loop diagrams. In Section 4 we compute the  $^{205}\text{Tl}$ ,  $n$ ,  $^{199}\text{Hg}$  and  $^2\text{H}^+$  EDMs in the CP-violating MSSM. Section 5 presents illustrative constraints on key soft SUSY-breaking parameters and CP-odd phases in the CPX, the trimixing and the MCPMFV scenarios. We summarize our conclusions in Section 6.

## 2 One-Loop EDMs of Leptons and Quarks

At the one-loop level, the charged leptons,  $e$ ,  $\mu$  and  $\tau$ , and the light quarks,  $u$ ,  $d$  and  $s$ , can have EDMs induced by charginos, neutralinos and gluinos. The  $u$ ,  $d$  and  $s$  quarks may also develop chromoelectric dipole moments (CEDMs) via the corresponding squark and gluino loop diagrams. In this Section we exhibit analytical formulae for the one-loop EDMs of charged leptons and light quarks, and the CEDMs of the quarks.

We denote the EDM of a fermion by  $d_f^E$  and the CEDM of a quark by  $d_q^C$ . The relevant (C)EDM interaction Lagrangian is given by

$$\mathcal{L}_{(\text{C})\text{EDM}} = -\frac{i}{2} d_f^E F^{\mu\nu} \bar{f} \sigma_{\mu\nu} \gamma_5 f - \frac{i}{2} d_q^C G^{a\mu\nu} \bar{q} \sigma_{\mu\nu} \gamma_5 T^a q, \quad (2.1)$$

where  $F^{\mu\nu}$  and  $G^{a\mu\nu}$  are the electromagnetic and strong field strengths, respectively, and the  $T^a = \lambda^a/2$  are the generators of the  $\text{SU}(3)_C$  group. The interaction Lagrangian (2.1) leads to a matrix element of the form:

$$i\mathcal{M} = -d_f^E \epsilon(q) \cdot (p + p') \bar{u}(p') \gamma_5 u(p), \quad (2.2)$$

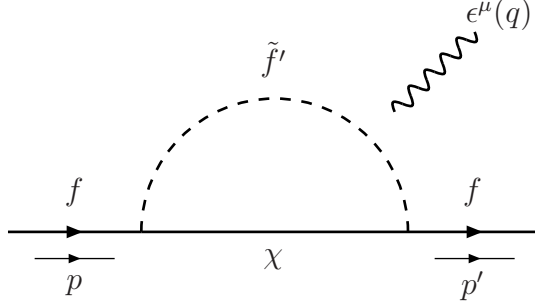


Figure 1: *Generic Feynman diagram for the EDM  $(d_f^E)^\chi$  of the fermion  $f$  induced by  $\chi$  exchange effects. The photon line can be attached to the sfermion  $\tilde{f}'$  line, or to the  $\chi$  line if  $\chi = \tilde{\chi}_i^\pm$ .*

where  $p = q + p'$  and  $\epsilon(q) \cdot p = \epsilon(q) \cdot p'$ , since  $\epsilon(q) \cdot q = 0$ . We use the convention  $\sigma^{\mu\nu} = \frac{i}{2}[\gamma^\mu, \gamma^\nu] = i(\gamma^\mu\gamma^\nu - g^{\mu\nu})$ .

To set our coupling notations and normalisations, we write down the generic interaction of a chargino  $\tilde{\chi}_{1,2}^\pm$ , neutralino  $\tilde{\chi}_{1,2,3,4}^0$  or gluino  $\tilde{g}^a$ , collectively denoted by  $\chi$ , with a fermion  $f$  and sfermion  $\tilde{f}'_{1,2}$ , as follows:<sup>†</sup>

$$\mathcal{L}_{\chi f \tilde{f}'} = g_{Lij}^{\chi f \tilde{f}'} (\bar{\chi}_i P_L f) \tilde{f}'_j^* + g_{Rij}^{\chi f \tilde{f}'} (\bar{\chi}_i P_R f) \tilde{f}'_j^* + \text{h.c.} \quad (2.3)$$

Likewise, the interaction Lagrangians for the couplings of a photon  $A^\mu$  with  $\chi$  and  $\tilde{f}'$  read:

$$\mathcal{L}_{\chi\chi A} = -e Q_\chi (\bar{\chi} \gamma_\mu \chi) A^\mu, \quad \mathcal{L}_{\tilde{f}' \tilde{f}' A} = -ie Q_{\tilde{f}'} \tilde{f}'^* \overleftrightarrow{\partial}_\mu \tilde{f}' A^\mu. \quad (2.4)$$

Employing (2.3) and (2.4) and taking into consideration the diagrams of Fig. 1, we calculate the one-loop fermion EDM,

$$\left(\frac{d_f^E}{e}\right)^\chi = \frac{m_{\chi_i}}{16\pi^2 m_{\tilde{f}'_j}^2} \Im \left[ (g_{Rij}^{\chi f \tilde{f}'})^* g_{Lij}^{\chi f \tilde{f}'} \right] \left[ Q_\chi A(m_{\chi_i}^2/m_{\tilde{f}'_j}^2) + Q_{\tilde{f}'} B(m_{\chi_i}^2/m_{\tilde{f}'_j}^2) \right], \quad (2.5)$$

where

$$A(r) = \frac{1}{2(1-r)^2} \left( 3 - r + \frac{2 \ln r}{1-r} \right), \quad B(r) = \frac{1}{2(1-r)^2} \left( 1 + r + \frac{2r \ln r}{1-r} \right), \quad (2.6)$$

with  $A(1) = -1/3$  and  $B(1) = 1/6$ . We have checked that our analytic expressions for the one-loop EDMs are in agreement with [9] and [11].

<sup>†</sup>Here the convention for the couplings  $g_L$  and  $g_R$  is different from that used in [9]:  $g_L = R_{ik}^*$  and  $g_R = L_{ik}^*$ .

We now present the individual one-loop contributions of charginos  $\tilde{\chi}^\pm$  to the EDMs of charged leptons  $(d_l^E/e)^{\tilde{\chi}^\pm}$ , up-type quarks  $(d_u^E/e)^{\tilde{\chi}^\pm}$  and down-type quarks  $(d_d^E/e)^{\tilde{\chi}^\pm}$ . In detail, these are given by

$$\left(\frac{d_l^E}{e}\right)^{\tilde{\chi}^\pm} = \frac{1}{16\pi^2} \sum_i \frac{m_{\tilde{\chi}_i^\pm}}{m_{\tilde{\nu}_l}^2} \Im[(g_{Ri}^{\tilde{\chi}^\pm l\bar{\nu}})^* g_{Li}^{\tilde{\chi}^\pm l\bar{\nu}}] Q_{\tilde{\chi}^-} A(m_{\tilde{\chi}_i^\pm}^2/m_{\tilde{\nu}_l}^2), \quad (2.7)$$

$$\left(\frac{d_u^E}{e}\right)^{\tilde{\chi}^\pm} = \frac{1}{16\pi^2} \sum_{i,j} \frac{m_{\tilde{\chi}_i^\pm}}{m_{\tilde{d}_j}^2} \Im[(g_{Rij}^{\tilde{\chi}^\pm u\bar{d}})^* g_{Lij}^{\tilde{\chi}^\pm u\bar{d}}] [Q_{\tilde{\chi}^+} A(m_{\tilde{\chi}_i^\pm}^2/m_{\tilde{d}_j}^2) + Q_{\tilde{d}} B(m_{\tilde{\chi}_i^\pm}^2/m_{\tilde{d}_j}^2)], \quad (2.8)$$

$$\left(\frac{d_d^E}{e}\right)^{\tilde{\chi}^\pm} = \frac{1}{16\pi^2} \sum_{i,j} \frac{m_{\tilde{\chi}_i^\pm}}{m_{\tilde{u}_j}^2} \Im[(g_{Rij}^{\tilde{\chi}^\pm d\bar{u}})^* g_{Lij}^{\tilde{\chi}^\pm d\bar{u}}] [Q_{\tilde{\chi}^-} A(m_{\tilde{\chi}_i^\pm}^2/m_{\tilde{u}_j}^2) + Q_{\tilde{u}} B(m_{\tilde{\chi}_i^\pm}^2/m_{\tilde{u}_j}^2)], \quad (2.9)$$

where the electric-charge assignments for the loop particles are:  $Q_{\tilde{\chi}^\pm} = \pm 1$ ,  $Q_{\tilde{u}} = 2/3$ ,  $Q_{\tilde{d}} = -1/3$ , and

$$g_{Li}^{\tilde{\chi}^\pm l\bar{\nu}} = -g(C_R)_{i1}, \quad g_{Ri}^{\tilde{\chi}^\pm l\bar{\nu}} = h_l^*(C_L)_{i2}, \quad (2.10)$$

$$g_{Lij}^{\tilde{\chi}^\pm u\bar{d}} = -g(C_L)_{i1}^*(U^{\tilde{d}})_{1j}^* + h_d(C_L)_{i2}^*(U^{\tilde{d}})_{2j}^*, \quad g_{Rij}^{\tilde{\chi}^\pm u\bar{d}} = h_u^*(C_R)_{i2}^*(U^{\tilde{d}})_{1j}^*, \quad (2.11)$$

$$g_{Lij}^{\tilde{\chi}^\pm d\bar{u}} = -g(C_R)_{i1}(U^{\tilde{u}})_{1j}^* + h_u(C_R)_{i2}(U^{\tilde{u}})_{2j}^*, \quad g_{Rij}^{\tilde{\chi}^\pm d\bar{u}} = h_d^*(C_L)_{i2}(U^{\tilde{u}})_{1j}^*. \quad (2.12)$$

We note that the coupling coefficients defined in (2.10)–(2.12) appear in (2.7)–(2.9), respectively.

Correspondingly, the contributions of neutralinos to the EDMs of charged leptons  $(d_l^E/e)^{\tilde{\chi}^0}$ , up-type quarks  $(d_u^E/e)^{\tilde{\chi}^0}$  and down-type quarks  $(d_d^E/e)^{\tilde{\chi}^0}$  may conveniently be expressed as

$$\left(\frac{d_f^E}{e}\right)^{\tilde{\chi}^0} = \frac{1}{16\pi^2} \sum_{i,j} \frac{m_{\tilde{\chi}_i^0}}{m_{\tilde{f}_j}^2} \Im[(g_{Rij}^{\tilde{\chi}^0 f\bar{f}})^* g_{Lij}^{\tilde{\chi}^0 f\bar{f}}] Q_{\tilde{f}} B(m_{\tilde{\chi}_i^0}^2/m_{\tilde{f}_j}^2), \quad (2.13)$$

with  $f = l, u, d$ . The neutralino-fermion-sfermion couplings are

$$\begin{aligned} g_{Lij}^{\tilde{\chi}^0 f\bar{f}} &= -\sqrt{2} g T_3^f N_{i2}^*(U^{\tilde{f}})_{1j}^* - \sqrt{2} g t_W (Q_f - T_3^f) N_{i1}^*(U^{\tilde{f}})_{1j}^* - h_f N_{i\alpha}^*(U^{\tilde{f}})_{2j}^*, \\ g_{Rij}^{\tilde{\chi}^0 f\bar{f}} &= \sqrt{2} g t_W Q_f N_{i1}(U^{\tilde{f}})_{2j}^* - h_f^* N_{i\alpha}(U^{\tilde{f}})_{1j}^*, \end{aligned} \quad (2.14)$$

where the Higgsino index  $\alpha = 3$  ( $f = l, d$ ) or  $4$  ( $f = u$ ),  $T_3^{l,d} = -1/2$  and  $T_3^u = +1/2$ .

In addition to charginos and neutralinos, gluinos also contribute to the quark EDMs  $(d_q^E/e)^{\tilde{g}}$ . In the gluino mass basis,  $(d_q^E/e)^{\tilde{g}}$  is given by

$$\left(\frac{d_q^E}{e}\right)^{\tilde{g}} = \frac{1}{3\pi^2} \sum_j \frac{|M_3|}{m_{\tilde{q}_j}^2} \Im[(g_{Rj}^{\tilde{g}q\bar{q}})^* g_{Lj}^{\tilde{g}q\bar{q}}] Q_{\tilde{q}} B(|M_3|^2/m_{\tilde{q}_j}^2), \quad (2.15)$$

where the gluino-quark-squark couplings are given by

$$g_{Lj}^{\tilde{g}q\bar{q}} = -\frac{g_s}{\sqrt{2}} e^{-i\Phi_3/2} (U^{\tilde{q}})_{1j}^*, \quad g_{Rj}^{\tilde{g}q\bar{q}} = +\frac{g_s}{\sqrt{2}} e^{+i\Phi_3/2} (U^{\tilde{q}})_{2j}^*. \quad (2.16)$$

As well as the EDMs, the chargino, neutralino and gluino loops can produce non-vanishing CEDMs for the quarks,  $(d_q^C)^{\chi^\pm, \chi^0, \tilde{g}}$ . Their individual contributions are as follows:

$$\begin{aligned}
(d_u^C)^{\tilde{\chi}^\pm} &= \frac{g_s}{16\pi^2} \sum_{i,j} \frac{m_{\tilde{\chi}_i^\pm}}{m_{\tilde{d}_j}^2} \Im[(g_{Rij}^{\tilde{\chi}^\pm u \tilde{d}})^* g_{Lij}^{\tilde{\chi}^\pm u \tilde{d}}] B(m_{\tilde{\chi}_i^\pm}^2/m_{\tilde{d}_j}^2), \\
(d_d^C)^{\tilde{\chi}^\pm} &= \frac{g_s}{16\pi^2} \sum_{i,j} \frac{m_{\tilde{\chi}_i^\pm}}{m_{\tilde{u}_j}^2} \Im[(g_{Rij}^{\tilde{\chi}^\pm d \tilde{u}})^* g_{Lij}^{\tilde{\chi}^\pm d \tilde{u}}] B(m_{\tilde{\chi}_i^\pm}^2/m_{\tilde{u}_j}^2), \\
(d_{q=u,d}^C)^{\tilde{\chi}^0} &= \frac{g_s}{16\pi^2} \sum_{i,j} \frac{m_{\tilde{\chi}_i^0}}{m_{\tilde{q}_j}^2} \Im[(g_{Rij}^{\tilde{\chi}^0 q \tilde{q}})^* g_{Lij}^{\tilde{\chi}^0 q \tilde{q}}] B(m_{\tilde{\chi}_i^0}^2/m_{\tilde{q}_j}^2), \\
(d_{q=u,d}^C)^{\tilde{g}} &= -\frac{g_s}{8\pi^2} \sum_j \frac{|M_3|}{m_{\tilde{q}_j}^2} \Im[(g_{Rj}^{\tilde{g} q \tilde{q}})^* g_{Lj}^{\tilde{g} q \tilde{q}}] C(|M_3|^2/m_{\tilde{q}_j}^2), \tag{2.17}
\end{aligned}$$

where

$$C(r) \equiv \frac{1}{6(1-r)^2} \left( 10r - 26 + \frac{2r \ln r}{1-r} - \frac{18 \ln r}{1-r} \right), \tag{2.18}$$

so that  $C(1) = 19/18$ .

Finally, it is important to stress that there are non-holomorphic threshold corrections to the light-quark Yukawa couplings that occur in the chargino and neutralino couplings. These corrections are proportional to the strong coupling  $\alpha_s$ , and become significant at large  $\tan \beta$ . We therefore resum these effects by redefining the light-quark Yukawa couplings as follows:

$$\begin{aligned}
h_u &= \frac{\sqrt{2}m_u}{vs_\beta} \frac{1}{1 + \Delta_u/t_\beta}, & h_c &= \frac{\sqrt{2}m_c}{vs_\beta} \frac{1}{1 + \Delta_c/t_\beta}, \\
h_d &= \frac{\sqrt{2}m_d}{vc_\beta} \frac{1}{1 + \Delta_d t_\beta}, & h_s &= \frac{\sqrt{2}m_s}{vc_\beta} \frac{1}{1 + \Delta_s t_\beta}, \tag{2.19}
\end{aligned}$$

where

$$\begin{aligned}
\Delta_u &= \frac{2\alpha_s}{3\pi} \mu^* M_3^* I(M_{U_1}^2, M_{Q_1}^2, |M_3|^2), & \Delta_c &= \frac{2\alpha_s}{3\pi} \mu^* M_3^* I(M_{U_2}^2, M_{Q_2}^2, |M_3|^2), \\
\Delta_d &= \frac{2\alpha_s}{3\pi} \mu^* M_3^* I(M_{D_1}^2, M_{Q_1}^2, |M_3|^2), & \Delta_s &= \frac{2\alpha_s}{3\pi} \mu^* M_3^* I(M_{D_2}^2, M_{Q_2}^2, |M_3|^2), \tag{2.20}
\end{aligned}$$

and

$$I(x, y, z) \equiv \frac{xy \ln(x/y) + yz \ln(y/z) + xz \ln(z/x)}{(x-y)(y-z)(x-z)} \tag{2.21}$$

is the one-loop function that takes account of the non-holomorphic threshold corrections.

### 3 Higher-Order Contributions to EDMs

Beyond the one-loop single-particle level, there are many CP-violating operators that can have significant effects on the EDMs. Of particular importance are the gluino- and Higgs-mediated dimension-6 Weinberg operator, the Higgs-exchange four-fermion operators, and

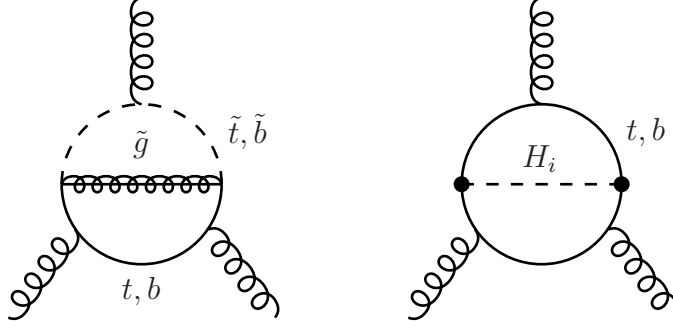


Figure 2: *Typical Feynman diagrams for  $(d^G)^{\tilde{g}}$  and  $(d^G)^H$ . The  $H_i$  lines denote all three neutral Higgs bosons including CP-violating Higgs-boson mixing. Heavy dots indicate resummation of threshold corrections to the corresponding Yukawa couplings.*

the two-loop Higgs-mediated Barr–Zee-type diagrams. We present detailed analytic expressions for all those contributions in this Section.

### 3.1 Weinberg Operator

We start by considering first the gluonic dimension-6 Weinberg operator. This is described by the interaction Lagrangian <sup>‡</sup> [21]:

$$\mathcal{L}_{\text{Weinberg}} = \frac{1}{3} d^G f_{abc} G_{\rho\mu}^a \tilde{G}^{b\mu\nu} G_{\nu\rho}^c, \quad (3.1)$$

where  $\tilde{G}^{\mu\nu} = \frac{1}{2}\epsilon^{\mu\nu\lambda\sigma} G_{\lambda\sigma}$  is the dual of the  $\text{SU}(3)_c$  field-strength tensor  $G_{\lambda\sigma}$ . In the MSSM,  $d^G$  is induced at two-loop order by  $\tilde{g}$  and  $\tilde{t}, \tilde{b}$ , and at three-loop order by CP-violating Higgs-boson mixing and non-holomorphic threshold corrections to the top- and bottom-quark Yukawa couplings. Hence, the Weinberg operator  $d^G$  is the sum of two terms:

$$d^G = (d^G)^{\tilde{g}} + (d^G)^H, \quad (3.2)$$

as illustrated in Fig. 2. The first term,  $(d^G)^{\tilde{g}}$ , is the quark-squark-gluino exchange contribution and is given by [19]

$$(d^G)^{\tilde{g}} = -\frac{3}{2\pi} \left( \frac{g_s}{4\pi|M_3|} \right)^3 \sum_{q=t,b} m_q \left\{ \sum_j \frac{m_{\tilde{q}_j}^2}{|M_3|^2} \Im[(g_{Rj}^{\tilde{g}q\tilde{q}})^* g_{Lj}^{\tilde{g}q\tilde{q}}] \right\} \\ \times H(m_{\tilde{q}_1}^2/|M_3|^2, m_{\tilde{q}_2}^2/|M_3|^2, m_q^2/|M_3|^2), \quad (3.3)$$

where

$$H(z_1, z_2, z_q) = \frac{1}{2} \int_0^1 dx \int_0^1 du \int_0^1 dy x(1-x)u \frac{N_1 N_2}{D^4} \quad (3.4)$$

<sup>‡</sup>Note the coefficient  $d^G$  has a different sign from that in [21]:  $d^G = -C$ .

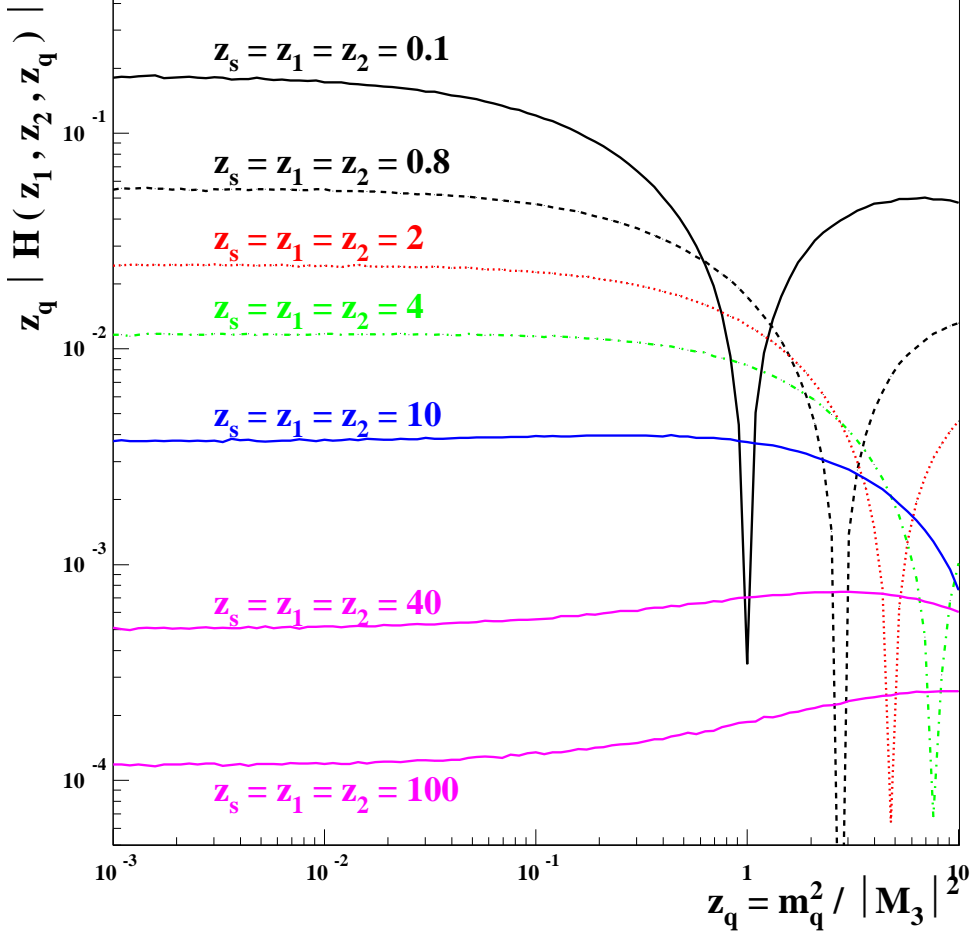


Figure 3: The functional dependence of  $z_q |H(z_1, z_2, z_q)|$  on  $z_q$  for several values of  $z_s \equiv z_1 = z_2$ . When  $z_s \leq 4$ ,  $H(z_1, z_2, z_q)$  becomes negative when  $z_q$  is larger than a specific value.

and

$$\begin{aligned}
 N_1 &= u(1-x) + z_q x(1-x)(1-u) - 2ux[z_1 y + z_2(1-y)], \\
 N_2 &= (1-x)^2(1-u)^2 + u^2 - \frac{1}{9}x^2(1-u)^2, \\
 D &= u(1-x) + z_q x(1-x)(1-u) + ux[z_1 y + z_2(1-y)].
 \end{aligned} \tag{3.5}$$

Figure 3 shows the functional dependence of  $z_q |H(z_1, z_2, z_q)|$  on  $z_q$  for several values of  $z_s \equiv z_1 = z_2$ . Our results are at variance with those presented in [19]. For instance, we find that when  $z_s \leq 4$ ,  $H(z_1, z_2, z_q)$  becomes negative beyond certain values of  $z_q$ <sup>§</sup>.

<sup>§</sup>We thank Oleg Lebedev and Pran Nath for useful comparisons and comments regarding the loop function  $H(z_1, z_2, z_q)$ .



The loop function  $H(z_1, z_2, z_q)$  simplifies considerably in specific regions of the parameter space. Specifically, if  $z_1 = z_2 = z_s$  and the limit  $z_q \rightarrow 0$  is taken, the following function may be defined:

$$\begin{aligned}\widehat{H}_0(z_s) &\equiv \lim_{z_q \rightarrow 0} z_q H(z_s, z_s, z_q) \\ &= \frac{1}{18(1-z_s)^4} \left[ 2(1-z_s)(1+11z_s) - (1-16z_s-9z_s^2) \ln z_s \right],\end{aligned}\quad (3.6)$$

with  $\widehat{H}_0(1) = 5/108$ . Hence, for  $z_q \lesssim 0.1$  and  $(z_2 - z_1)^2/(z_2 + z_1)^2 \ll 1$ , the loop function  $H(z_1, z_2, z_q)$  may be approximated as follows:

$$H(z_1, z_2, z_q) \approx \frac{1}{z_q} \left[ \widehat{H}_0\left(\frac{z_1+z_2}{2}\right) + \frac{(z_2-z_1)^2}{(z_1+z_2)^2} \widehat{H}_1\left(\frac{z_1+z_2}{2}\right) \right],\quad (3.7)$$

where

$$\begin{aligned}\widehat{H}_1(z_s) &\equiv \frac{1}{108(1-z_s)^6} \left[ (1-z_s)(1+7z_s+295z_s^2+177z_s^3) \right. \\ &\quad \left. + 6z_s^2(21+50z_s+9z_s^2) \ln(z_s) \right],\end{aligned}\quad (3.8)$$

with  $\widehat{H}_1(1) = 11/1080$ .

The second term in (3.2),  $(d^G)^H$ , is the neutral Higgs contribution [20,21], which may be cast into the form:

$$(d^G)^H = \frac{4\sqrt{2}G_F g_s^3}{(4\pi)^4} \sum_{q=t,b} \left[ \sum_i g_{H_i \bar{q}q}^S g_{H_i \bar{q}q}^P h(z_{iq}) \right],\quad (3.9)$$

where  $z_{iq} \equiv M_{H_i}^2/m_q^2$  and

$$h(z) = \frac{1}{4} \int_0^1 dx \int_0^1 du \frac{u^3 x^3 (1-x)}{[x(1-ux) + z(1-u)(1-x)]^2},\quad (3.10)$$

with  $h(0) = 1/16$ . We note that for the loop function  $h(z)$  we follow [20], whose result is smaller by a factor 2 than the one given in [21].

### 3.2 CP-Odd Four-Fermion Interactions

CP-odd four-fermion interactions play a significant role in the EDMs. These interactions may be generically described by the Lagrangian

$$\mathcal{L}_{4f} = \sum_{f,f'} C_{ff'} (\bar{f}f)(\bar{f}'i\gamma_5 f').\quad (3.11)$$

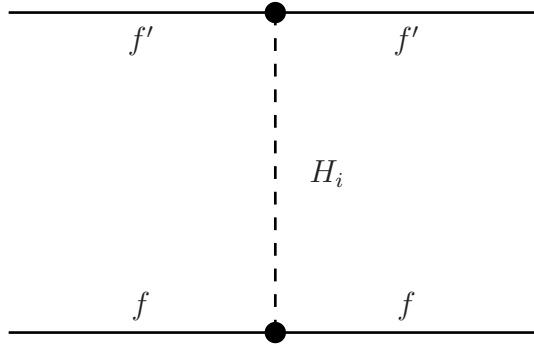


Figure 4: *Feynman diagrams for CP-odd four-fermion operators. The  $H_i$  line denotes all three neutral Higgs bosons including CP-violating Higgs-boson mixing. Heavy dots indicate resummation of threshold corrections to the corresponding Yukawa couplings.*

The CP-odd four-fermion operators in (3.11) are generated by CP-violating neutral Higgs-boson mixing in the  $t$ -channel and by CP-violating Yukawa threshold corrections, see Fig. 4. The combined effect of these two contributions gives rise to the CP-odd coefficients

$$(C_{ff'})^H = g_f g_{f'} \sum_i \frac{g_{H_i \bar{f} f}^S g_{H_i \bar{f}' f'}^P}{M_{H_i}^2}, \quad (3.12)$$

where  $g_f = m_f/v$  with  $v = 2M_W/g$  for  $f = l, d, u$ . Possible sub-dominant contributions from box diagrams [17] have been neglected.

### 3.3 Barr–Zee Graphs

Finally, there are additional Higgs-boson quantum effects that contribute significantly to the EDMs beyond the one-loop level. For the Thallium EDM, these are the two-loop Barr–Zee graphs, denoted as  $(d_e^E)^H$ , and the CP-odd electron-nucleon interaction  $\mathcal{L}_{C_S} = C_S \bar{e} i \gamma_5 e \bar{N} N$  [12,13], which is induced by CP-violating gluon-gluon-Higgs couplings,  $(C_S)^g$ . As shown in Fig. 5, the electron EDM  $(d_e^E)^H$  is induced by CP-violating phases of third-generation fermions and sfermions and of charginos. More explicitly,  $(d_e^E)^H$  is given by

$$\begin{aligned} \left(\frac{d_e^E}{e}\right)^H &= \sum_{q=t,b} \left\{ \frac{3\alpha_{\text{em}} Q_q^2 m_e}{32\pi^3} \sum_{i=1}^3 \frac{g_{H_i e^+ e^-}^P}{M_{H_i}^2} \sum_{j=1,2} g_{H_i \tilde{q}_j^* \tilde{q}_j} F(\tau_{\tilde{q}_j i}) \right. \\ &+ \frac{3\alpha_{\text{em}}^2 Q_q^2 m_e}{8\pi^2 s_W^2 M_W^2} \sum_{i=1}^3 \left[ g_{H_i e^+ e^-}^P - g_{H_i \bar{q} q}^S f(\tau_{q_i}) + g_{H_i e^+ e^-}^S - g_{H_i \bar{q} q}^P g(\tau_{q_i}) \right] \left. \right\} \\ &+ \frac{\alpha_{\text{em}} m_e}{32\pi^3} \sum_{i=1}^3 \frac{g_{H_i e^+ e^-}^P}{M_{H_i}^2} \sum_{j=1,2} g_{H_i \tilde{\tau}_j^* \tilde{\tau}_j} F(\tau_{\tilde{\tau}_j i}) \\ &+ \frac{\alpha_{\text{em}}^2 m_e}{8\pi^2 s_W^2 M_W^2} \sum_{i=1}^3 \left[ g_{H_i e^+ e^-}^P - g_{H_i \tau^+ \tau^-}^S f(\tau_{\tau i}) + g_{H_i e^+ e^-}^S - g_{H_i \tau^+ \tau^-}^P g(\tau_{\tau i}) \right] \end{aligned}$$

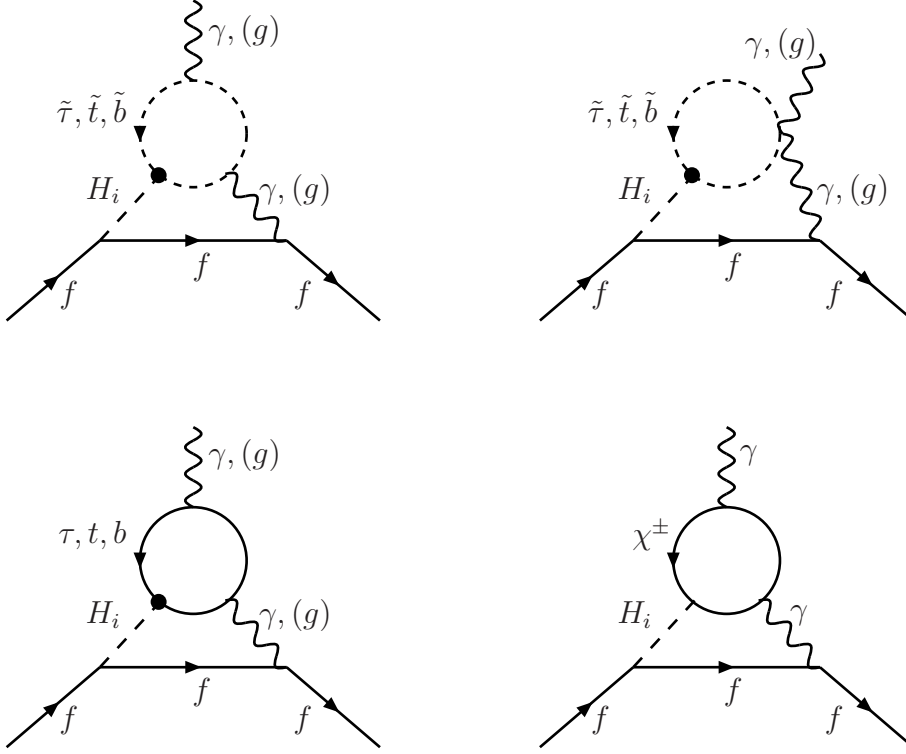


Figure 5: *Barr-Zee diagrams: the  $H_i$  lines denote all three neutral Higgs bosons, including CP-violating Higgs-boson mixing, and heavy dots indicate resummation of threshold corrections to the corresponding Yukawa couplings.*

$$\begin{aligned}
& + \frac{\alpha_{\text{em}}^2 m_e}{4\sqrt{2}\pi^2 s_W^2 M_W} \\
& \times \sum_{i=1}^3 \sum_{j=1,2} \frac{1}{m_{\chi_j^\pm}} \left[ g_{H_i e^+ e^-}^P g_{H_i \chi_j^+ \chi_j^-}^S f(\tau_{\chi_j^\pm i}) + g_{H_i e^+ e^-}^S g_{H_i \chi_j^+ \chi_j^-}^P g(\tau_{\chi_j^\pm i}) \right],
\end{aligned} \tag{3.13}$$

with  $\tau_{xi} = m_x^2/M_{H_i}^2$ . The Higgs-mediated two-loop quark EDMs ( $d_{q=u,d,s}^E$ )<sup>H</sup> are also calculated similarly. In the above, the two-loop functions  $F(\tau)$ ,  $f(\tau)$ , and  $g(\tau)$  are given by

$$\begin{aligned}
F(\tau) &= \int_0^1 dx \frac{x(1-x)}{\tau - x(1-x)} \ln \left[ \frac{x(1-x)}{\tau} \right], \\
f(\tau) &= \frac{\tau}{2} \int_0^1 dx \frac{1 - 2x(1-x)}{x(1-x) - \tau} \ln \left[ \frac{x(1-x)}{\tau} \right], \\
g(\tau) &= \frac{\tau}{2} \int_0^1 dx \frac{1}{x(1-x) - \tau} \ln \left[ \frac{x(1-x)}{\tau} \right].
\end{aligned} \tag{3.14}$$

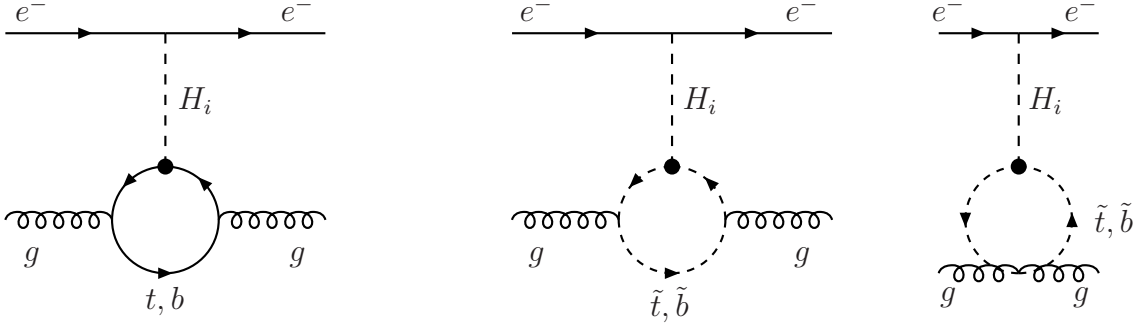


Figure 6: *Feynman graphs contributing to  $(C_S)^g$ : the  $H_i$  lines denote all three neutral Higgs bosons, including CP-violating Higgs-boson mixing, and heavy dots indicate resummation of threshold corrections to the corresponding Yukawa couplings.*

There are subleading two-loop contributions which we neglect [28, 29]. Instead, we consider the gluon-gluon-Higgs contribution to  $C_S$ , see Fig. 6. This is given by

$$(C_S)^g = (0.1 \text{ GeV}) \frac{m_e}{v^2} \sum_{i=1}^3 \frac{g_{H_i gg}^S g_{H_i \bar{e}e}^P}{M_{H_i}^2}, \quad (3.15)$$

where  $\langle N | \frac{\alpha_s}{8\pi} G^{a, \mu\nu} G_{\mu\nu}^a | N \rangle = -(0.1 \text{ GeV}) \bar{N} N$  is used, and we use the tree-level value  $g_{H_i \bar{e}e}^P = -\tan \beta O_{ai}$ . In addition,  $g_{H_i gg}^S$  is the scalar form factor  $S_i^g$  in the heavy (s)quark limit:

$$g_{H_i gg}^S = \sum_{q=t,b} \left\{ \frac{2x_q}{3} g_{H_i \bar{q}q}^S - \frac{v^2}{12} \sum_{j=1,2} \frac{g_{H_i \bar{q}_j^* \bar{q}_j}}{m_{\bar{q}_j}^2} \right\}, \quad (3.16)$$

where  $x_t = 1$  and  $x_b = (1 - 0.25\kappa)$  with  $\kappa \equiv \langle N | m_s \bar{s} s | N \rangle / 220 \text{ MeV} \simeq 0.50 \pm 0.25$  [cf. (4.4)].

Apart from EDMs, the two-loop Barr-Zee graphs also generate CEDMs for the  $u$  and  $d$  quarks. These additional contributions are given by

$$\begin{aligned} (d_{q_l}^C)^H &= - \sum_{q=t,b} \left\{ \frac{g_s \alpha_s m_{q_l}}{64\pi^3} \sum_{i=1}^3 \frac{g_{H_i \bar{q}_l q_l}^P}{M_{H_i}^2} \sum_{j=1,2} g_{H_i \bar{q}_j^* \bar{q}_j} F(\tau_{\bar{q}_j i}) \right. \\ &\quad \left. + \frac{g_s \alpha_s \alpha_{\text{em}} m_{q_l}}{16\pi^2 s_W^2 M_W^2} \sum_{i=1}^3 \left[ g_{H_i \bar{q}_l q_l}^P g_{H_i \bar{q}q}^S f(\tau_{q_i}) + g_{H_i \bar{q}_l q_l}^S g_{H_i \bar{q}q}^P g(\tau_{q_i}) \right] \right\}, \quad (3.17) \end{aligned}$$

with  $q_l = u, d$ .

## 4 Thallium, Neutron, Mercury and Deuteron EDMs

In this Section we present analytic expressions for the Thallium, neutron, Mercury and deuteron EDMs in terms of the constituent particle (C)EDMs and the coefficients of the

dimension-six Weinberg operator and the four-fermion operators.

## 4.1 Thallium

We first consider the atomic EDM  $d_{\text{Tl}}$  of  $^{205}\text{Tl}$ . This receives contributions mainly from two terms [30, 31]:

$$d_{\text{Tl}} [e \text{ cm}] = -585 \cdot d_e^E [e \text{ cm}] - 8.5 \times 10^{-19} [e \text{ cm}] \cdot (C_S \text{ TeV}^2) + \dots, \quad (4.1)$$

where  $d_e^E$  is the electron EDM, which is given by the sum

$$d_e^E = (d_e^E)^{\tilde{\chi}^\pm} + (d_e^E)^{\tilde{\chi}^0} + (d_e^E)^H. \quad (4.2)$$

The coefficient  $C_S$  is calculated as

$$C_S = (C_S)^{4f} + (C_S)^g, \quad (4.3)$$

where the (down-type) quark contribution is given by [17]

$$(C_S)^{4f} = C_{de} \frac{29 \text{ MeV}}{m_d} + C_{se} \frac{\kappa \times 220 \text{ MeV}}{m_s}. \quad (4.4)$$

We neglect the  $u$ - and  $c$ -quark contributions and absorb the  $b$ -quark contribution into  $(C_S)^g$  together with the top and heavy-squark contributions [cf. (3.16)]. We recall that the ratio  $C_{qe}/m_q \propto m_e/v^2$  is scale-invariant [17]. More details concerning the calculations of these coefficients are given in Appendix A.

## 4.2 Neutron

We now turn to the calculation of the neutron EDM,  $d_n$ . Its magnitude is somewhat uncertain, because of non-perturbative dynamics at the hadron level. We consider three different hadronic approaches for computing  $d_n$ : (i) the Chiral Quark Model (CQM), (ii) the Parton Quark Model (PQM) and (iii) the QCD sum-rule technique.

The CQM is a non-relativistic model, where the quark EDMs are estimated via naive dimensional analysis (NDA) [32], and the neutron EDM is given by

$$\begin{aligned} d_n &= \frac{4}{3} d_d^{\text{NDA}} - \frac{1}{3} d_u^{\text{NDA}}, \\ d_{q=u,d}^{\text{NDA}} &= \eta^E d_q^E + \eta^C \frac{e}{4\pi} d_q^C + \eta^G \frac{e\Lambda}{4\pi} d_q^G, \\ d_{q=u,d}^{E(C)} &= (d_q^{E(C)})^{\tilde{\chi}^\pm} + (d_q^{E(C)})^{\tilde{\chi}^0} + (d_q^{E(C)})^{\tilde{g}} + (d_q^{E(C)})^H, \end{aligned} \quad (4.5)$$

where the chiral symmetry breaking scale  $\Lambda \simeq 1.19 \text{ GeV}$  and the  $\eta^{E,C,G}$  are QCD correction factors that describe the renormalization-group (RG) evolution of  $d_q^{E,C}$  and  $d_q^G$  from the

electroweak (EW) scale, e.g., the  $Z$ -boson mass  $M_Z$ , down to the hadronic scale. These QCD correction factors are given in [33] as

$$\eta^E \simeq 1.53, \quad \eta^C \simeq \eta^G \simeq 3.4. \quad (4.6)$$

We note that the EDM operators  $d_q^{E,C}$  and  $d^G$  in (4.5) are computed at the EW scale.

Another approach to computing the neutron EDM is based on the PQM, which uses low-energy data related to the constituent-quark contributions to the proton spin combined with isospin symmetry [34]. In the PQM, the neutron EDM is given by

$$d_n = \eta^E (\Delta_d^{\text{PQM}} d_d^E + \Delta_u^{\text{PQM}} d_u^E + \Delta_s^{\text{PQM}} d_s^E), \quad (4.7)$$

where we consider the following particular values, to contrast with the PQM predictions ¶

$$\Delta_d^{\text{PQM}} = 0.746, \quad \Delta_u^{\text{PQM}} = -0.508, \quad \Delta_s^{\text{PQM}} = -0.226. \quad (4.8)$$

As in the CQM,  $d_q^E$ 's in (4.7) are evaluated at the EW scale.

The third approach to computing the neutron EDM employs QCD sum rule techniques [17, 35–38]. With the aid of these techniques, the neutron EDM is determined by

$$\begin{aligned} d_n &= d_n(d_q^E, d_q^C) + d_n(d^G) + d_n(C_{bd}) + \dots, \\ d_n(d_q^E, d_q^C) &= (1.4 \pm 0.6) (d_d^E - 0.25 d_u^E) + (1.1 \pm 0.5) e (d_d^C + 0.5 d_u^C)/g_s, \\ d_n(d^G) &\sim \pm e (20 \pm 10) \text{ MeV } d^G, \\ d_n(C_{bd}) &\sim \pm e 2.6 \times 10^{-3} \text{ GeV}^2 \left[ \frac{C_{bd}}{m_b} + 0.75 \frac{C_{db}}{m_b} \right], \end{aligned} \quad (4.9)$$

where  $d_q^E$  and  $d_q^C$  should be evaluated at the EW scale and  $d^G$  at the 1 GeV scale ¶. We note that the contribution of  $d^G$  to  $d_n$  is a factor  $\sim 2$  smaller than in the CQM. We calculate the coefficients  $C_{bd}$  and  $C_{db}$  by means of (3.12) and evaluate the coefficients  $g_b$  and  $g_d$ , at the energy scales  $m_b$  and 1 GeV, respectively. For definiteness, in our numerical estimates we assume that both  $d^G$  and  $C_{bd}$  contribute positively to  $d_n$ .

The comparisons between the results obtained in these three approaches indicates the significance of the non-perturbative uncertainties in calculating  $d_n$ . Related uncertainties appear also in the calculations of EDMs of nuclei. In Section 5, we present numerical estimates of the neutron EDM based on the CQM, the PQM and QCD sum-rules.

---

¶We note that isospin symmetry between the neutron  $n$  and the proton  $p$  implies that  $\Delta_d = (\Delta_u)_p = 4/3$ ,  $\Delta_u = (\Delta_d)_p = -1/3$ . Furthermore, in the relativistic Naive Quark Model (NQM), one has  $\Delta_s = (\Delta_s)_p = 0$ .

¶Here we make use of the relation:  $d^G|_{1 \text{ GeV}} \simeq (\eta^G/0.4) d^G|_{\text{EW}} \simeq 8.5 d^G|_{\text{EW}}$  [37].

### 4.3 Mercury

Using QCD sum rules [17, 38] to calculate the Mercury EDM, one finds that

$$\begin{aligned}
d_{\text{Hg}} &= 7 \times 10^{-3} e (d_u^C - d_d^C)/g_s + 10^{-2} d_e^E \\
&\quad - 1.4 \times 10^{-5} e \text{ GeV}^2 \left[ \frac{0.5C_{dd}}{m_d} + 3.3\kappa \frac{C_{sd}}{m_s} + (1 - 0.25\kappa) \frac{C_{bd}}{m_b} \right] \\
&\quad + (3.5 \times 10^{-3} \text{ GeV}) e C_S \\
&\quad + (4 \times 10^{-4} \text{ GeV}) e \left[ C_P + \left( \frac{Z - N}{A} \right)_{\text{Hg}} C'_P \right]. \tag{4.10}
\end{aligned}$$

The parameters  $C_P$  and  $C'_P$  are the couplings of the CP-odd singlet and triplet electron-nucleon interactions, respectively, and are described by the interaction Lagrangian

$$\mathcal{L}_{C_P} = C_P \bar{e} e \bar{N} i \gamma_5 N + C'_P \bar{e} e \bar{N} i \gamma_5 \tau_3 N. \tag{4.11}$$

Making use of the SU(2) isospin symmetry of the nucleon  $N = (p, n)$ , one may evaluate the triplet contribution  $C'_P$ , which is suppressed by a factor  $[(Z - N)/A]_{\text{Hg}} = -0.2$  with respect to the singlet one  $C_P$ . In detail, the contribution of four-fermion interactions to  $C_P$  and  $C'_P$  is given by

$$\begin{aligned}
C_P &= (C_P)^{4f} \simeq -375 \text{ MeV} \sum_{q=c,s,t,b} \frac{C_{eq}}{m_q}, \\
C'_P &= (C'_P)^{4f} \simeq -806 \text{ MeV} \frac{C_{ed}}{m_d} - 181 \text{ MeV} \sum_{q=c,s,t,b} \frac{C_{eq}}{m_q}, \tag{4.12}
\end{aligned}$$

where the  $u$ -quark contribution has been neglected. For a detailed discussion, see Appendix B.

On the basis of above results, we improve upon an earlier calculation of the Mercury EDM [31]\*\*. More explicitly, including the CP-odd triplet electron-nucleon interaction, the Mercury EDM is given by

$$\begin{aligned}
d_{\text{Hg}} &= (1.8 \times 10^{-3} \text{ GeV}^{-1}) e \bar{g}_{\pi NN}^{(1)} + 10^{-2} d_e^E + (3.5 \times 10^{-3} \text{ GeV}) e C_S \\
&\quad + (4 \times 10^{-4} \text{ GeV}) e \left[ C_P + \left( \frac{Z - N}{A} \right)_{\text{Hg}} C'_P \right], \\
\bar{g}_{\pi NN}^{(1)} &= 2_{-1}^{+4} \times 10^{-12} \frac{(d_u^C - d_d^C)/g_s}{10^{-26} \text{ cm}} \frac{|\langle \bar{q}q \rangle|}{(225 \text{ MeV})^3}, \\
\bar{g}_{\pi NN}^{(1)} &\sim -8 \times 10^{-3} \text{ GeV}^3 \left[ \frac{0.5C_{dd}}{m_d} + 3.3\kappa \frac{C_{sd}}{m_s} + (1 - 0.25\kappa) \frac{C_{bd}}{m_b} \right], \tag{4.13}
\end{aligned}$$

where  $\mathcal{L}_{\pi NN} \supset \bar{g}_{\pi NN}^{(1)} \bar{N} N \pi^0$ . We note that the factors  $1.8 \times 10^{-3} \text{ GeV}^{-1}$  and  $-8 \times 10^{-3} \text{ GeV}^3$  are known only up to 50 % accuracy [39].

---

\*\*We also correct the errors in the contributions of  $\bar{g}_{\pi NN}^{(1)}$  to  $d_{\text{Hg}}$  and of four-fermion interactions to  $\bar{g}_{\pi NN}^{(1)}$  [39].

## 4.4 Deuteron

Finally, the deuteron EDM may be calculated by using QCD sum rules. We include the contributions from the pion-nucleon-nucleon isospin-triplet coupling  $\bar{g}_{\pi NN}^{(1)}$  [40], the constituent proton and neutron EDMs [36], and the dimension-six Weinberg operator [21, 37]. The deuteron EDM  $d_D$  is then found to be [6]

$$\begin{aligned}
d_D &= d_D^{\pi NN} + d_D(d_n, d_p) + d_D(d^G), \\
d_D^{\pi NN} &= -\frac{e g_{\pi NN} \bar{g}_{\pi NN}^{(1)}}{12\pi m_\pi} \frac{1 + \xi}{(1 + 2\xi)^2} \simeq -(1.3 \pm 0.3) e \bar{g}_{\pi NN}^{(1)} \text{ GeV}^{-1}, \\
d_D(d_n, d_p) &\simeq (0.5 \pm 0.3)(d_u^E + d_d^E) - (0.6 \pm 0.3) e [(d_u^C - d_d^C)/g_s + 0.3(d_u^C + d_d^C)/g_s], \\
d_D(d^G) &\simeq d_n(d^G) + d_p(d^G) \sim \pm e (20 \pm 10) \text{ MeV } d^G,
\end{aligned} \tag{4.14}$$

where  $g_{\pi NN} \simeq 13.45$  and  $\xi = \sqrt{m_p \epsilon}/m_\pi$ , with  $\epsilon = 2.23$  MeV being the deuteron binding energy. Collecting all the above intermediate results, we may write  $d_D$  in the more compact form:

$$\begin{aligned}
d_D &\simeq -\left[5_{-3}^{+11} + (0.6 \pm 0.3)\right] e (d_u^C - d_d^C)/g_s \\
&\quad - (0.2 \pm 0.1) e (d_u^C + d_d^C)/g_s + (0.5 \pm 0.3)(d_u^E + d_d^E) \\
&\quad + (1 \pm 0.2) \times 10^{-2} e \text{ GeV}^2 \left[ \frac{0.5 C_{dd}}{m_d} + 3.3\kappa \frac{C_{sd}}{m_s} + (1 - 0.25\kappa) \frac{C_{bd}}{m_b} \right] \\
&\quad \pm e (20 \pm 10) \text{ MeV } d^G.
\end{aligned} \tag{4.15}$$

In the above,  $d^G$  is evaluated at the 1 GeV scale, and the coupling coefficients  $g_{d,s,b}$  that occur in  $C_{dd, sd, bd}$  are computed at energies 1 GeV, 1 GeV and  $m_b$ , respectively. All other EDM operators are calculated at the EW scale. We observe that the leading dependence of  $d_D$  on  $d_{u,d}^C$  is the same as in  $d_{\text{Hg}}$ . In the numerical estimates given in the next Section, we assume that  $d^G$  contributes positively to  $d_D$ .

## 5 EDM Constraints

In this Section, we present illustrative constraints on key soft SUSY-breaking parameters and CP phases in the trimixing, the CPX and the MCPMFV scenarios. We use the following current experimental limits on the Thallium [1], neutron [2], and Mercury [3] EDMs:

$$\begin{aligned}
|d_{\text{Tl}}| &< 9 \times 10^{-25} \text{ e cm}, \\
|d_{\text{Hg}}| &< 2 \times 10^{-28} \text{ e cm}, \\
|d_n| &< 3 \times 10^{-26} \text{ e cm}.
\end{aligned} \tag{5.1}$$

On the other hand, the projected sensitivity to the deuteron EDM is [4]

$$|d_D| < (1 - 3) \times 10^{-27} \text{ e cm}. \tag{5.2}$$



For our numerical study, we take  $3 \times 10^{-27}$  e cm as a representative expected value. However, we note that much better statistical precision at the level of  $10^{-29}$  e cm may be possible in principle [5].

## 5.1 Trimixing Scenario

The trimixing scenario is characterized by large  $\tan\beta$  and a light charged Higgs boson, resulting in a strongly-mixed system of three neutral Higgs bosons with mass differences smaller than the decay widths [25]:

$$\begin{aligned}
\tan\beta &= 50, \quad M_{H^\pm} = 155 \text{ GeV}, \\
M_{\tilde{Q}_3} &= M_{\tilde{U}_3} = M_{\tilde{D}_3} = M_{\tilde{L}_3} = M_{\tilde{E}_3} = M_{\text{SUSY}} = 0.5 \text{ TeV}, \\
|\mu| &= 0.5 \text{ TeV}, \quad |A_{t,b,\tau}| = 1 \text{ TeV}, \quad |M_2| = |M_1| = 0.3 \text{ TeV}, \quad |M_3| = 1 \text{ TeV}, \\
\Phi_\mu &= 0^\circ, \quad \Phi_1 = \Phi_2 = 0^\circ, \quad \Phi_{A_\tau} = \Phi_{A_e} = \Phi_{A_u} = \Phi_{A_c} = \Phi_{A_d} = \Phi_{A_s} = 0^\circ.
\end{aligned} \tag{5.3}$$

Note that, in this scenario, only two independent CP-violating phases generate EDMs:  $\Phi_A = \Phi_{A_t} = \Phi_{A_b}$  and  $\Phi_3$ . In addition, we introduce a common hierarchy factor  $\rho$  between the masses of the first two and third generations:

$$M_{\tilde{X}_{1,2}} = \rho M_{\tilde{X}_3}, \tag{5.4}$$

with  $X = Q, U, D, L, E$ . For the size of first two generation  $A$  terms, we take  $|A_e| = |A_\tau|$ ,  $|A_{u,c}| = |A_t|$ , and  $|A_{d,s}| = |A_b|$ . Note that in this scenario, only  $d_{u,d,s}^E$  and  $d_{u,d}^C$  depend on the hierarchy factor  $\rho$  through the resummed threshold corrections (2.19).

In Fig. 7, we show the absolute value of the Thallium EDM divided by its current experimental limit, in the  $\Phi_3$ - $\Phi_A$  plane (left) and as a function of  $\Phi_3$  taking  $\Phi_A = 60^\circ$  (right). In the left frame, the plane is divided into 4 regions:  $|d_{\text{Tl}}/d^{\text{EXP}}| < 1$  (black),  $1 \leq |d_{\text{Tl}}/d^{\text{EXP}}| < 10$  (red),  $10 \leq |d_{\text{Tl}}/d^{\text{EXP}}| < 100$  (green), and  $100 \leq |d_{\text{Tl}}/d^{\text{EXP}}|$  (magenta). The unshaded region is not allowed theoretically. In the right frame, the constituent contributions from the electron EDM  $d_e^E$  and the CP-odd electron-nucleon interaction  $C_S$  are shown in the thin solid and dashed lines, respectively. The thick solid line is for the total. Note the non-trivial cancellation between  $d_e^E$  and  $C_S$  contributions around  $\Phi_3 = 275^\circ$  in the right frame.

In Fig. 8, we show the neutron EDM calculated in the CQM for two values of the hierarchy factor  $\rho$ :  $\rho = 1$  (upper) and 3 (lower). In the left frames, the regions are shaded as in the Thallium case, Fig. 7. In the right frames, the constituent contributions from the quark EDMs  $d_{u,d}^E$ , the quark CEDMs  $d_{u,d}^C$ , the Weinberg operator  $d^G$  are shown in the thin solid, dashed, and dotted lines, respectively. The thick lines are again for the total. We note first that  $d_{u,d}^E$  and  $d_{u,d}^C$  do not vanish, even though we are taking  $\Phi_{1,2} = \Phi_{A_{u,d}} = 0^\circ$  in this scenario. This is because the non-vanishing  $\Phi_3$  enters the Yukawa

couplings through the threshold corrections and the two-loop Higgs-mediated graphs. The  $d_{u,d}^{E,C}$  contributions decrease for larger  $\rho$ , whilst the  $d^G$  contribution is independent of  $\rho$ . For larger  $\rho = 3$ , the  $d^G$  contribution is almost dominating. The non-vanishing  $\rho$ -independent  $d_{u,d}^{E,C}$  at  $\Phi_3 = 0^\circ, 180^\circ$  comes from the two-loop Higgs-mediated diagrams. A non-trivial cancellation occurs, for example, between the  $d_{u,d}^C$  and  $d^G$  contributions around  $\Phi_3 = 10^\circ$  in the lower-right frame.

In Fig. 9, we display the neutron EDM calculated in the PQM. The shaded regions and lines are the same as in Fig. 8, except for the constituent contributions in the right frames: the thin solid, dashed, and dotted lines are for the contributions from the EDMs of  $u$ ,  $d$ , and  $s$  quarks, respectively. In this model, the neutron EDM is dominated by the  $d_s^E$  contribution and decreases as  $\rho$  increases. The dips in the lower-right frames are due to the cancellation between the contributions to  $d_s^E$  from the Higgs-mediated and other diagrams.

Figure 10 shows the predictions for the neutron EDM calculated using the QCD sum rule approach. In the right frames, the thin solid, dashed, dotted, and dash-dotted lines are for the constituent contributions  $d_{u,d}^E$ ,  $d_{u,d}^C$ ,  $d^G$ , and  $C_{bd,db}$ , respectively. Compared to the CQM,  $d_{u,d}^C$  contribution is about 3 times larger and  $d^G$  one about 2 times smaller. The  $C_{bd,db}$  contribution is significant because of the large value of  $\tan\beta$  and the light Higgs spectrum in this scenario.

Comparing Figs. 8, 9 and 10, we see that they yield qualitatively similar overall results, but with important detail differences. In particular, the appearances and locations of non-trivial cancellations are model-dependent.

Finally, Fig. 11 gives our numerical estimates for the Mercury EDM. In the right frames, the thin solid, dashed, dotted, and dash-dotted lines are for the constituent contributions from  $d_e^E$ ,  $d_{u,d}^C$ ,  $C_{4f} \equiv C_{dd,sd,bd}$ , and  $C_{S,P}^{(l)}$ , respectively. When  $\rho = 1$ , the Mercury EDM is dominated by  $d_{u,d}^C$ . However, as  $\rho$  increases, the  $d_{u,d}^C$  contribution decreases while other four contributions remain the same. Cancellations occur more easily for larger  $\rho$ , in which case all the contributions become more or less comparable, and we see a non-trivial example in the lower-right frame.

## 5.2 CPX Scenario

In the CPX scenario [24], the product of  $\mu$  and the third-generation  $A$  terms are larger than the common SUSY scale of the third-generation squarks by a factor of 8:

$$\begin{aligned} M_{\tilde{Q}_3} &= M_{\tilde{U}_3} = M_{\tilde{D}_3} = M_{\tilde{L}_3} = M_{\tilde{E}_3} = M_{\text{SUSY}}, \\ |\mu| &= 4 M_{\text{SUSY}}, \quad |A_{t,b,\tau}| = 2 M_{\text{SUSY}}, \quad |M_3| = 1 \text{ TeV}. \end{aligned} \quad (5.5)$$

As an example, we have fixed  $|M_2| = 2|M_1| = 100 \text{ GeV}$ , and taken the charged Higgs-boson pole mass  $M_{H^\pm} = 300 \text{ GeV}$  and the common SUSY scale  $M_{\text{SUSY}} = 0.5 \text{ TeV}$ , but the

parameter  $\tan\beta$  is varied. The  $A$ -term phases of first two generations are set to vanish, as in the trimixing scenario:  $\Phi_{A_\tau} = \Phi_{A_e} = \Phi_{A_u} = \Phi_{A_c} = \Phi_{A_d} = \Phi_{A_s} = 0^\circ$ . For the size of the  $A$  terms of the first two generations, we also take  $|A_e| = |A_\tau|$ ,  $|A_{u,c}| = |A_t|$ , and  $|A_{d,s}| = |A_b|$ . As for the CP-violating phases, initially we vary two phases generating EDMs,  $\Phi_A$  and  $\Phi_3$ , taking  $\Phi_1 = \Phi_2 = 0$ . The effects of non-trivial  $\Phi_1$  and  $\Phi_2$  are described later.

Taking  $\Phi_1 = \Phi_2 = 0^\circ$ , in Figs. 12, 13, 14, 15, and 16, we show the Thallium, neutron, and Mercury EDMs on the  $\Phi_3 - \Phi_A$  plane (left) and as functions of  $\Phi_3$  taking  $\Phi_A = 90^\circ$  (right). We take two values of  $\tan\beta = 5$  (upper) and 50 (lower) but with fixed  $\rho = 1$ . The shaded regions and the lines are the same as in Figs. 7, 8, 9, 10, and 11, respectively.

We observe the Thallium EDM, shown in Fig. 12, is dominated by the two-loop Higgs-mediated electron EDM for both cases, with only mild dependence on  $\Phi_3$ . For small  $\tan\beta$ , we always have  $|d_{Tl}/d^{\text{EXP}}| < 10$ , independently of  $\Phi_{3,A}$ , as can be seen from the upper-left frame. For large  $\tan\beta$ , the sub-leading  $C_S$  contribution becomes larger by two orders of magnitude, whilst the electron EDM contribution is larger by one order of magnitude as seen by comparing the two right frames.

Turning now to the neutron EDM in the CQM, shown in Fig. 13, we see that the three contributions from  $d_{u,d}^E$ ,  $d_{u,d}^C$ , and  $d^G$  are comparable. The most important contributions to the down-quark EDM  $d_d^E$  and CEDM  $d_d^C$  come from the one-loop gluino diagrams, explaining the mild  $\Phi_A$  dependence. The different dependence on  $\Phi_3$  for large  $\tan\beta$  is due to the enhanced two-loop Higgs-mediated contribution to  $d_d^{E,C}$ , and we note a non-trivial cancellation in the lower-right panel when  $\Phi_3 \sim 325^\circ$ . The neutron EDM in the PQM, Fig. 14, and that found using the QCD sum rules, Fig. 15, are somewhat larger in general and show a similar behaviour, due to the dominance by the  $d_s^E$  and the  $d_d^C$  contributions, respectively. The Mercury EDM, Fig. 16, is also dominated by the  $d_d^C$  contribution. However, the sub-dominant contributions from  $d_e^E$ ,  $C_{4f} \equiv C_{dd,sd,bd}$ , and  $C_{S,P}^{(\prime)}$  become larger for large  $\tan\beta$ .

We now study the effects of non-zero  $\Phi_1$  and  $\Phi_2$ , and some cancellation properties, varying the common hierarchy factor  $\rho$  and assuming maximal CP violation in  $\Phi_A$  and  $\Phi_3$ , i.e.,  $\Phi_A = \Phi_3 = 90^\circ$ . The one-loop contributions decrease as  $\rho$  increases but the contributions from the Weinberg operator and the two-loop Higgs mediated diagrams remain constant.

In the upper frames of Fig. 17, we show the Thallium EDM as a function of  $\rho$  for two values of  $\tan\beta$ : 5 (upper-left) and 50 (upper-right). The four lines are for  $(\Phi_1, \Phi_2) = (0^\circ, 0^\circ)$  (solid),  $(90^\circ, 0^\circ)$  (dashed),  $(0^\circ, 90^\circ)$  (dotted), and  $(0^\circ, 270^\circ)$  (dash-dotted). When  $(\Phi_1, \Phi_2) = (0^\circ, 0^\circ)$ , the Thallium EDM is independent of  $\rho$  because the main contribution from the electron EDM is dominated by the two-loop Higgs-mediated diagrams, see Fig. 12. The two dips around  $\rho = 1.5$  and 4 when  $(\Phi_1, \Phi_2) = (90^\circ, 0^\circ)$  and  $(0^\circ, 90^\circ)$  are due to the cancellations between the  $\rho$ -independent two-loop Higgs and neutralino and chargino

contributions to the electron EDM, respectively. In the lower frames we show explicitly the chargino-Higgs cancellation in the  $(0^\circ, 90^\circ)$  case. In the lower frames, the thick solid line is for the total electron EDM and the thin solid, dashed, horizontal dash-dotted lines are for the chargino, neutralino, and Higgs contributions to it, respectively.

In Fig. 18, we compare the three calculations of the neutron EDM: the CQM (upper row), the PQM (middle row), and the QCD sum-rule technique (lower row). The lines are the same as in Fig. 17. The cases with  $(\Phi_1, \Phi_2) = (0^\circ, 0^\circ)$  (solid) and  $(90^\circ, 0^\circ)$  (dashed) are hardly distinguishable from each other. The PQM calculation (middle) is most sensitive to  $\Phi_2$ , whilst the QCD sum-rule approach shows the least sensitivity. We observe that the value of  $\rho$  where the cancellation occurs varies on the models and approaches. In all cases, the neutron EDM calculations saturate to certain values determined by the  $\rho$ -independent contribution from the Weinberg operator or the two-loop Higgs mediated diagrams, as shown below.

In Figs. 19 and 20, we show details of the neutron EDM taking the cases  $(\Phi_1, \Phi_2) = (0^\circ, 90^\circ)$  and  $(0^\circ, 270^\circ)$ , respectively, as examples. In Fig. 19, the thick line is for the total neutron EDM and the thin solid, dashed and horizontal dotted lines are for the contributions from the EDMs of quarks  $d_{u,d}^E$ , the CEDMs  $d_{u,d}^C$ , and the Weinberg operator  $d^G$ , respectively. The EDMs and CEDMs are dominated by those of the down quark. In the lower-right frame, the lower horizontal dash-dotted line is for the contribution from the bottom-down four-fermion operator,  $C_{bd,db}$ . We observe the dips of the thick lines are determined by the interplay of the three main contributions. For example, in the upper-left frames with  $\tan\beta = 5$ , cancellation occurs at  $\rho = 2$  in the CQM. On the other hand, in the QCD sum-rule approach where the contribution from  $d^G$  ( $d_{u,d}^C$ ) is suppressed (enhanced) compared to the CQM, the cancellation occurs at  $\rho \sim 3.6$ . Taking into account of the uncertainty involved in the calculation of the  $d^G$  contribution, the  $\rho$  value where the cancellation occurs may change by  $\sim \pm 1$ , at least. The more significant contribution from  $d_{u,d}^E$  in the CQM explains why this calculation is more sensitive to  $\Phi_2$  than the QCD sum-rule approach. The dips in the thin solid lines for  $d_{u,d}^E$  are due to three-way cancellations among the one-loop gluino, one-loop chargino and two-loop Higgs-mediated diagrams. For large  $\tan\beta$ , no cancellation occurs due to the dominance of  $d_{u,d}^C$ .

Figure 20 displays our numerical estimates for the neutron EDM in the PQM when  $(\Phi_1, \Phi_2) = (0^\circ, 270^\circ)$ . In the upper frames, the thick lines are for the total EDM, and the thin solid, dashed, and dotted lines are for the contributions from the EDMs of the up  $d_u^E$ , down  $d_d^E$ , and the strange quark  $d_s^E$ , respectively. In the lower frame, we show the dominating contribution from the strange-quark EDM  $d_s^E$  (thick solid) together with its constituent contributions from the one-loop chargino  $\chi^\pm$  (thin solid), one-loop neutralino  $\chi^0$  (thin dashed), one-loop gluino  $\tilde{g}$  (thin dotted), and two-loop Higgs-mediated  $H^0$  (horizontal thin dashed-dotted) diagrams. We observe that there is a cancellation between the chargino, gluino, and Higgs contributions at  $\rho \sim 4$ .

The above examples demonstrate that the interpretation of neutron EDM measurements is subject to uncertainties in non-perturbative QCD, which are reflected in the specific models discussed.

In Fig. 21, we show the Mercury EDM. It shows barely any sensitivity to  $\Phi_1$  and  $\Phi_2$ , due to the dominance by the down-quark CEDM  $d_d^C$ , which is dominated by the one-loop gluino and two-loop Higgs-mediated diagrams, as shown in the lower frames. In the lower frames, the lines are the same as in the lower frames of Fig. 20.

Taking into account the uncertainty of the  $d^G$  contribution to the neutron EDM, and that involved in the Mercury EDM calculation, there is a possibility of evading all the three EDM constraints by taking  $(\Phi_1, \Phi_2) \sim (0^\circ, 90^\circ)$  and  $\rho \sim 4$  in the CPX scenario with  $\Phi_A = \Phi_3 = 90^\circ$  when  $\tan \beta = 5$ , if one calculates the neutron EDM using the QCD sum-rule approach.

Finally, in Fig. 22 we show the deuteron EDM. It is not sensitive to  $\Phi_1$  and  $\Phi_2$ , as it is dominated by the  $d^G$  and  $d_d^C$  contributions. At high  $\rho$ , the EDM is given by the sum of the  $d^G$  contribution and the contribution to  $d_d^C$  from the two-loop Higgs-mediated diagrams. In the lower frames, the thick line is for the total EDM and the thin solid, dashed, horizontal dashed, horizontal dash-dotted lines are for the contributions from  $d_{u,d}^E$ ,  $d_{u,d}^C$ ,  $C_{4f} \equiv C_{dd,sd,bd}$ , and  $d^G$ .

### 5.3 MCPMFV Scenario

In the MCPMFV scenario, in contrast to the trimixing and CPX scenarios, the soft SUSY-breaking parameters are specified at the gauge coupling unification (GUT) scale where the MFV condition is imposed [26,41]. This scenario has a total of 19 parameters, including 6 CP-violating phases and 13 real mass parameters. As a numerical example, in order to study the effects of the CP-violating phases on EDMs in this framework, we consider a CP-violating variant of a SPS1a-like [42] scenario:

$$\begin{aligned}
|M_{1,2,3}| &= 250 \text{ GeV}, \\
M_{H_u}^2 &= M_{H_d}^2 = \widetilde{M}_Q^2 = \widetilde{M}_U^2 = \widetilde{M}_D^2 = (100 \text{ GeV})^2, \\
\widetilde{M}_L^2 &= \widetilde{M}_E^2 = (200 \text{ GeV})^2, \\
|A_u| &= |A_d| = |A_e| = 100 \text{ GeV},
\end{aligned}
\tag{5.6}$$

with  $\tan \beta (M_{\text{SUSY}}) = 40$ . As for the CP-violating phases, we adopt the convention that  $\Phi_\mu = 0^\circ$ , and we vary separately the three phases of the gaugino mass parameters,  $\Phi_{1,2,3}$ , taking however vanishing  $A$ -term phases at the GUT scale:  $\Phi_{A_u}^{\text{GUT}} = \Phi_{A_d}^{\text{GUT}} = \Phi_{A_e}^{\text{GUT}} = 0^\circ$ . At the low-energy  $M_{\text{SUSY}}$  scale,  $A$ -term phases may be generated by the CP-violating phases of the gaugino mass parameters  $\Phi_{1,2,3}$ , even though we are taking real  $A$  terms at the GUT scale [26,43].

In the upper-left frame of Fig. 23, we show the Thallium EDM as a function of  $\Phi_2$  for several values of  $(\Phi_1, \Phi_3)$ :  $(0^\circ, 0^\circ)$  (solid),  $(0^\circ, 90^\circ)$  (dashed),  $(90^\circ, 0^\circ)$  (dotted), and  $(270^\circ, 0^\circ)$  (dash-dotted). We see the Thallium EDM is nearly independent of  $\Phi_3$ , cf., the two overlapping lines for  $(\Phi_1, \Phi_3) = (0^\circ, 0^\circ)$  and  $(0^\circ, 90^\circ)$ . This is because the Thallium EDM is dominated by the electron EDM. In the upper-right, lower-left, and lower-right frames, we show the electron EDM as a function of  $\Phi_2$  when  $(\Phi_1, \Phi_3) = (0^\circ, 90^\circ)$ ,  $(90^\circ, 0^\circ)$ , and  $(270^\circ, 90^\circ)$ , respectively. In the lower frames, we observe the neutralino contribution becomes less dependent on  $\Phi_2$  when  $\Phi_1 = 90^\circ$  and  $270^\circ$  and cancels the chargino one around  $\Phi_2 = \pm 4^\circ$ , resulting in the dips in the upper-left frame.

Figure 24 presents numerical estimates of the neutron EDM in the CQM as a function of  $\Phi_2$ . We observe that the EDM is nearly independent of  $\Phi_1$  and  $\Phi_3$ . This is because of the dominance of the down-quark EDM  $d_d^E$ , see the upper-right frame with  $(\Phi_1, \Phi_3) = (0^\circ, 0^\circ)$  in which the thin solid line for  $d_{u,d}^E$  is overlapped by the total thick line. The electric EDM of the down quark still plays a dominant role even when  $\Phi_3$  has a non-trivial value, because of an accidental cancellation between the contributions from the Weinberg operator  $d^G$  (dotted line) and the down-quark CEDM  $d_d^C$  (dashed line) as shown in the lower frames for  $(\Phi_1, \Phi_3) = (180^\circ, 90^\circ)$  (lower-left) and  $(180^\circ, 270^\circ)$  (lower-right). This accidental cancellation is lifted when the EDM is calculated using the QCD sum-rule approach, in which  $d^G$  and  $d_d^C$  contribute differently to the total EDM, see the lower-frames of Fig. 26.

In the upper-left frame of Fig. 25, we show the neutron EDM calculated in the PQM. We find that the neutron EDM is nearly independent of  $\Phi_3$ . The dominant contribution comes from the strange-quark EDM  $d_s^E$ , and we show it together with the constituent contributions in the other frames taking  $(\Phi_1, \Phi_3) = (0^\circ, 0^\circ)$  (upper-right),  $(0^\circ, 10^\circ)$  (lower-left), and  $(0^\circ, 90^\circ)$  (lower-right). The thick lines are for the total EDM and the thin solid, dashed, dotted, and dash-dotted lines are for the contributions from the one-loop chargino  $\chi^\pm$ , neutralino  $\chi^0$ , gluino  $\tilde{g}$ , and the two-loop Higgs-mediated  $H^0$  diagrams. When  $\Phi_3 = 0^\circ$ ,  $d_s^E$  is dominated by the chargino contribution, see the upper-right frame. As shown in the lower frames, the  $\Phi_3$  dependence of the strange-quark EDM is largely cancelled in the two main chargino and gluino contributions, explaining the  $\Phi_3$  independence of the neutron EDM shown in the upper-left frame. We note that this cancellation resulting in  $\Phi_3$  independence also occurs in the down-quark EDM  $d_d^E$ , see the thin solid  $d_{u,d}^E$  lines in the lower frames of Figs. 24 and 26.

Figure 26 gives the predicted values for the neutron EDM calculated using the QCD sum-rule approach. In the upper-right and lower frames, the lines are the same as in Fig. 24, but for different combinations of  $\Phi_1$  and  $\Phi_3$ . The non-trivial three-way cancellation among the contributions from  $d_{u,d}^E$ ,  $d_{u,d}^C$ , and  $d^G$  explains the dips in the upper-left frame when  $\Phi_3 = 20^\circ$  and  $340^\circ$ .

In Fig. 27, we present numerical estimates for the Mercury EDM. In the upper-right and lower frames, we see that the dominant contributions come from the electron EDM



$d_e^E$  and the down-quark CEDM  $d_d^C$ . The cancellation between them results in the dips in the upper-left frame. Note that  $\Phi_3 = 90^\circ$  could generate an EDM larger than the current experimental limit by a factor  $\sim 400$ , nearly independent of  $\Phi_2$ , see the nearly horizontal thin solid line in the upper-left frame.

Finally, Fig. 28 shows theoretical predictions for the deuteron EDM. The deuteron EDM is dominated by the down-quark CEDM  $d_d^C$ . The sub-leading contributions are from the Weinberg operator  $d^G$  and the down-quark EDM  $d_d^E$ . In the upper-right and lower frames, we show the constituent contributions to  $d_d^C$ . The chargino and neutralino contributions are dominant when  $\Phi_3 = 0$ , see the upper-right and lower-left frames. However, as  $\Phi_3$  grows, the gluino contribution rapidly increases, see the lower-right frame. We note that the dip around  $\Phi_2 = -20^\circ$  in the upper-left frame when  $(\Phi_1, \Phi_3) = (0^\circ, 10^\circ)$  is due to a cancellation between the  $d_d^C$  and  $d_d^E$  contributions.

## 6 Conclusions

We have performed a fully-fledged analysis of the Thallium, neutron, Mercury and deuteron EDMs within the general CP-violating framework of the MSSM. In our analysis, we have taken into account the complete set of one-loop graphs, the dominant Higgs-mediated Barr–Zee diagrams, the complete CP-odd dimension-six Weinberg operator and the Higgs-mediated four-fermion operators. Our study has also improved earlier calculations in two important aspects. First, it includes CP-violating Higgs-boson mixing effects and, secondly, it properly implements resummation effects due to threshold corrections to the Yukawa couplings of all up- and down-type quarks and charged leptons. Not only do these two effects turn out to be significant for the existing one- and two-loop EDMs, but also they give rise to additional higher-order contributions within the MSSM, such as the original Weinberg operator induced by  $t$  and  $b$  quarks with Higgs bosons in the loop. In addition, we have improved the Mercury EDM calculation by including the contribution due to the CP-odd triplet electron-nucleon interaction.

Having established the latest state-of-art theoretical framework as described above, we have then explored the EDM constraints on the CPX, trimixing and MCPMFV scenarios. Clearly, sufficiently small values of the CP-violating parameters survive the experimental upper limits on the EDMs. However, we have also found that larger values of the CP-violating parameters may be allowed exceptionally by accidental cancellations among the CP-violating contributions to the three measured EDMs, i.e.,  $d_{\text{Tl}}$ ,  $d_n$  and  $d_{\text{Hg}}$ , in all the above scenarios. In detail, the results of our analysis may be summarized as follows.

First, we studied the trimixing scenario. We have explored the impact on the three measured EDMs resulting from an hierarchy of the soft SUSY-breaking masses between the first two and third generations,  $\rho$ , and the CP phases  $\Phi_A = \Phi_{A_t} = \Phi_{A_b}$  and  $\Phi_3$  related to

the third generation  $A$ -terms and the gluino mass parameter, respectively. In the case of the Thallium EDM, large CP-violating phases are allowed due to the cancellation between the contributions from the CP-odd electron-nucleon interaction  $C_S$  and the two-loop Higgs-mediated electron EDM  $(d_e^E)^H$ . The two contributions are found to be independent of  $\rho$  in the scenario under consideration.

The neutron EDM has been computed within three different models and approaches: (i) the CQM, (ii) the PQM and (iii) a QCD sum-rule approach. In the CQM and QCD sum-rule approaches, the neutron EDM is dominated by the EDM and CEDM of the down quark  $d_d^{E,C}$  and the contribution from the dimension-six Weinberg operator  $d^G$ . In the QCD sum rule approach,  $d^G$  ( $d_d^C$ ) becomes less (more) important than in the CQM. The down-quark EDM and CEDM  $d_d^{E,C}$  are generated through the resummed threshold corrections at one loop by  $\Phi_3$  and the two-loop Higgs-mediated diagrams. The latter remains the same for large  $\rho$ . The  $d_d^{E,C}$  contributions depend on  $\rho$ , whilst the one due to  $d^G$  is  $\rho$ -independent. The bottom-down four-quark interaction  $C_{bd,db}$  is also independent of  $\rho$  and becomes significant in the QCD sum rule approach. Interestingly, cancellations may occur among  $d_d^{E,C}$ ,  $d^G$  and  $C_{bd,db}$  more easily when  $\rho$  is large. In the PQM, on the other hand, the neutron EDM is dominated by the strange-quark EDM  $d_s^E$ , which is generated by one-loop threshold corrections at the one-loop level and by the two-loop Barr–Zee graphs. Again, cancellations occur between the two contributions when  $\rho$  is large. All the three different hadronic models or approaches for computing the neutron EDM give comparable estimates. However, there are significant differences of detail, implying that the interpretation of neutron EDM measurements is model-dependent.

As far as the Mercury EDM in the trimixing scenario is concerned, the  $d$ -quark CEDM  $d_d^C$  was found to be dominant for small values of  $\rho$ , whilst it gets suppressed for large values of  $\rho$ . In addition, the  $\rho$ -independent contributions from  $C_S$ , the four-quark operators  $C_{dd,sd,bd}$ , the CP-odd singlet and triplet electron-nucleon interactions,  $C_P$  and  $C'_P$ , and the electron EDM become all relevant, leading to an interesting cancellation pattern.

In the CPX scenario, we have analyzed the dependence of EDMs on the hierarchy factor  $\rho$ , the CP phases  $\Phi_A = \Phi_{A_t} = \Phi_{A_b}$  and  $\Phi_{1,2,3}$ , for a relatively low and large value of  $\tan\beta$ :  $\tan\beta = 5$  and  $50$ . In the absence of any mass hierarchy between the first two and third generation of squarks and sleptons, i.e.,  $\rho = 1$ , and for  $\Phi_1 = \Phi_2 = 0^\circ$ , we have found that the Thallium EDM is dominated by the electron EDM, whilst  $C_S$  starts becoming important only for  $\tan\beta \gtrsim 10$ . Correspondingly, the neutron EDM receives the largest contribution from  $d_d^{E,C}$  and  $d^G$  in the CQM and the QCD sum-rule approach. The main contributions to  $d_d^{E,C}$  come from the one-loop gluino diagrams and the two-loop Higgs-mediated diagrams. The latter become important when  $\tan\beta$  is large. In the PQM, the neutron EDM mainly results from  $d_s^E$ . Finally, the Mercury EDM receives its biggest contribution from  $d_d^C$ , whilst the contribution due to  $d_e^E$  becomes important only for large  $\tan\beta$ .



Varying  $\rho$  and the CP phases  $\Phi_1$  and  $\Phi_2$ , we have found that several cancellations can occur within the CPX scenario. Specifically, one-loop neutralino and chargino effects and the two-loop Barr–Zee graphs may add up destructively and suppress the electron EDM  $d_e^E$ . Likewise, cancellations among the one-loop chargino and gluino graphs and two-loop Higgs-mediated diagrams lead to suppressed strange- and down-quark EDMs  $d_{d,s}^E$  and to an equally small down-quark CEDM  $d_d^C$ . As a consequence of the suppressed  $d_e^E$ ,  $d_s^E$  and  $d_d^C$ , the Thallium, neutron (in the PQM) and Mercury EDMs were all found to come out well below their experimental limits. A similar result has been obtained in the CQM or QCD sum-rule approach, where the Weinberg operator  $d^G$  plays an important role. In particular, we have demonstrated explicitly the possibility of evading all the three EDM constraints from  $d_{\text{Tl}}$ ,  $d_n$  and  $d_{\text{Hg}}$  in the CPX scenario with  $\Phi_A \sim \Phi_3 \sim 90^\circ$ , if one assumes that  $(\Phi_1, \Phi_2) \sim (0^\circ, 90^\circ)$  and  $\rho \sim 4$  when  $\tan \beta = 5$ , provided  $d_n$  is calculated using QCD sum-rule techniques. Finally, the deuteron EDM [4, 5], whose size crucially depends on  $d^G$  and  $d_d^C$ , can constrain dramatically the CP-violating phases by a factor of about 100 [6].

A third benchmark scenario of the MSSM that has been analyzed was the MCPMFV scenario. For definiteness, we have used SPS1a-like input parameters given at the GUT scale, for which  $\Phi_{A_u}^{\text{GUT}} = \Phi_{A_u}^{\text{GUT}} = \Phi_{A_e}^{\text{GUT}} = 0^\circ$  and  $\tan \beta = 40$ . This choice results in a relatively light SUSY spectrum, where phases for the  $A$ -terms are generated by RG running down to the electroweak scale. Within this particular MCPMFV scenario, we have studied the implications of the CP-violating phases  $\Phi_1$ ,  $\Phi_2$  and  $\Phi_3$  for the three EDMs  $d_{\text{Tl}}$ ,  $d_n$  and  $d_{\text{Hg}}$ . The Thallium EDM was found to be nearly independent of  $\Phi_3$ , since the electron EDM  $d_e^E$  turns out to be the dominant contribution. Moreover, we have noticed that one-loop chargino and neutralino effects may cancel each other in  $d_e^E$ . The neutron EDM in the CQM was also found to be nearly independent of  $\Phi_1$  and  $\Phi_3$ , due to an accidental cancellation between the Weinberg operator  $d^G$  and the down-quark CEDM  $d_d^C$ . Unlike in the CQM, this cancellation is no longer present when the QCD sum rule approach is used, leading to a strong dependence on  $\Phi_3$ . In the PQM, like in the CQM, the neutron EDM does not depend strongly on  $\Phi_3$ , since there is a cancellation between the chargino and gluino effects on the dominant strange-quark EDM  $d_s^E$ . The Mercury EDM  $d_{\text{Hg}}$  in the MCPMFV scenario was found to receive its biggest contribution from the electron EDM  $d_e^E$  and the down-quark CEDM  $d_d^C$ . A non-vanishing gluino phase  $\Phi_3$  can drive  $d_{\text{Hg}}$  to quite large values that could easily exceed the current experimental limit. Finally, the leading effect on the deuteron EDM comes from  $d_d^C$ , whilst  $d^G$  and  $d_d^E$  remain sub-leading. Since the deuteron EDM is expected to be a factor  $\sim 100$  more sensitive than  $d_{\text{Hg}}$  [4, 5], it will lead to much tighter constraints on the CP-violating phases [6].

Our detailed study has shown that the three measured EDMs provide correlated constraints on the 6 CP-violating phases in MCPMFV scenario, leaving open the possibility of relatively large contributions to other CP-violating observables. In particular, the deuteron EDM [4, 5] will probe the unconstrained CP phases of the MCPMFV scenario.

The analytic expressions for the EDMs are implemented in an updated version of the code `CPsuperH2.0`. This new feature of `CPsuperH2.0` will be particularly valuable in future explorations for possible new-physics phenomena in the  $K$ - and  $B$ -meson systems.

## **Acknowledgements**

We thank Yannis Semertzidis for valuable information on the deuteron EDM. The work of J.S.L. was supported in part by the National Science Council of Taiwan, R.O.C. under Grant No. NSC 96-2811-M-008-068. The work of A.P. was supported in part by the STFC research grant: PP/D000157/1.

## A Calculation of $C_S$

In this appendix we calculate the coefficient  $C_S$ . Our starting point is the interaction Lagrangians:

$$\mathcal{L}_{C_S} = C_S \bar{e} i \gamma_5 e \bar{N} N, \quad \mathcal{L}_{4f} = C_{qe} \bar{q} q \bar{e} i \gamma_5 e. \quad (\text{A.1})$$

Given the relation  $\langle N | \mathcal{L}_{C_S} | N \rangle = \langle N | \mathcal{L}_{4f} | N \rangle$ , one may identify

$$[(C_S)^{4f}]_q = C_{qe} \frac{\langle N | \bar{q} q | N \rangle}{\langle N | \bar{N} N | N \rangle}, \quad (\text{A.2})$$

where  $q$  could be a light quark, e.g.  $u, d$ , or a heavy one such as the  $b$  quark.

We first derive the light-quark contribution to  $(C_S)^{4f}$ ,  $[(C_S)^{4f}]_{q=u,d}$ . To this end, we need to know  $\langle N | \bar{u} u | N \rangle$  and  $\langle N | \bar{d} d | N \rangle$ . Using the relation [17]

$$(m_u + m_d) \langle N | \bar{u} u + \bar{d} d | N \rangle \simeq 90 \text{ MeV} \langle N | \bar{N} N | N \rangle, \quad (\text{A.3})$$

and assuming that the triplet contribution vanishes, i.e.

$$\langle N | \bar{u} u - \bar{d} d | N \rangle = 0, \quad (\text{A.4})$$

we obtain

$$\frac{\langle N | \bar{u} u | N \rangle}{\langle N | \bar{N} N | N \rangle} = \frac{\langle N | \bar{d} d | N \rangle}{\langle N | \bar{N} N | N \rangle} \simeq \frac{1}{2} \frac{90 \text{ MeV}}{(m_u + m_d)} \simeq \frac{29 \text{ MeV}}{m_d} = \left( \frac{m_u}{m_d} \right) \frac{29 \text{ MeV}}{m_u}, \quad (\text{A.5})$$

with  $m_u/m_d = 0.55$ . Putting everything together, we find that

$$\begin{aligned} [(C_S)^{4f}]_u &\simeq C_{ue} \left( \frac{m_u}{m_d} \right) \frac{29 \text{ MeV}}{m_u} \simeq C_{ue} \frac{16 \text{ MeV}}{m_u}, \\ [(C_S)^{4f}]_d &\simeq C_{de} \frac{29 \text{ MeV}}{m_d}. \end{aligned} \quad (\text{A.6})$$

The very last expression was used to obtain the first term in Eq. (4.4).

As for the heavy-quark contribution to  $C_S$ , there are two approaches that can be considered. We illustrate these by taking the  $b$ -quark as an example. The first way is to include the heavy-quark contribution directly to  $(C_S)^{4f}$  [17], i.e.

$$[(C_S)^{4f}]_b = C_{be} \frac{66 \text{ MeV} (1 - 0.25\kappa)}{m_b}. \quad (\text{A.7})$$

The second method uses the QCD trace anomaly and the heavy quark is integrated out in the gluon-gluon-Higgs vertex  $(C_S)^g$  [cf. (3.15)]:

$$[(C_S)^g]_b = (0.1 \text{ GeV}) \frac{m_e}{v^2} \sum_{i=1}^3 \frac{[g_{H_i gg}^S]_b g_{H_i \bar{e} e}^P}{M_{H_i}^2} = C_{be} \frac{2 (0.1 \text{ GeV})}{3 m_b}, \quad (\text{A.8})$$

where we made use of the relation  $[g_{H_i gg}^S]_b = 2/3 g_{H_i \bar{b} b}^S$  [cf. (3.16) and (3.12)]. Notice that, apart from the  $\kappa$ -dependent term, the two approaches are equivalent to each other.

## B Calculation of $C_P$ and $C'_P$

Here we compute the iso-scalar and iso-triplet coefficients  $C_P$  and  $C'_P$  that are relevant in the determination of the Mercury EDM. To this end, we start considering the interaction Lagrangians,

$$\mathcal{L}_{C_P} = C_P \bar{e} e \bar{N} i \gamma_5 N + C'_P \bar{e} e \bar{N} i \gamma_5 \tau_3 N, \quad \mathcal{L}_{4f} = C_{eq} \bar{e} e \bar{q} i \gamma_5 q. \quad (\text{B.1})$$

Imposing the relation  $\langle N | \mathcal{L}_{C_P} | N \rangle = \langle N | \mathcal{L}_{4f} | N \rangle$ , we may project out the iso-scalar and iso-triplet contributions as follows:

$$\left[ (C_P)^{4f} \right]_q = C_{eq} \frac{\langle N | \bar{q} i \gamma_5 q | N \rangle}{\langle N | \bar{N} i \gamma_5 N | N \rangle}, \quad \left[ (C'_P)^{4f} \right]_q = C_{eq} \frac{\langle N | \bar{q} i \gamma_5 q | N \rangle}{\langle N | \bar{N} i \gamma_5 \tau_3 N | N \rangle}. \quad (\text{B.2})$$

As in Appendix A, we need to consider the light- and heavy-quark contributions separately. Our approach closely follows [44]. Thus, taking into account all the relations that follow from isospin invariance, i.e.

$$\begin{aligned} \langle N | m_u \bar{u} i \gamma_5 u + m_d \bar{d} i \gamma_5 d | N \rangle &= \frac{m_u - m_d}{m_u + m_d} m_N (-g_A) \langle N | \bar{N} i \gamma_5 \tau_3 N | N \rangle, \\ \langle N | \bar{u} i \gamma_5 u | N \rangle &= -\langle N | \bar{d} i \gamma_5 d | N \rangle, \end{aligned} \quad (\text{B.3})$$

we obtain

$$\begin{aligned} m_u \langle N | \bar{u} i \gamma_5 u | N \rangle &= m_N (-g_A) \frac{m_u}{m_u + m_d} \langle N | \bar{N} i \gamma_5 \tau_3 N | N \rangle, \\ m_d \langle N | \bar{d} i \gamma_5 d | N \rangle &= -m_N (-g_A) \frac{m_d}{m_u + m_d} \langle N | \bar{N} i \gamma_5 \tau_3 N | N \rangle, \end{aligned} \quad (\text{B.4})$$

where  $(-g_A) = 1.25$  is the axial nucleon form factor. From all the above relations, it is then not difficult to derive that

$$\begin{aligned} \left[ (C'_P)^{4f} \right]_u &= \frac{C_{eu}}{m_u} m_N (-g_A) \frac{m_u}{m_u + m_d} \simeq C_{eu} \frac{444 \text{ MeV}}{m_u}, \\ \left[ (C'_P)^{4f} \right]_d &= -\frac{C_{ed}}{m_d} m_N (-g_A) \frac{m_d}{m_u + m_d} \simeq -C_{ed} \frac{806 \text{ MeV}}{m_d}, \end{aligned} \quad (\text{B.5})$$

where we assume that  $m_N = 1 \text{ GeV}$  and  $m_u/m_d = 0.55$ . Observe that the light quarks do not contribute to the singlet coefficient  $(C_P)^{4f}$ .

To calculate the heavy-quark contributions to  $C_P$  and  $C'_P$ , we first consider the chiral anomaly relations [44]:

$$\begin{aligned} \langle N | \partial^\mu J_\mu^5 | N \rangle &= 2 \langle N | m_u \bar{u} i \gamma_5 u + m_d \bar{d} i \gamma_5 d | N \rangle \\ &\quad + 2 \sum_{q=c,s,t,b} \langle N | m_q \bar{q} i \gamma_5 q | N \rangle + 6 \langle N | \frac{\alpha_s}{8\pi} G \tilde{G} | N \rangle, \\ \langle N | \partial^\mu J_\mu^5 | N \rangle &= \left( -g_A^{(0)} \right) 2 m_N \langle N | \bar{N} i \gamma_5 N | N \rangle, \end{aligned} \quad (\text{B.6})$$

where  $n_l = 2$  and  $n_h = 4$  are assumed to be the numbers of the light and heavy quarks, respectively, and  $g_A^{(0)} = (3/5)g_A$  in the relativistic quark model. After integrating out the heavy quarks by employing the relation

$$\langle N|m_q \bar{q}i\gamma_5 q|N\rangle|_{q=c,s,t,b} = -\frac{1}{2} \langle N|\frac{\alpha_s}{8\pi}G\tilde{G}|N\rangle, \quad (\text{B.7})$$

we get

$$\langle N|m_u \bar{u}i\gamma_5 u + m_d \bar{d}i\gamma_5 d|N\rangle + \langle N|\frac{\alpha_s}{8\pi}G\tilde{G}|N\rangle = (-g_A^{(0)}) m_N \langle N|\bar{N}i\gamma_5 N|N\rangle. \quad (\text{B.8})$$

From (B.3) and (B.7), we finally obtain

$$\begin{aligned} \langle N|m_q \bar{q}i\gamma_5 q|N\rangle &= -\frac{1}{2} m_N (-g_A^{(0)}) \langle N|\bar{N}i\gamma_5 N|N\rangle \\ &\quad + \frac{1}{2} \frac{m_u - m_d}{m_u + m_d} m_N (-g_A) \langle N|\bar{N}i\gamma_5 \tau_3 N|N\rangle \end{aligned} \quad (\text{B.9})$$

for each of the heavy quarks  $q = c, s, t, b$ . The first and second terms in (B.9) give the heavy-quark contributions to  $(C_P)^{4f}$  and  $(C'_P)^{4f}$ , respectively. More explicitly, we have

$$\begin{aligned} [(C_P)^{4f}]_{q=c,s,t,b} &= \frac{C_{eq}}{m_q} \left[ -\frac{1}{2} m_N (-g_A^{(0)}) \right] \simeq -C_{eq} \frac{375 \text{ MeV}}{m_q}, \\ [(C'_P)^{4f}]_{q=c,s,t,b} &= \frac{C_{eq}}{m_q} \left[ \frac{1}{2} \frac{m_u - m_d}{m_u + m_d} m_N (-g_A) \right] \simeq -C_{eq} \frac{181 \text{ MeV}}{m_q}, \end{aligned} \quad (\text{B.10})$$

where  $m_N = 1 \text{ GeV}$  and  $m_u/m_d = 0.55$  were used in our numerical estimates.

## C CPsuperH2.0 Interface

- Input: For the complex  $A$  parameters of first two generations, part of auxiliary array CAUX\_H is used as

$$\begin{aligned} A_e &= \text{CAUX\_H}(995), \\ A_u &= \text{CAUX\_H}(996), \quad A_c = \text{CAUX\_H}(997), \\ A_d &= \text{CAUX\_H}(998), \quad A_s = \text{CAUX\_H}(999). \end{aligned} \quad (\text{C.1})$$

- Output: For output, part of auxiliary array RAUX\_H is used.

– The electron EDM in units of cm:

$$\text{RAUX\_H}(200) = d_e^E/e = (d_e^E/e)^{\tilde{\chi}^\pm} + (d_e^E/e)^{\tilde{\chi}^0} + (d_e^E/e)^{\tilde{g}} + (d_e^E/e)^H, \quad (\text{C.2})$$

where the constituent contributions are

$$\begin{aligned} \text{RAUX\_H}(201) &= (d_e^E/e)^{\tilde{\chi}^\pm}, \quad \text{RAUX\_H}(202) = (d_e^E/e)^{\tilde{\chi}^0} \\ \text{RAUX\_H}(203) &= (d_e^E/e)^{\tilde{g}}, \quad \text{RAUX\_H}(204) = (d_e^E/e)^H. \end{aligned}$$

– The electric EDM of the  $u$  quark in units of cm:

$$\text{RAUX\_H}(210) = d_u^E/e = (d_u^E/e)\tilde{\chi}^\pm + (d_u^E/e)\tilde{\chi}^0 + (d_u^E/e)\tilde{g} + (d_u^E/e)^H, \quad (\text{C.3})$$

where the constituent contributions are

$$\begin{aligned} \text{RAUX\_H}(211) &= (d_u^E/e)\tilde{\chi}^\pm, & \text{RAUX\_H}(212) &= (d_u^E/e)\tilde{\chi}^0 \\ \text{RAUX\_H}(213) &= (d_u^E/e)\tilde{g}, & \text{RAUX\_H}(214) &= (d_u^E/e)^H. \end{aligned} \quad (\text{C.4})$$

– The electric EDM of the  $d$  quark in units of cm:

$$\text{RAUX\_H}(220) = d_d^E/e = (d_d^E/e)\tilde{\chi}^\pm + (d_d^E/e)\tilde{\chi}^0 + (d_d^E/e)\tilde{g} + (d_d^E/e)^H, \quad (\text{C.5})$$

where the constituent contributions are

$$\begin{aligned} \text{RAUX\_H}(221) &= (d_d^E/e)\tilde{\chi}^\pm, & \text{RAUX\_H}(222) &= (d_d^E/e)\tilde{\chi}^0 \\ \text{RAUX\_H}(223) &= (d_d^E/e)\tilde{g}, & \text{RAUX\_H}(224) &= (d_d^E/e)^H. \end{aligned} \quad (\text{C.6})$$

– The electric EDM of the  $s$  quark in units of cm:

$$\text{RAUX\_H}(230) = d_s^E/e = (d_s^E/e)\tilde{\chi}^\pm + (d_s^E/e)\tilde{\chi}^0 + (d_s^E/e)\tilde{g} + (d_s^E/e)^H, \quad (\text{C.7})$$

where the constituent contributions are

$$\begin{aligned} \text{RAUX\_H}(231) &= (d_s^E/e)\tilde{\chi}^\pm, & \text{RAUX\_H}(232) &= (d_s^E/e)\tilde{\chi}^0 \\ \text{RAUX\_H}(233) &= (d_s^E/e)\tilde{g}, & \text{RAUX\_H}(234) &= (d_s^E/e)^H. \end{aligned} \quad (\text{C.8})$$

– The chromo-electric EDM of the  $u$  quark in units of cm:

$$\text{RAUX\_H}(240) = d_u^C = (d_u^C)\tilde{\chi}^\pm + (d_u^C)\tilde{\chi}^0 + (d_u^C)\tilde{g} + (d_u^C)^H, \quad (\text{C.9})$$

where the constituent contributions are

$$\begin{aligned} \text{RAUX\_H}(241) &= (d_u^C)\tilde{\chi}^\pm, & \text{RAUX\_H}(242) &= (d_u^C)\tilde{\chi}^0 \\ \text{RAUX\_H}(243) &= (d_u^C)\tilde{g}, & \text{RAUX\_H}(244) &= (d_u^C)^H. \end{aligned} \quad (\text{C.10})$$

– The chromo-electric EDM of the  $d$  quark in units of cm:

$$\text{RAUX\_H}(250) = d_d^C = (d_d^C)\tilde{\chi}^\pm + (d_d^C)\tilde{\chi}^0 + (d_d^C)\tilde{g} + (d_d^C)^H, \quad (\text{C.11})$$

where the constituent contributions are

$$\begin{aligned} \text{RAUX\_H}(251) &= (d_d^C)\tilde{\chi}^\pm, & \text{RAUX\_H}(252) &= (d_d^C)\tilde{\chi}^0 \\ \text{RAUX\_H}(253) &= (d_d^C)\tilde{g}, & \text{RAUX\_H}(254) &= (d_d^C)^H. \end{aligned} \quad (\text{C.12})$$

- The purely gluonic dimension-six Weinberg operator in units of cm/GeV:

$$\text{RAUX\_H}(260) = d^G = (d^G)^H + (d^G)^{\tilde{g}}, \quad (\text{C.13})$$

where the constituent contributions are

$$\text{RAUX\_H}(261) = (d^G)^H, \quad \text{RAUX\_H}(262) = (d^G)^{\tilde{g}}. \quad (\text{C.14})$$

In the distributed version, Eq. (3.7) is used to evaluate the function  $H(z_1, z_2, z_q)$  for  $(d^G)^{\tilde{g}}$ . For a full calculation, especially when  $z_q \gtrsim 0.1$ , the user should provide a dedicated routine, see Fig. 3.

- $C_S$ ,  $C_P$ , and,  $C'_P$  in units of cm/GeV:

$$\text{RAUX\_H}(270) = C_S, \quad \text{RAUX\_H}(271) = C_P, \quad \text{RAUX\_H}(272) = C'_P. \quad (\text{C.15})$$

- The coefficients of four-fermion operators in units of cm/GeV<sup>2</sup>:

$$\begin{aligned} \text{RAUX\_H}(280) &= C_{de}/m_d, & \text{RAUX\_H}(281) &= C_{se}/m_s, \\ \text{RAUX\_H}(282) &= C_{ed}/m_d, & \text{RAUX\_H}(283) &= C_{es}/m_s, & \text{RAUX\_H}(284) &= C_{eb}/m_b, \\ \text{RAUX\_H}(285) &= C_{ec}/m_c, & \text{RAUX\_H}(286) &= C_{et}/m_t, \\ \text{RAUX\_H}(287) &= C_{dd}/m_d, & \text{RAUX\_H}(288) &= C_{sd}/m_s, \\ \text{RAUX\_H}(289) &= C_{bd}/m_b, & \text{RAUX\_H}(290) &= C_{db}/m_b. \end{aligned} \quad (\text{C.16})$$

- The Thallium EDM in units of  $e$  cm:

$$\text{RAUX\_H}(300) = d_{\text{Tl}} = d_{\text{Tl}}(d_e^E) + d_{\text{Tl}}(C_S) \quad (\text{C.17})$$

where the constituent contributions are

$$\text{RAUX\_H}(301) = d_{\text{Tl}}(d_e^E), \quad \text{RAUX\_H}(302) = d_{\text{Tl}}(C_S).$$

- The neutron EDM in units of  $e$  cm:

- \* Chiral quark model:

$$\text{RAUX\_H}(310) = d_n = d_n(d_{u,d}^E) + d_n(d_{u,d}^C) + d_n(d^G) \quad (\text{C.18})$$

where the constituent contributions are

$$\text{RAUX\_H}(311) = d_n(d_{u,d}^E), \quad \text{RAUX\_H}(312) = d_n(d_{u,d}^C). \quad \text{RAUX\_H}(313) = d_n(d^G).$$

- \* Parton quark model:

$$\text{RAUX\_H}(320) = d_n = d_n(d_u^E) + d_n(d_d^E) + d_n(d_s^E) \quad (\text{C.19})$$

where the constituent contributions are

$$\text{RAUX\_H}(321) = d_n(d_u^E), \quad \text{RAUX\_H}(322) = d_n(d_d^E). \quad \text{RAUX\_H}(323) = d_n(d_s^E).$$

\* QCD sum rule approach:

$$\text{RAUX\_H(330)} = d_n = d_n(d_{u,d}^E) + d_n(d_{u,d}^C) + d_n(d^G) + d_n(C_{bd,db}) \quad (\text{C.20})$$

where the constituent contributions are

$$\begin{aligned} \text{RAUX\_H(331)} &= d_n(d_{u,d}^E), & \text{RAUX\_H(332)} &= d_n(d_{u,d}^C), \\ \text{RAUX\_H(332)} &= d_n(d^G), & \text{RAUX\_H(334)} &= d_n(C_{bd,db}). \end{aligned}$$

– The Mercury EDM in units of  $e$  cm:

$$\text{RAUX\_H(340)} = d_{\text{Hg}} = d_{\text{Hg}}(d_e^E) + d_{\text{Hg}}(d_{u,d}^C) + d_{\text{Hg}}(C_{4f}) + d_{\text{Hg}}(C_S) + d_{\text{Hg}}(C_P^{(\prime)}) \quad (\text{C.21})$$

where the constituent contributions are

$$\begin{aligned} \text{RAUX\_H(341)} &= d_{\text{Hg}}(d_e^E), & \text{RAUX\_H(342)} &= d_{\text{Hg}}(d_{u,d}^C), \\ \text{RAUX\_H(343)} &= d_{\text{Hg}}(C_{4f}), & \text{RAUX\_H(344)} &= d_{\text{Hg}}(C_S). & \text{RAUX\_H(345)} &= d_{\text{Hg}}(C_P^{(\prime)}). \end{aligned}$$

– The deuteron EDM in units of  $e$  cm:

$$\text{RAUX\_H(350)} = d_D = d_D(d_{u,d}^E) + d_D(d_{u,d}^C) + d_n(C_{4f}) + d_n(d^G) \quad (\text{C.22})$$

where the constituent contributions are

$$\begin{aligned} \text{RAUX\_H(351)} &= d_D(d_{u,d}^E), & \text{RAUX\_H(352)} &= d_D(d_{u,d}^C), \\ \text{RAUX\_H(353)} &= d_D(C_{4f}), & \text{RAUX\_H(354)} &= d_D(d^G). \end{aligned}$$

- IFLAG\_H(18)=1 is used to print out the Thallium, neutron, Mercury and deuteron EDMs. Using the `run` shell-script file distributed, the sample output obtained with  $\Phi_{A_e} = \Phi_{A_\tau}$ ,  $\Phi_{A_u} = \Phi_{A_c} = \Phi_{A_t}$ , and  $\Phi_{A_d} = \Phi_{A_s} = \Phi_{A_b}$ , and the hierarchy factor  $\rho_{\tilde{Q}} = \rho_{\tilde{U}} = \rho_{\tilde{D}} = \rho_{\tilde{L}} = \rho_{\tilde{E}} = 1$  is

```
-----
Thallium EDM in units of [e cm]: d^Tl/[e cm]
-----
d^Tl/(e cm) [Total]= -.9371E-24
Each contribution to d^Tl from
      [d^E_e]= -.9082E-24
      [C_S ]= -.2890E-25
-----

Neutron EDM in units of [e cm]: d^n/[e cm]
-----
```



(1) Chiral Quark Model

$$d^n/(e \text{ cm}) \quad [\text{Total}] = -.4196\text{E-}23$$

Each contribution to  $d^n$  from

$$[d^E_u \ \& \ d^E_d] = -.3994\text{E-}23$$

$$[d^C_u \ \& \ d^C_d] = -.2066\text{E-}23$$

$$[\text{Weinberg-6D}] = 0.1863\text{E-}23$$

(2) Parton Quark Model

$$d^n/(e \text{ cm}) \quad [\text{Total}] = 0.1278\text{E-}22$$

Each contribution to  $d^n$  from

$$[d^E_u \quad \quad \quad ] = -.6868\text{E-}25$$

$$[d^E_d \quad \quad \quad ] = -.2209\text{E-}23$$

$$[d^E_s \quad \quad \quad ] = 0.1506\text{E-}22$$

(3) QCD sum rule technique

$$d^n/(e \text{ cm}) \quad [\text{Total}] = -.7240\text{E-}23$$

Each contribution to  $d^n$  from

$$[d^E_u \ \& \ d^E_d] = -.2741\text{E-}23$$

$$[d^C_u \ \& \ d^C_d] = -.5483\text{E-}23$$

$$[\text{Weinberg-6D}] = 0.9836\text{E-}24$$

$$[C_{bd} \ \& \ C_{db}] = 0.1749\text{E-}28$$

---

Mercury EDM in units of  $[e \text{ cm}]$ :  $d^{\text{Hg}}/[e \text{ cm}]$

---

$$d^{\text{Hg}}/(e \text{ cm}) \quad [\text{Total}] = 0.3383\text{E-}25$$

Each contribution to  $d^{\text{Hg}}$  from

$$[d^E_e \quad \quad \quad ] = 0.1553\text{E-}28$$

$$[d^C_u \ \& \ d^C_d] = 0.3381\text{E-}25$$

$$[C_{4f} \quad \quad \quad ] = -.1094\text{E-}29$$

$$[C_S \quad \quad \quad ] = 0.2348\text{E-}29$$

$$[C_P \ \& \ C_{P^{\text{pr}}}] = 0.2229\text{E-}29$$

---

Deuteron EDM in units of  $[e \text{ cm}]$ :  $d^{\text{D}}/[e \text{ cm}]$

---

$$d^{\text{D}}/(e \text{ cm}) \quad [\text{Total}] = -.2598\text{E-}22$$

Each contribution to  $d^{\text{D}}$  from

$$[d^E_u \ \& \ d^E_d] = -.9236\text{E-}24$$

$$[d^C_u \ \& \ d^C_d] = -.2604\text{E-}22$$

$$[C_{4f} \quad \quad \quad ] = 0.7811\text{E-}27$$

$$[\text{Weinberg-6D}] = 0.9836\text{E-}24$$

- IFLAG\_H(18)=2 is used to print out the EDMs of the electron and the up, down, and strange quarks, the CEDMs of the up, down, and strange quarks, etc.

The Electric EDMs of particles in cm: e, u, d, s:

```

-----
d^E_e/e[Total]: 0.1553E-26
d^E_u/e[Total]: 0.8836E-25
d^E_d/e[Total]: -.1936E-23
d^E_s/e[Total]: -.4355E-22
d^E_e/e[C,N,G1,H]: 0.0000E+00 -.2833E-26 0.0000E+00 0.4386E-26
d^E_u/e[C,N,G1,H]: 0.4467E-28 0.1755E-26 0.8717E-25 -.6115E-27
d^E_d/e[C,N,G1,H]: 0.9825E-25 -.3481E-26 -.2042E-23 0.1170E-25
d^E_s/e[C,N,G1,H]: 0.2211E-23 -.7832E-25 -.4595E-22 0.2631E-24
-----

```

The Chromo-Electric EDMs of particles in cm: u, d:

```

-----
d^C_u [Total]: -.1208E-24
d^C_d [Total]: -.5756E-23
d^C_u [C,N,G1,H]: -.8956E-28 0.3073E-26 -.1180E-24 -.5825E-26
d^C_d [C,N,G1,H]: 0.1626E-25 0.1218E-25 -.5554E-23 -.2306E-24
-----

```

Purely-gluonic D-6 Weinberg operator in cm/GeV:

```

-----
d^G [Total]: 0.5786E-23
d^G[Higgs,Gluino]: 0.2046E-26 0.5784E-23
-----

```

Four-fermion couplings needed for EDMs in cm/GeV<sup>2</sup>:

```

-----
C4_de/m_d: -.2432E-26
C4_se/m_s: -.2432E-26
C4_ed/m_d: -.2432E-26
C4_es/m_s: -.2432E-26
C4_eb/m_b: -.1547E-25
C4_ec/m_c: -.9727E-28
C4_et/m_t: 0.3965E-27
C4_dd/m_d: -.3565E-25
C4_sd/m_s: -.3565E-25
-----

```

C4\_bd/m\_b: 0.1769E-24  
C4\_db/m\_b: -.2269E-24

---

C\_S, C\_P, and C\_P^prime in cm/GeV and in 1/GeV^2:

---

C_S	:	0.6710E-27	0.3400E-13
C_P	:	0.6602E-26	0.3346E-12
C_P^prime:		0.5147E-26	0.2608E-12

---

## References

- [1] B. C. Regan, E. D. Commins, C. J. Schmidt and D. DeMille, Phys. Rev. Lett. **88** (2002) 071805.
- [2] C. A. Baker *et al.*, Phys. Rev. Lett. **97** (2006) 131801.
- [3] M. V. Romalis, W. C. Griffith and E. N. Fortson, Phys. Rev. Lett. **86** (2001) 2505.
- [4] Y. K. Semertzidis *et al.* [EDM Collaboration], AIP Conf. Proc. **698** (2004) 200.
- [5] Y. F. Orlov, W. M. Morse and Y. K. Semertzidis, Phys. Rev. Lett. **96** (2006) 214802; also see [http://www.bnl.gov/edm/deuteron-proposal\\_080423\\_final.pdf](http://www.bnl.gov/edm/deuteron-proposal_080423_final.pdf).
- [6] O. Lebedev, K. A. Olive, M. Pospelov and A. Ritz, Phys. Rev. D **70** (2004) 016003.
- [7] H. P. Nilles, Phys. Rept. **110** (1984) 1; H. E. Haber and G. L. Kane, Phys. Rept. **117** (1985) 75.
- [8] For example, see,  
M. S. Carena, J. M. Moreno, M. Quiros, M. Seco and C. E. M. Wagner, Nucl. Phys. B **599** (2001) 158;  
M. S. Carena, M. Quiros, M. Seco and C. E. M. Wagner, Nucl. Phys. B **650** (2003) 24;  
T. Konstandin, T. Prokopec, M. G. Schmidt and M. Seco, Nucl. Phys. B **738** (2006) 1;  
D. J. H. Chung, B. Garbrecht, M. J. Ramsey-Musolf and S. Tulin, arXiv:0808.1144 [hep-ph].
- [9] For a recent review, see,  
T. Ibrahim and P. Nath, Rev. Mod. Phys. **80** (2008) 577.
- [10] J. Ellis, S. Ferrara and D. V. Nanopoulos, Phys. Lett. B **114** (1982) 231;  
W. Buchmüller and D. Wyler, Phys. Lett. B **121** (1983) 321;  
J. Polchinski and M. Wise, Phys. Lett. B **125** (1983) 393;  
F. del Aguila, M. Gavela, J. Grifols and A. Mendez, Phys. Lett. B **126** (1983) 71;  
D. V. Nanopoulos and M. Srednicki, Phys. Lett. B **128** (1983) 61;  
M. Dugan, B. Grinstein and L. Hall, Nucl. Phys. B **255** (1985) 413;  
P. Nath, Phys. Rev. Lett. **66** (1991) 2565;  
Y. Kizukuri and N. Oshimo, Phys. Rev. D **46** (1992) 3025;  
W. Fischler, S. Paban and S. D. Thomas, Phys. Lett. B **289** (1992) 373;  
R. Garisto and J.D. Wells, Phys. Rev. D **55** (1997) 1611;  
S. Pokorski, J. Rosiek and C.A. Savoy, Nucl. Phys. B **570** (2000) 81;  
E. Accomando, R. Arnowitt and B. Dutta, Phys. Rev. D **61** (2000) 115003;  
A. Bartl, T. Gajdosik, W. Porod, P. Stockinger and H. Stremnitzer, Phys. Rev. D **60**

- (1999) 073003;  
T. Ibrahim and P. Nath, Phys. Rev. D **58** (1998) 111301 [Erratum-ibid. D **60** (1999) 099902];  
M. Brhlik, L. L. Everett, G. L. Kane and J. D. Lykken, Phys. Rev. Lett. **83** (1999) 2124;  
S. Yaser Ayazi and Y. Farzan, Phys. Rev. D **74** (2006) 055008;  
S. Y. Ayazi and Y. Farzan, JHEP **0706** (2007) 013.
- [11] S. Abel, S. Khalil and O. Lebedev, Nucl. Phys. B **606** (2001) 151.
- [12] D. Chang, W. Y. Keung and A. Pilaftsis, Phys. Rev. Lett. **82** (1999) 900 [Erratum-ibid. **83** (1999) 3972].
- [13] A. Pilaftsis, Nucl. Phys. B **644** (2002) 263.
- [14] J. R. Ellis, J. S. Lee and A. Pilaftsis, Phys. Rev. D **72** (2005) 095006.
- [15] S. M. Barr and A. Zee, Phys. Rev. Lett. **65** (1990) 21.
- [16] O. Lebedev and M. Pospelov, Phys. Rev. Lett. **89** (2002) 101801.
- [17] D. A. Demir, O. Lebedev, K. A. Olive, M. Pospelov and A. Ritz, Nucl. Phys. B **680** (2004) 339.
- [18] S. Barr, Phys. Rev. Lett. **68** (1992) 1822; Int. J. Mod. Phys. A **8** (1993) 209.
- [19] J. Dai, H. Dykstra, R. G. Leigh, S. Paban and D. Dicus, Phys. Lett. B **237** (1990) 216 [Erratum-ibid. B **242** (1990) 547].
- [20] D. A. Dicus, Phys. Rev. D **41** (1990) 999.
- [21] S. Weinberg, Phys. Rev. Lett. **63** (1989) 2333.
- [22] A. Pilaftsis, Phys. Rev. D **58** (1998) 096010; Phys. Lett. B **435** (1998) 88;  
A. Pilaftsis and C. E. M. Wagner, Nucl. Phys. B **553** (1999) 3;  
D. A. Demir, Phys. Rev. **D60** (1999) 055006;  
S. Y. Choi, M. Drees and J. S. Lee, Phys. Lett. **B481** (2000) 57;  
M. S. Carena, J. R. Ellis, A. Pilaftsis and C. E. M. Wagner, Nucl. Phys. B **586** (2000) 92;  
T. Ibrahim and P. Nath, Phys. Rev. D **63** (2001) 035009;  
M. Frank, T. Hahn, S. Heinemeyer, W. Hollik, H. Rzehak and G. Weiglein, JHEP **0702** (2007) 047.

- [23] T. Banks, Nucl. Phys. B **303** (1988) 172;  
 E. Ma, Phys. Rev. D **39** (1989) 1922;  
 R. Hempfling, Phys. Rev. D **49** (1994) 6168;  
 L. J. Hall, R. Rattazzi and U. Sarid, Phys. Rev. D **50** (1994) 7048;  
 M. Carena, M. Olechowski, S. Pokorski and C. E. M. Wagner, Nucl. Phys. B **426** (1994) 269;  
 D. M. Pierce, J. A. Bagger, K. T. Matchev and R. j. Zhang, Nucl. Phys. B **491** (1997) 3;  
 F. Borzumati, G. R. Farrar, N. Polonsky and S. D. Thomas, Nucl. Phys. B **555** (1999) 53.
- [24] M. Carena, J. R. Ellis, A. Pilaftsis and C. E. M. Wagner, Phys. Lett. B **495** (2000) 155.
- [25] J. R. Ellis, J. S. Lee and A. Pilaftsis, Phys. Rev. D **70** (2004) 075010.
- [26] J. Ellis, J. S. Lee and A. Pilaftsis, Phys. Rev. D **76** (2007) 115011.
- [27] J. S. Lee, A. Pilaftsis, M. Carena, S. Y. Choi, M. Drees, J. R. Ellis and C. E. M. Wagner, Comput. Phys. Commun. **156** (2004) 283;  
 J. S. Lee, M. Carena, J. Ellis, A. Pilaftsis and C. E. M. Wagner, arXiv:0712.2360 [hep-ph].
- [28] A. Pilaftsis, Phys. Lett. B **471** (1999) 174;  
 D. Chang, W. F. Chang and W. Y. Keung, Phys. Lett. B **478** (2000) 239;  
 A. Pilaftsis, Phys. Rev. D **62** (2000) 016007;  
 D. Chang, W. F. Chang and W. Y. Keung, Phys. Rev. D **66** (2002) 116008;  
 D. Chang, W. F. Chang and W. Y. Keung, Phys. Rev. D **71** (2005) 076006;  
 Y. Li, S. Profumo and M. Ramsey-Musolf, arXiv:0806.2693 [hep-ph].
- [29] T. H. West, Phys. Rev. D **50** (1994) 7;  
 T. Kadoyoshi and N. Oshimo, Phys. Rev. D **55** (1997) 1481.
- [30] I.B. Khriplovich and S.K. Lamoreaux, *CP Violation Without Strangeness* (Springer, New York, 1997).
- [31] M. Pospelov and A. Ritz, Annals Phys. **318** (2005) 119.
- [32] A. Manohar and H. Georgi, Nucl. Phys. B **234** (1984) 189;  
 R. Arnowitt, J. L. Lopez and D. V. Nanopoulos, Phys. Rev. D **42** (1990) 2423;  
 R. Arnowitt, M. J. Duff and K. S. Stelle, Phys. Rev. D **43** (1991) 3085.
- [33] T. Ibrahim and P. Nath, Phys. Rev. D **57** (1998) 478 [Erratum-ibid. D **58** (1998) ERRAT,D60,079903.1999 ERRAT,D60,119901.1999) 019901]

- [34] J. R. Ellis and R. A. Flores, Phys. Lett. B **377** (1996) 83.
- [35] M. Pospelov and A. Ritz, Phys. Rev. Lett. **83** (1999) 2526;  
M. Pospelov and A. Ritz, Nucl. Phys. B **573** (2000) 177.
- [36] M. Pospelov and A. Ritz, Phys. Rev. D **63** (2001) 073015.
- [37] D. A. Demir, M. Pospelov and A. Ritz, Phys. Rev. D **67** (2003) 015007.
- [38] K. A. Olive, M. Pospelov, A. Ritz and Y. Santoso, Phys. Rev. D **72** (2005) 075001.
- [39] M. Pospelov and A. Ritz, in private communication.
- [40] I. B. Khriplovich and R. A. Korkin, Nucl. Phys. A **665** (2000) 365.
- [41] For a similar suggestion, see,  
M. Argyrou, A. B. Lahanas and V. C. Spanos, JHEP **0805** (2008) 026.
- [42] M. Battaglia *et al.*, Eur. Phys. J. C **22** (2001) 535;  
B. C. Allanach *et al.*, arXiv:hep-ph/0202233;  
N. Ghodbane and H. U. Martyn, arXiv:hep-ph/0201233;  
M. Battaglia, A. De Roeck, J. R. Ellis, F. Gianotti, K. A. Olive and L. Pape, Eur. Phys. J. C **33** (2004) 273.
- [43] T. Goto, Y. Y. Keum, T. Nihei, Y. Okada and Y. Shimizu, Phys. Lett. B **460** (1999) 333.
- [44] A. A. Anselm, V. E. Bunakov, V. P. Gudkov and N. G. Uraltsev, Phys. Lett. B **152** (1985) 116 [JETP Lett. **40** (1984 ZFPRA,40,310-313.1984) 1102].

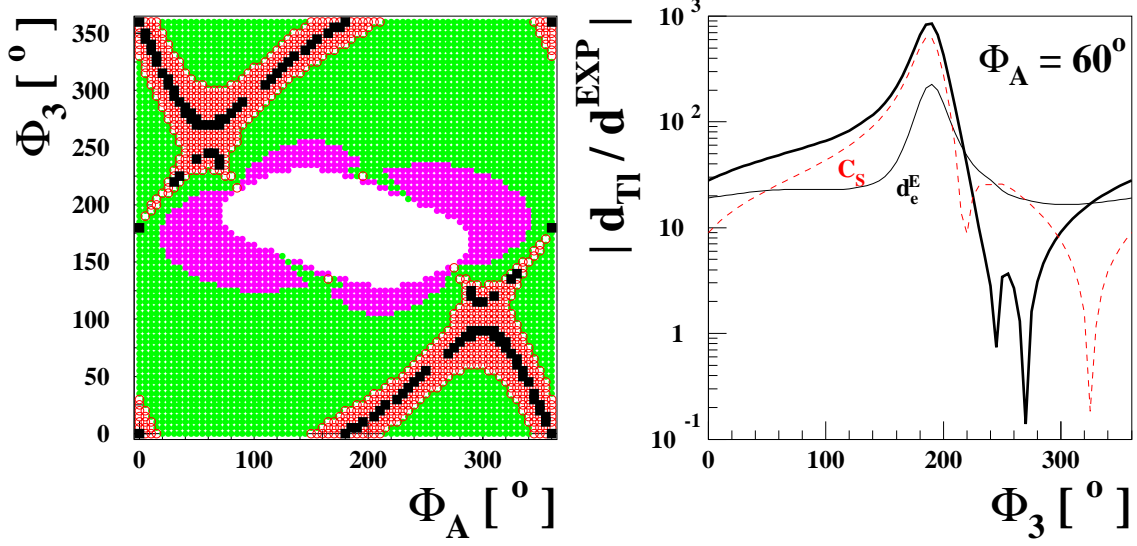


Figure 7: The absolute value of the Thallium EDM divided by its current experimental limit,  $d_{\text{Tl}}^{\text{EXP}} = 9 \times 10^{-25}$  e cm, in the  $\Phi_3$ - $\Phi_A$  plane (left) and as a function of  $\Phi_3$  taking  $\Phi_A = 60^\circ$  (right). The trimixing scenario has been taken. In the left frame, the plane is divided into 4 regions:  $|d_{\text{Tl}}/d^{\text{EXP}}| < 1$  (black),  $1 \leq |d_{\text{Tl}}/d^{\text{EXP}}| < 10$  (red),  $10 \leq |d_{\text{Tl}}/d^{\text{EXP}}| < 100$  (green), and  $100 \leq |d_{\text{Tl}}/d^{\text{EXP}}|$  (magenta). The unshaded region is not allowed theoretically. In the right frame, the constituent contributions from  $d_e^E$  and  $C_S$  are shown as the thin solid and dashed lines, respectively. The thick solid line is for the total EDM.



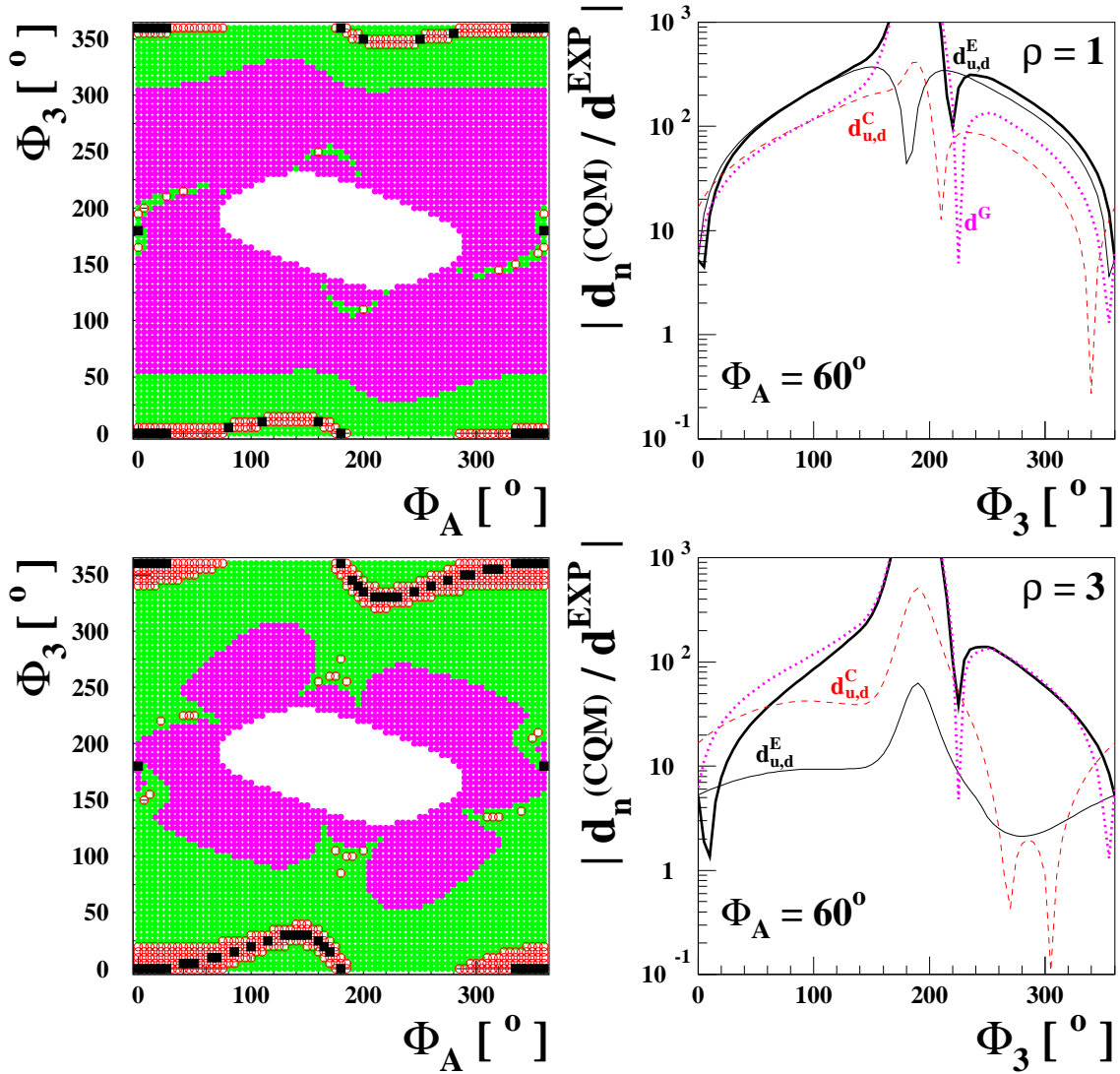


Figure 8: The absolute value of the neutron EDM in the CQM divided by its current experimental limit,  $d_n^{\text{EXP}} = 3 \times 10^{-26}$  e cm, in the  $\Phi_3$ - $\Phi_A$  plane (left) and as a function of  $\Phi_3$  taking  $\Phi_A = 60^\circ$  (right). The trimixing scenario has been taken with the common hierarchy factor  $\rho = 1$  (upper) and 3 (lower). In the left frames, the shaded regions are the same as in Fig. 7. In the right frames, the constituent contributions from  $d_{u,d}^E$ ,  $d_{u,d}^C$ , and  $d^G$  are shown in the thin solid, dashed, dotted lines, respectively. The thick solid line is for the total EDM.

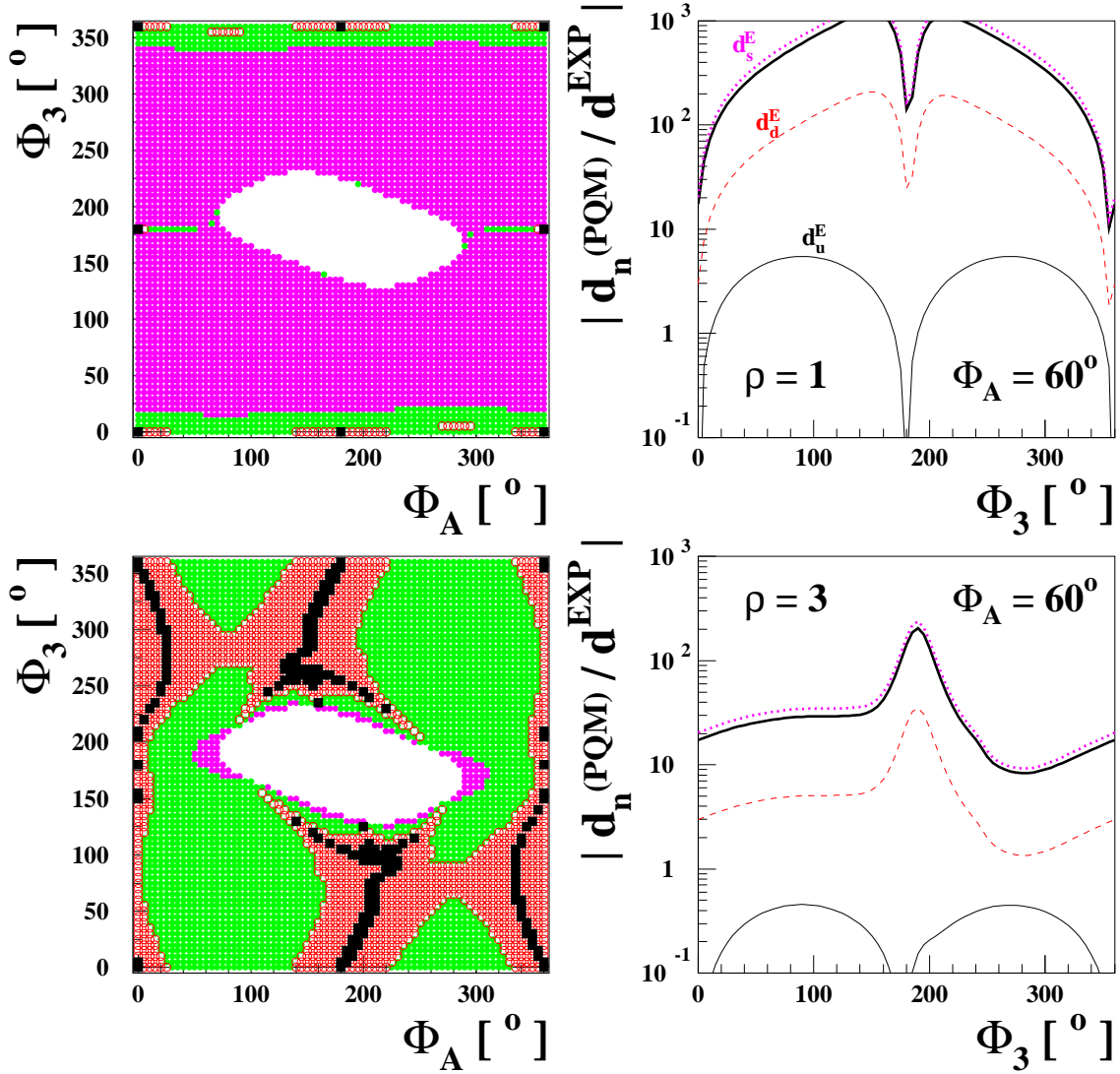


Figure 9: *The same as in Fig. 8, but using the PQM for the calculation. In the right frames, the constituent contributions from  $d_u^E$ ,  $d_d^E$ , and  $d_s^E$  are shown as the thin solid, dashed, dotted lines, respectively. The thick solid line is for the total EDM.*

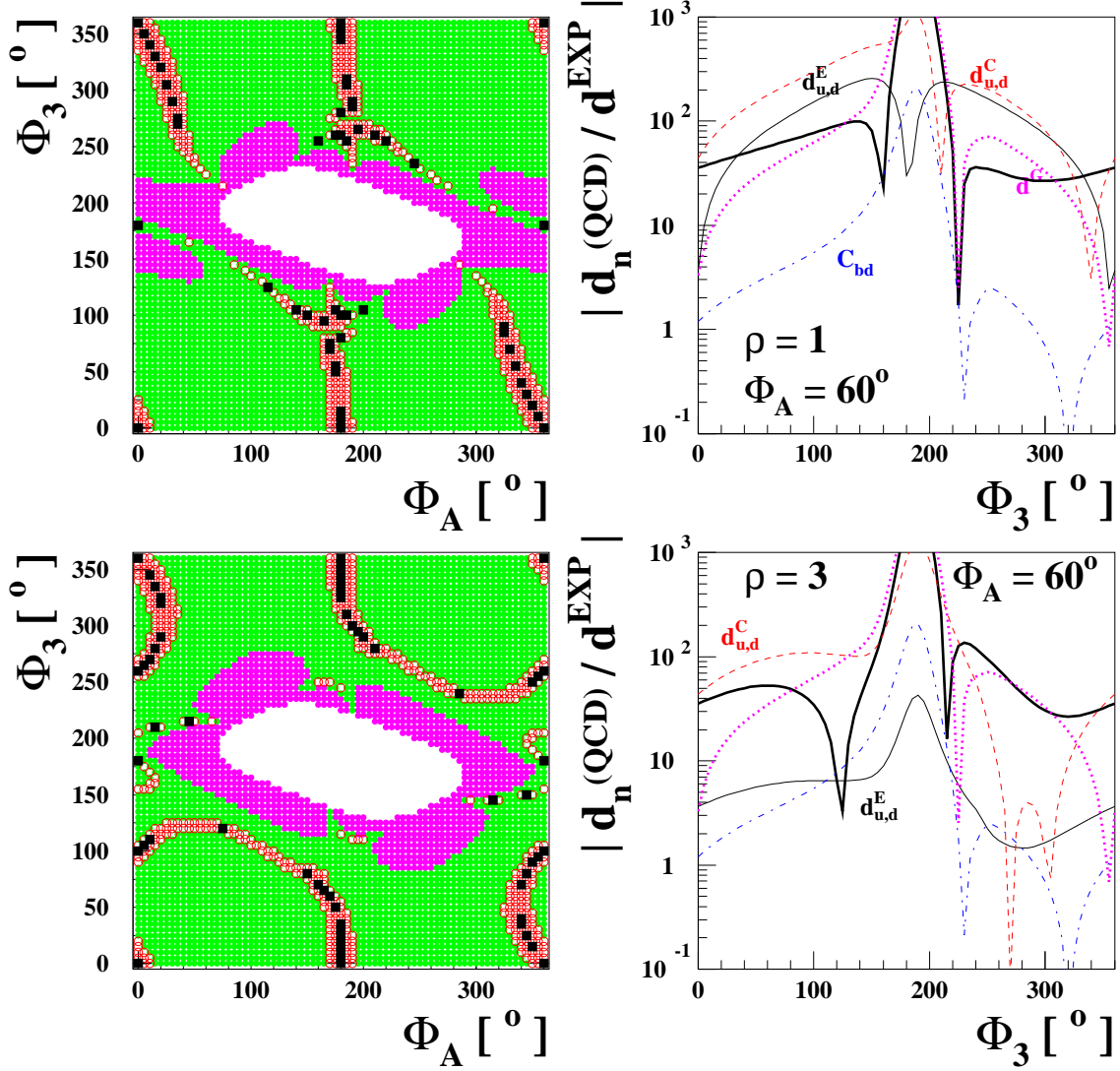


Figure 10: The same as in Fig. 8 but using the QCD sum rule approach for the calculation. In the right frames, the constituent contributions from  $d_{u,d}^E$ ,  $d_{u,d}^C$ ,  $d^G$ , and  $C_{bd,db}$  are shown as the thin solid, dashed, dotted, dash-dotted lines, respectively. The thick solid line is for the total EDM.

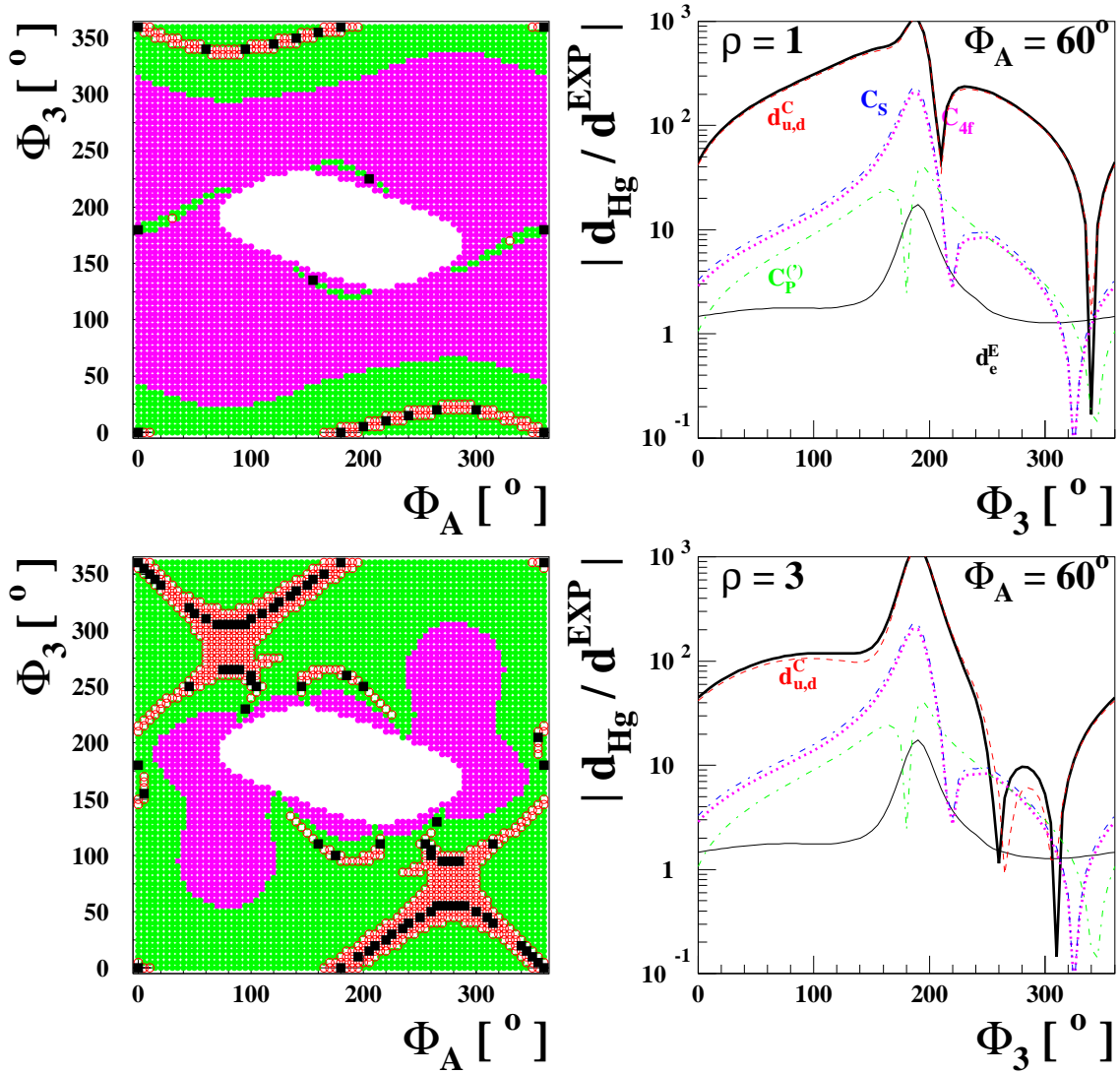


Figure 11: *The absolute value of the Mercury EDM divided by its current experimental limit,  $d_{\text{Hg}}^{\text{EXP}} = 2 \times 10^{-28}$  e cm, on the  $\Phi_3$ - $\Phi_A$  plane (left) and as a function of  $\Phi_3$  taking  $\Phi_A = 60^\circ$  (right). The trimixing scenario has been taken with the common hierachy factor  $\rho = 1$  (upper) and 3 (lower). In the left frames, the shaded regions are the same as in Fig. 7. In the right frames, the constituent contributions from  $d_e^E$ ,  $d_{u,d}^C$ ,  $C_{4f} \equiv C_{dd,sd,bd}$ , and  $C_{S,P}^{(l)}$  are shown as the thin solid, dashed, dotted, and dash-dotted lines, respectively. The thick solid line is for the total EDM.*

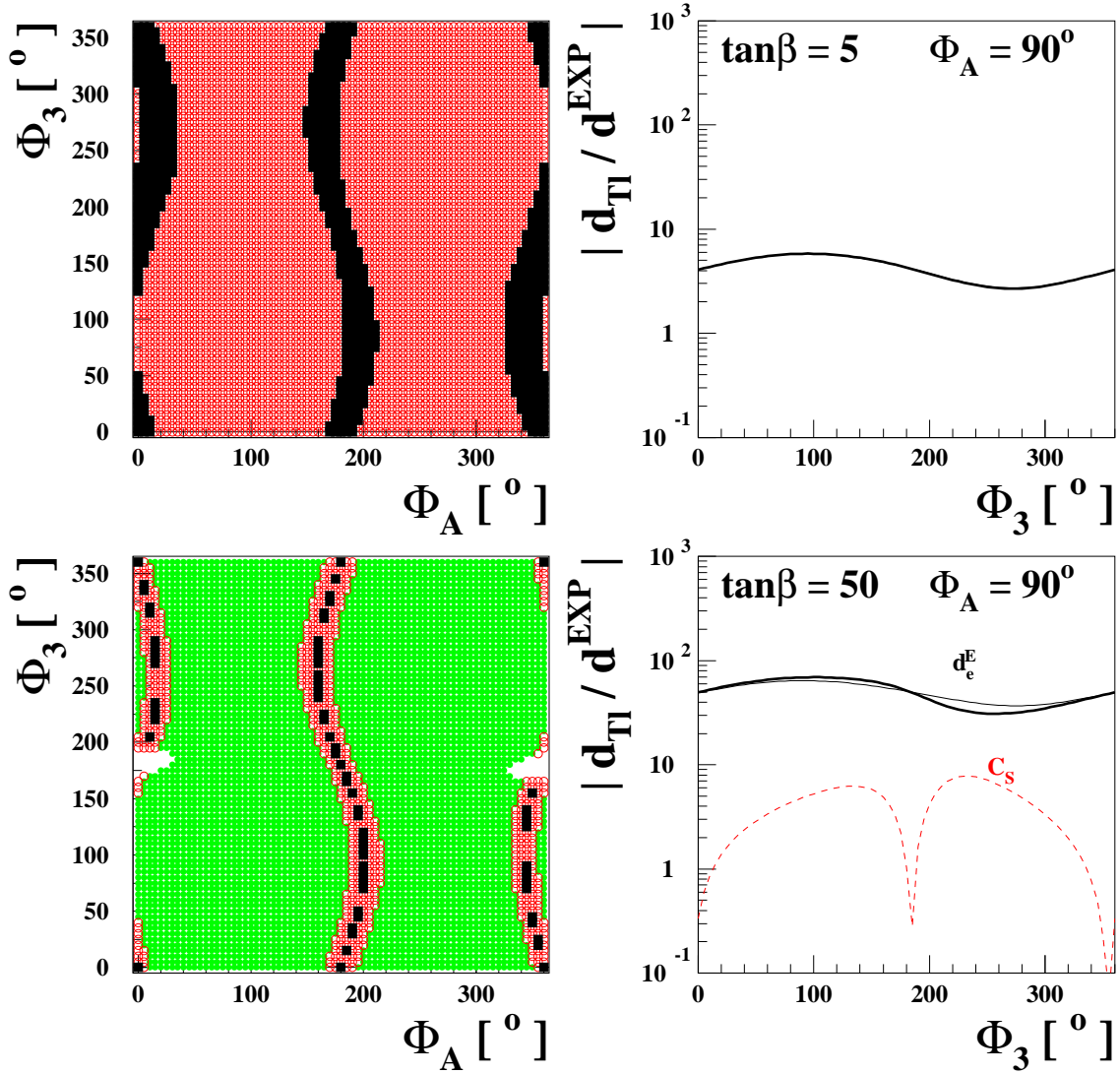


Figure 12: *The Thallium EDM in the CPX scenario. The upper frames are for  $\tan\beta = 5$  and the lower ones for  $\tan\beta = 50$  with  $\Phi_A = 90^\circ$ . The shaded regions and lines are the same as in Fig. 7.*

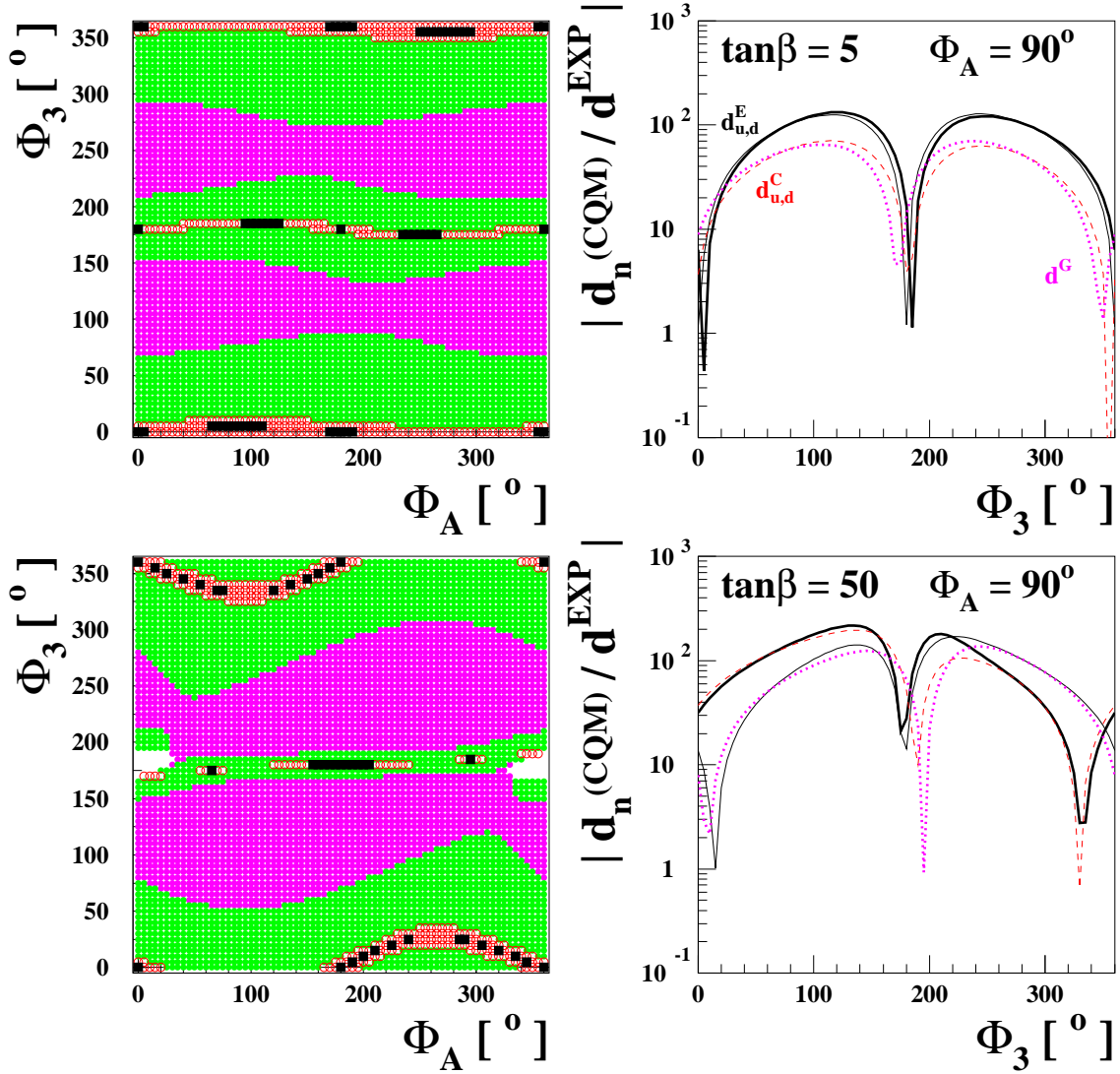


Figure 13: *The neutron EDM in the CPX scenario calculated in the CQM. The upper frames are for  $\tan\beta = 5$  and the lower ones for  $\tan\beta = 50$  with  $\Phi_A = 90^\circ$ . The shaded regions and lines are the same as in Fig. 8.*



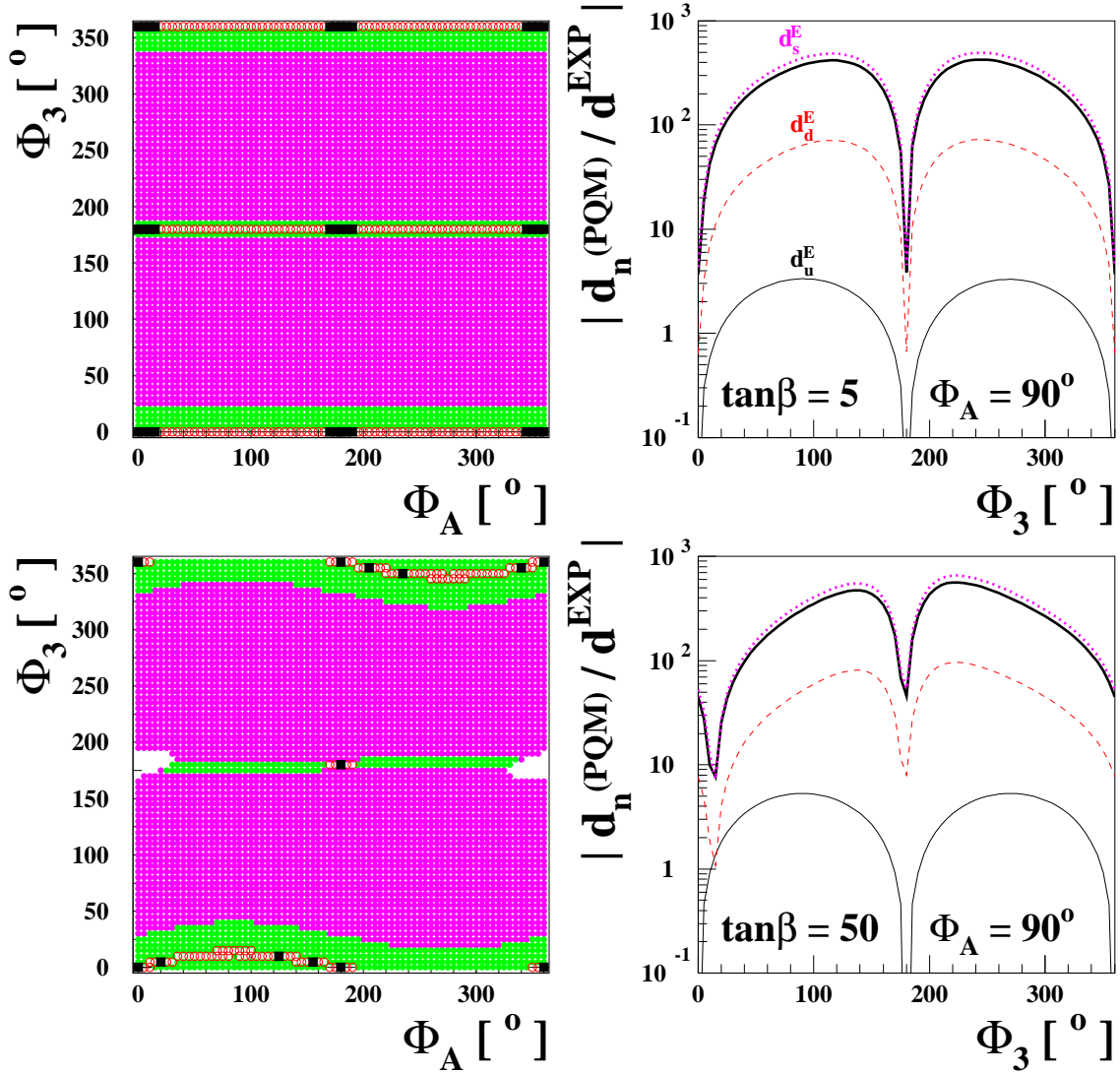


Figure 14: *The neutron EDM in the CPX scenario calculated in the PQM. The upper frames are for  $\tan\beta = 5$  and the lower ones for  $\tan\beta = 50$  with  $\Phi_A = 90^\circ$ . The shaded regions and lines are the same as in Fig. 9.*

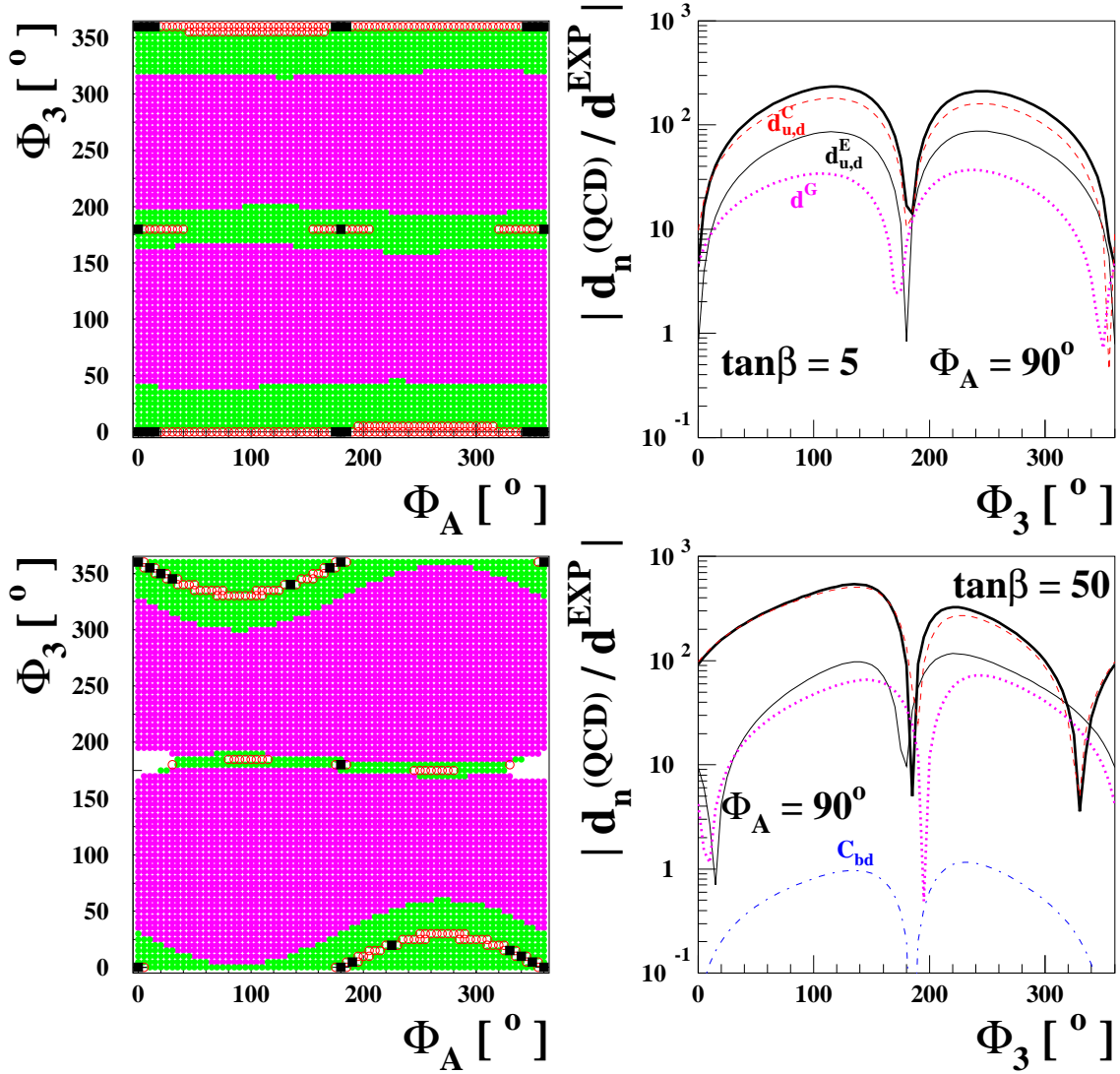


Figure 15: *The neutron EDM in the CPX scenario calculated using the QCD sum rule approach. The upper frames are for  $\tan\beta = 5$  and the lower ones for  $\tan\beta = 50$  with  $\Phi_A = 90^\circ$ . The shaded regions and lines are the same as in Fig. 10.*



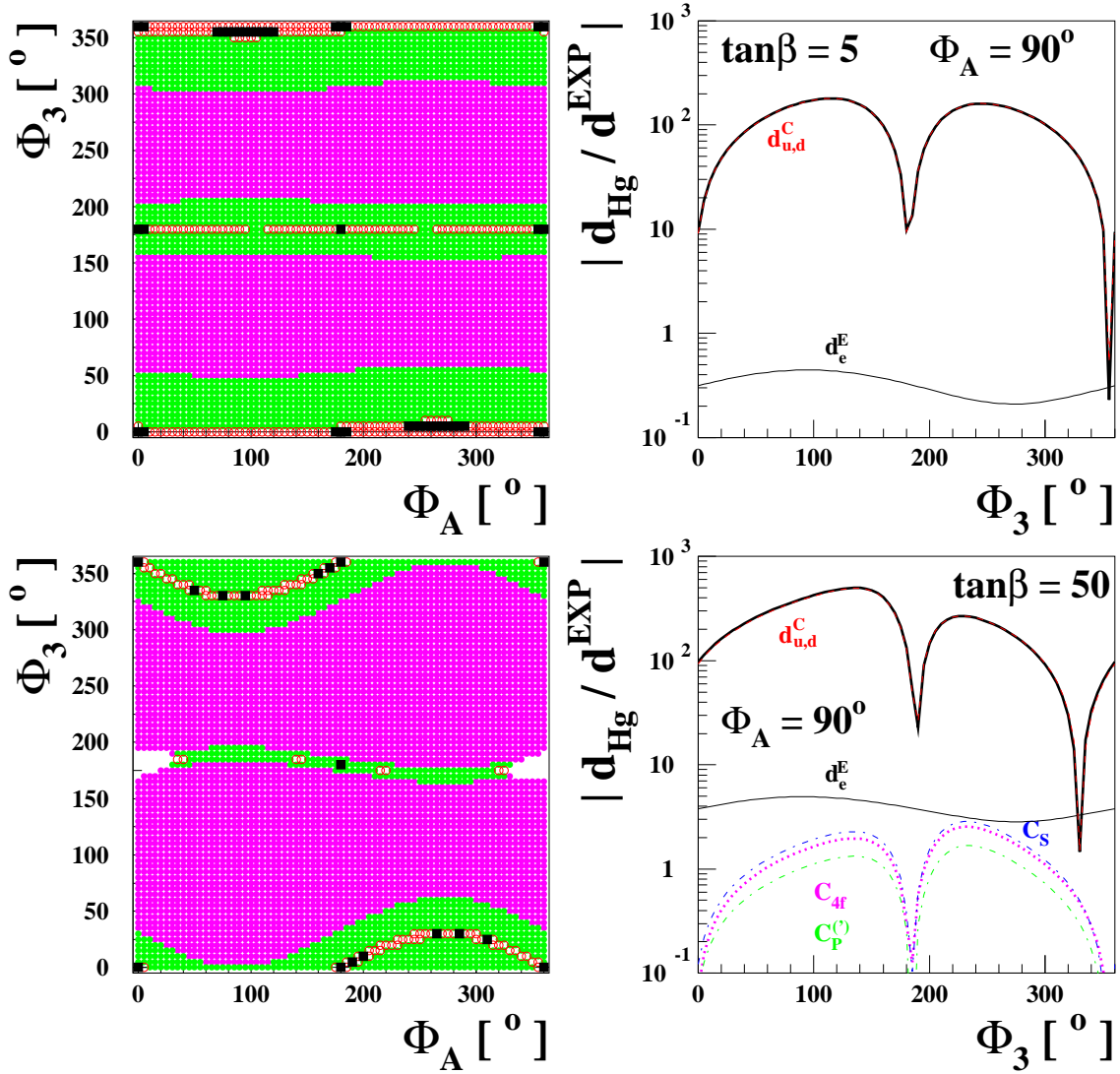


Figure 16: *The Mercury EDM in the CPX scenario. The upper frames are for  $\tan\beta = 5$  and the lower ones for  $\tan\beta = 50$  with  $\Phi_A = 90^\circ$ . The shaded regions and lines are the same as in Fig. 11.*

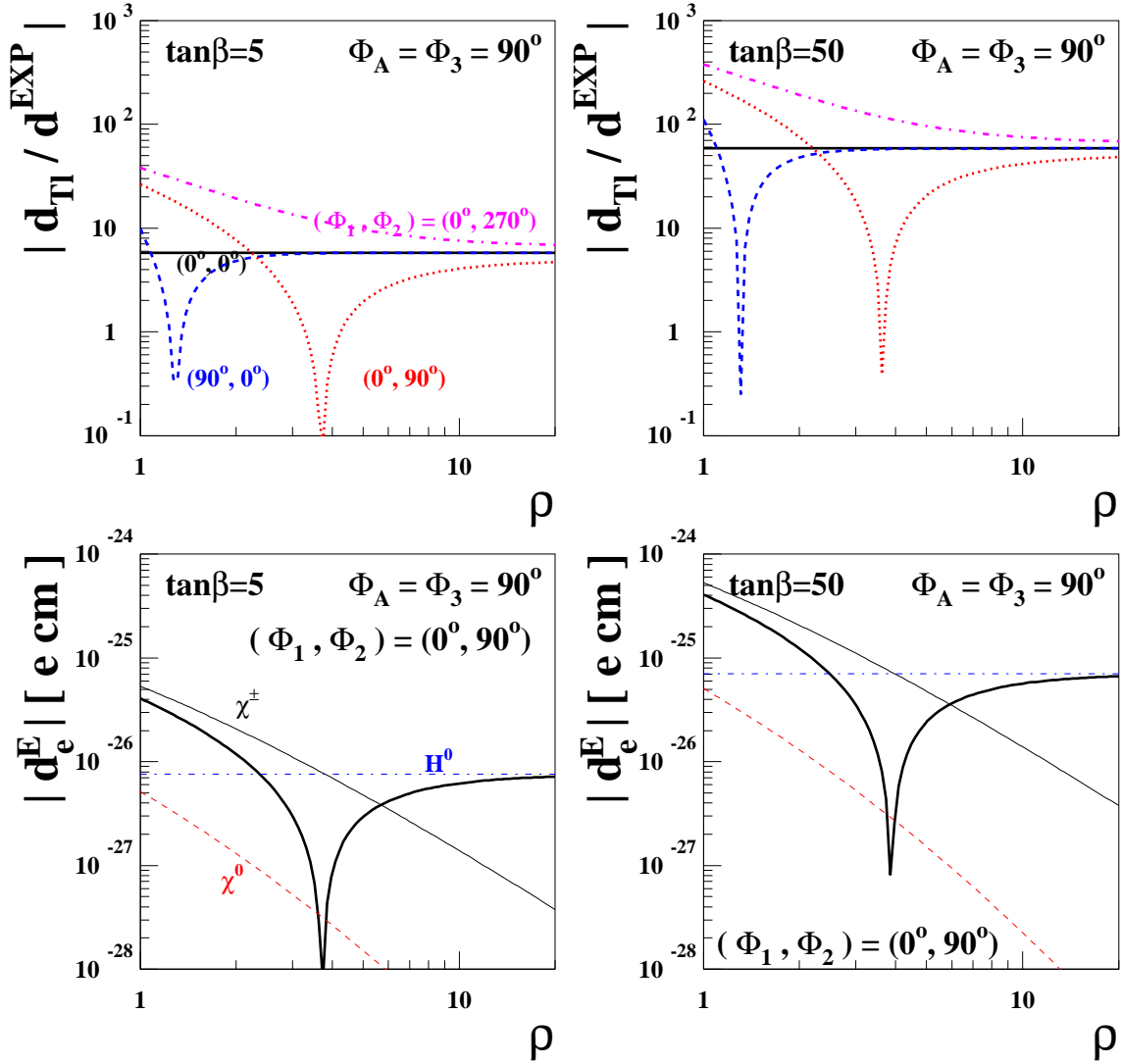


Figure 17: In the upper frames, we show the Thallium EDM in the CPX scenario as a function of the common hierarchy factor  $\rho$  with several non-trivial values of  $(\Phi_1, \Phi_2)$ :  $(\Phi_1, \Phi_2) = (0^\circ, 0^\circ)$  (solid),  $(90^\circ, 0^\circ)$  (dashed),  $(0^\circ, 90^\circ)$  (dotted), and  $(0^\circ, 270^\circ)$  (dash-dotted). The left frame is for  $\tan\beta = 5$  and the right one for  $\tan\beta = 50$ . The lower frames are for the electron EDM, which makes the main contribution to the Thallium EDM, in the given scenario, exemplifying the case with  $(\Phi_1, \Phi_2) = (0^\circ, 90^\circ)$  from each upper frame. Shown separately are the different contributions to the electron EDM from the chargino- (thin solid), neutralino- (thin dashed), and two-loop Higgs- (thin dash-dotted) mediated diagrams. The thick solid lines are for the total EDM. We have taken  $\Phi_A = \Phi_3 = 90^\circ$  in all frames.

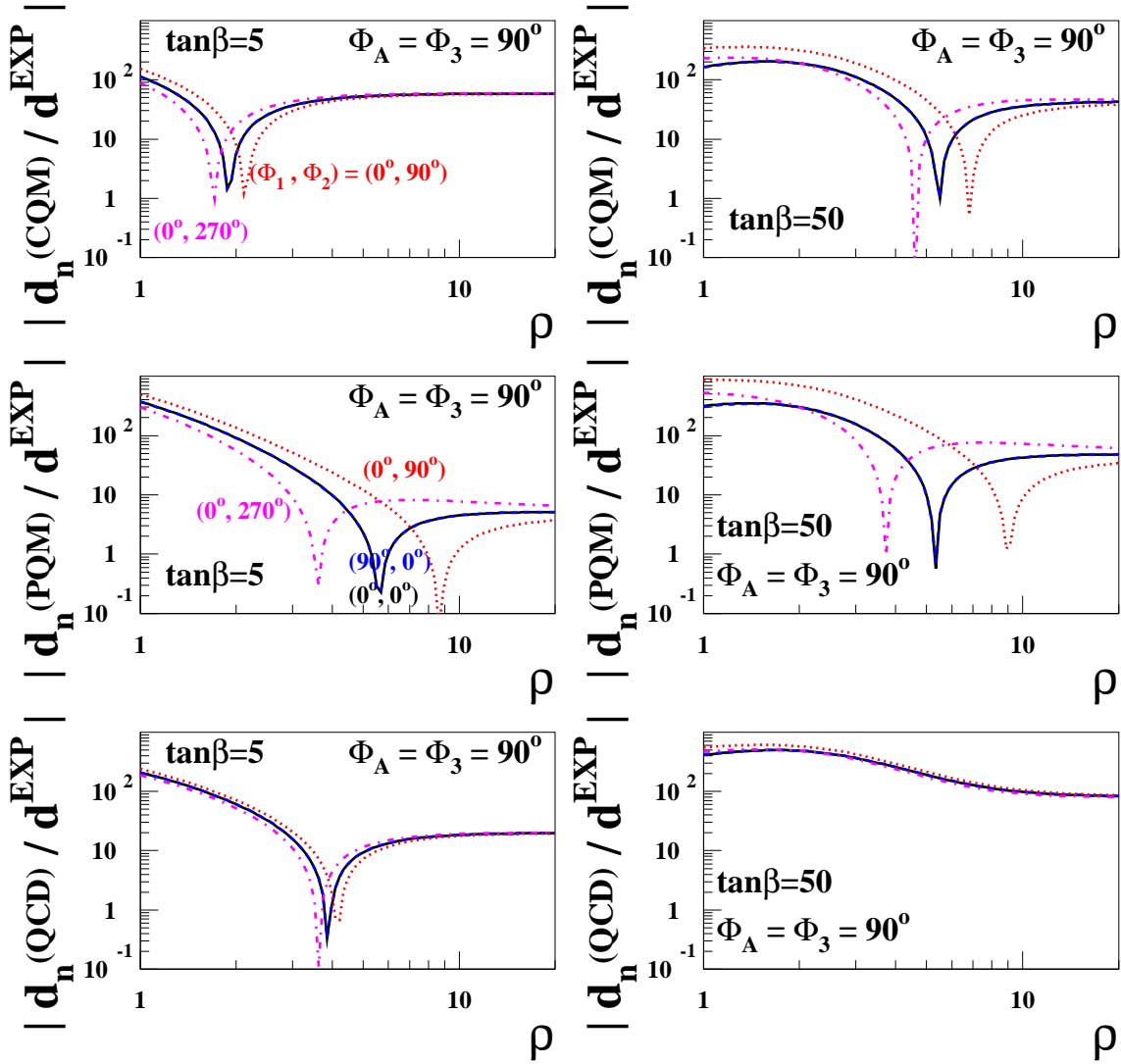


Figure 18: *The neutron EDM in the CPX scenario with  $\Phi_A = \Phi_3 = 90^\circ$  as a function of the common hierarchy factor  $\rho$  calculated in the CQM (upper), the PQM (middle), and using the QCD sum rule approach (lower) for  $\tan\beta = 5$  (left) and  $\tan\beta = 50$  (right). The cases with several non-trivial values of  $(\Phi_1, \Phi_2)$  are considered as in Fig. 17. The cases with  $(\Phi_1, \Phi_2) = (0^\circ, 0^\circ)$  and  $(90^\circ, 0^\circ)$  are hardly distinguishable from each other.*

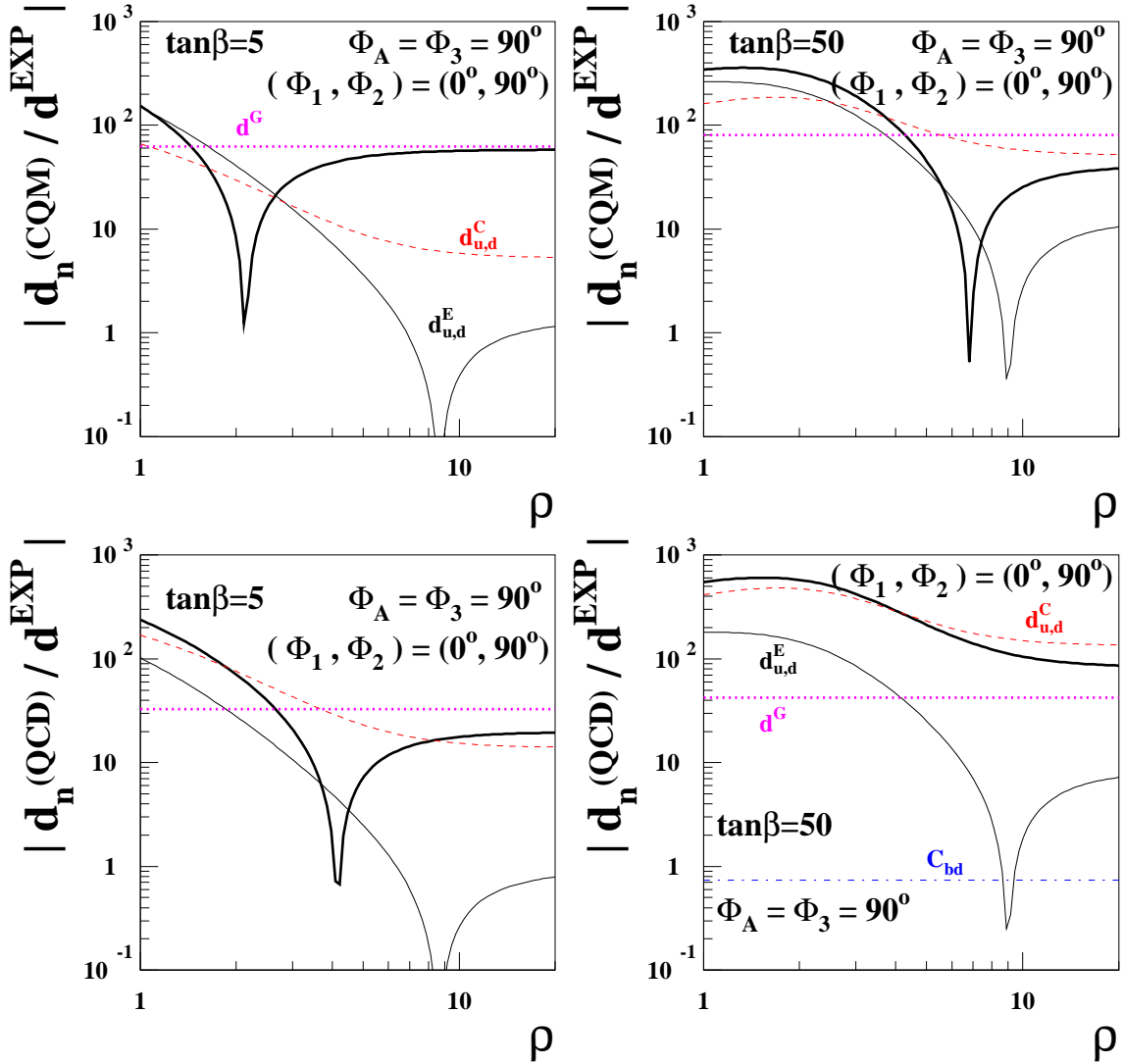


Figure 19: Comparison of the neutron EDM calculated in the CQM (upper) and using the QCD sum rule approach (lower). Among the lines in Fig. 18, the case with  $(\Phi_1, \Phi_2) = (0^\circ, 90^\circ)$  is shown together with the constituent contributions:  $d_{u,d}^E$  (thin solid),  $d_{u,d}^C$  (thin dashed),  $d^G$  (thin horizontal dotted), and  $C_{bd,db}$  (thin horizontal dash-dotted). The thick solid lines are for the total EDM.

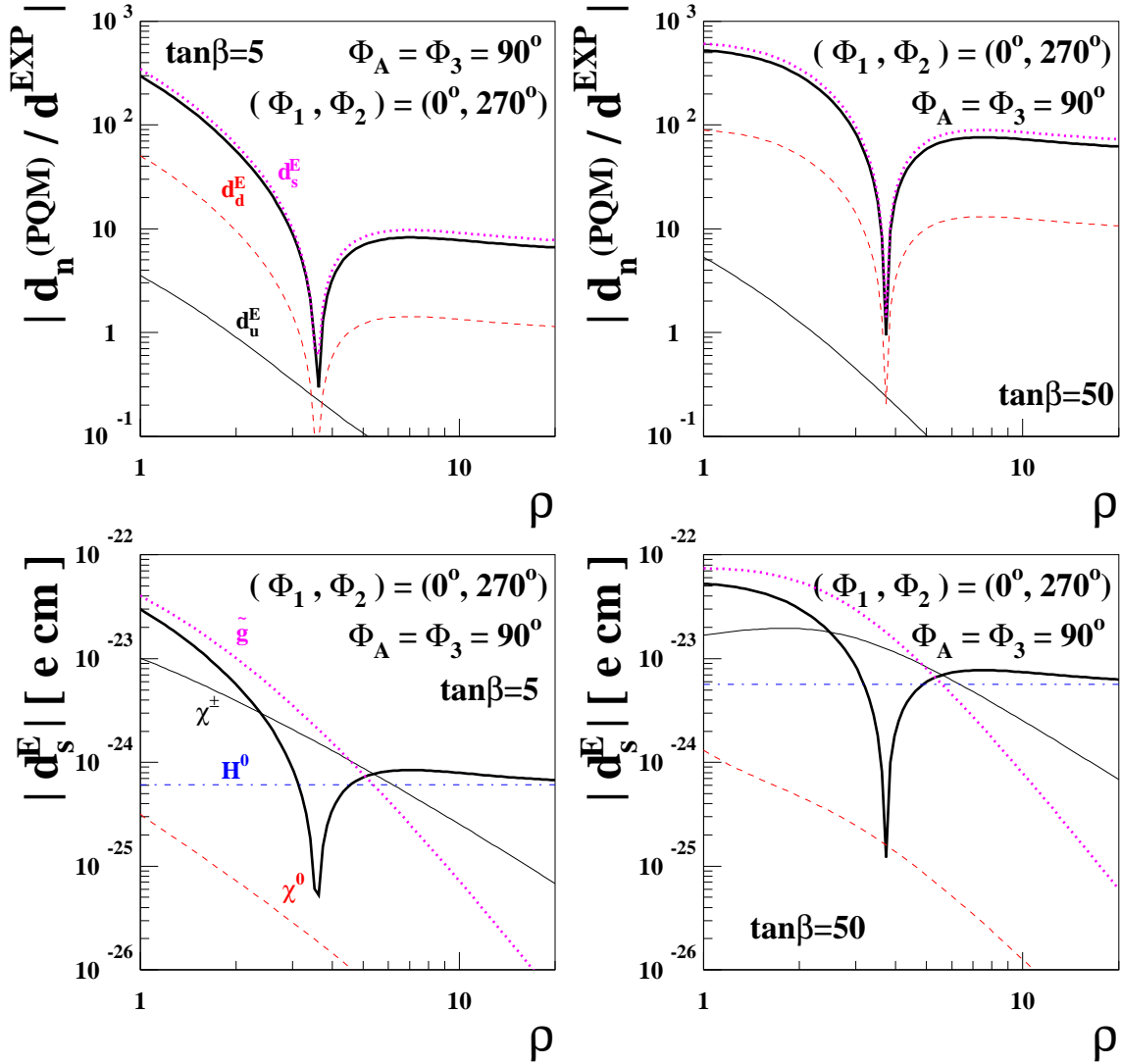


Figure 20: The neutron EDM calculated in the PQM. In the upper frames, among the lines in the middle frames of Fig. 18, the case with  $(\Phi_1, \Phi_2) = (0^\circ, 270^\circ)$  is shown together with the constituent contributions:  $d_u^E$  (thin solid),  $d_d^E$  (thin dashed), and the main contribution from  $d_s^E$  (thin dotted). In the lower frames, the strange-quark EDM is shown as functions of the common hierarchy factor  $\rho$ . The thin solid, dashed, dotted lines, and horizontal dash-dotted lines are for the contributions from the chargino-, neutralino-, gluino- and two-loop Higgs-mediated diagrams. The thick solid lines are for the total EDM.

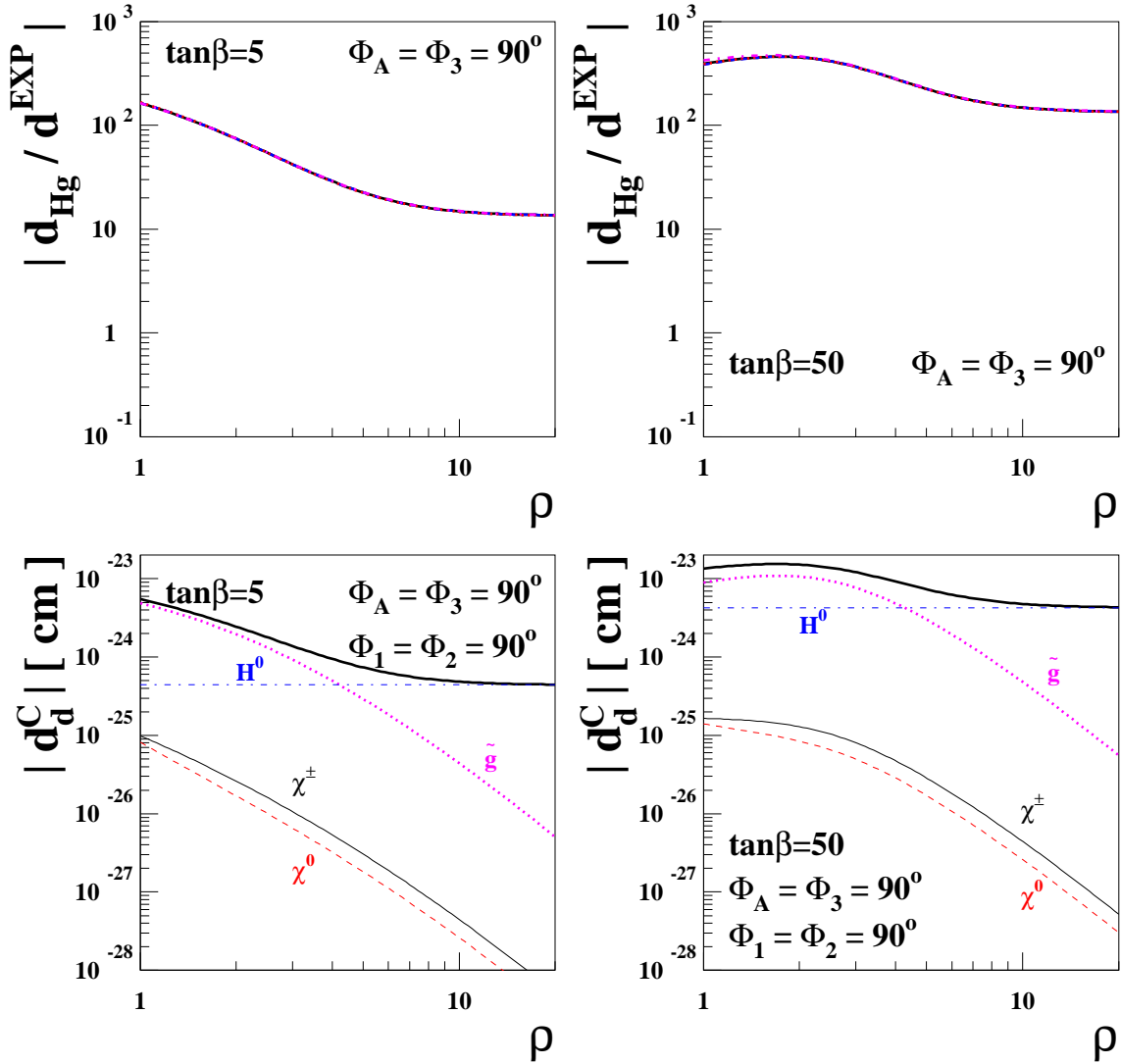


Figure 21: In the upper frames, we show the Mercury EDM in the CPX scenario with  $\Phi_A = \Phi_3 = 90^\circ$  as a function of the common hierarchy factor  $\rho$  for  $\tan\beta = 5$  (left) and  $\tan\beta = 50$  (right). It is hardly affected by  $(\Phi_1, \Phi_2)$ , because of the dominance of the contribution from  $d_{u,d}^C$ , see Fig. 16. In the lower frames, we show the dominant CEDM of the down quark,  $d_d^C$ , as a function of  $\rho$ . The lines are the same as in the lower frames of Fig. 20.

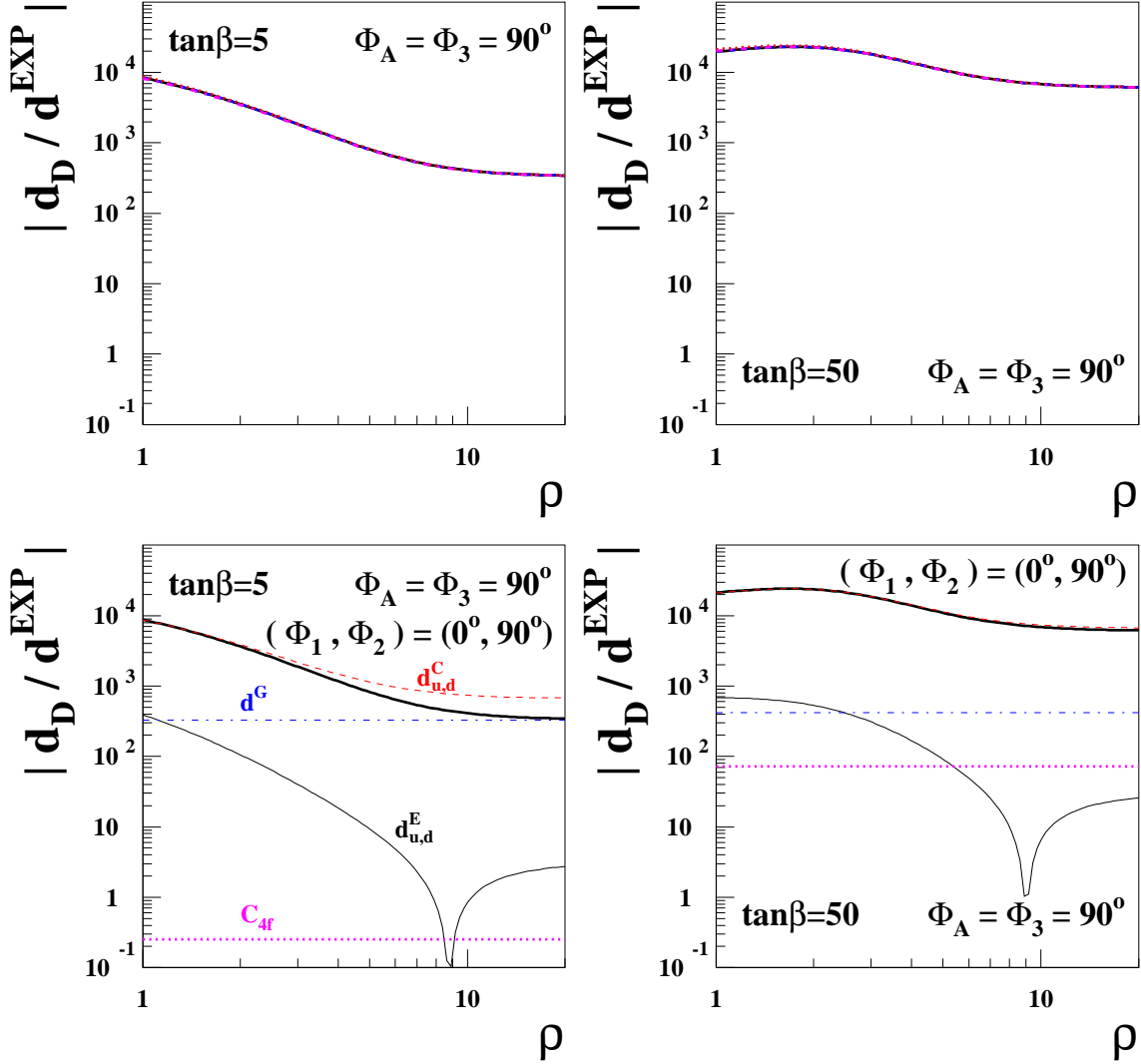


Figure 22: The deuteron EDM in the CPX scenario with  $\Phi_A = \Phi_3 = 90^\circ$  as a function of the common hierarchy factor  $\rho$  for  $\tan\beta = 5$  (left) and  $\tan\beta = 50$  (right). We have taken  $d_D^{\text{EXP}} = 3 \times 10^{-27} \text{e cm}$ . It is hardly affected by  $(\Phi_1, \Phi_2)$ , see the upper frames. In the lower frames, the case with  $(\Phi_1, \Phi_2) = (0^\circ, 90^\circ)$  is shown together with the constituent contributions:  $d_{u,d}^E$  (thin solid),  $d_{u,d}^C$  (thin dashed),  $C_{4f} \equiv C_{dd,sd,bd}$  (thin lower horizontal dotted), and  $d^G$  (thin upper horizontal dash-dotted). The thick lines are for the total EDM.

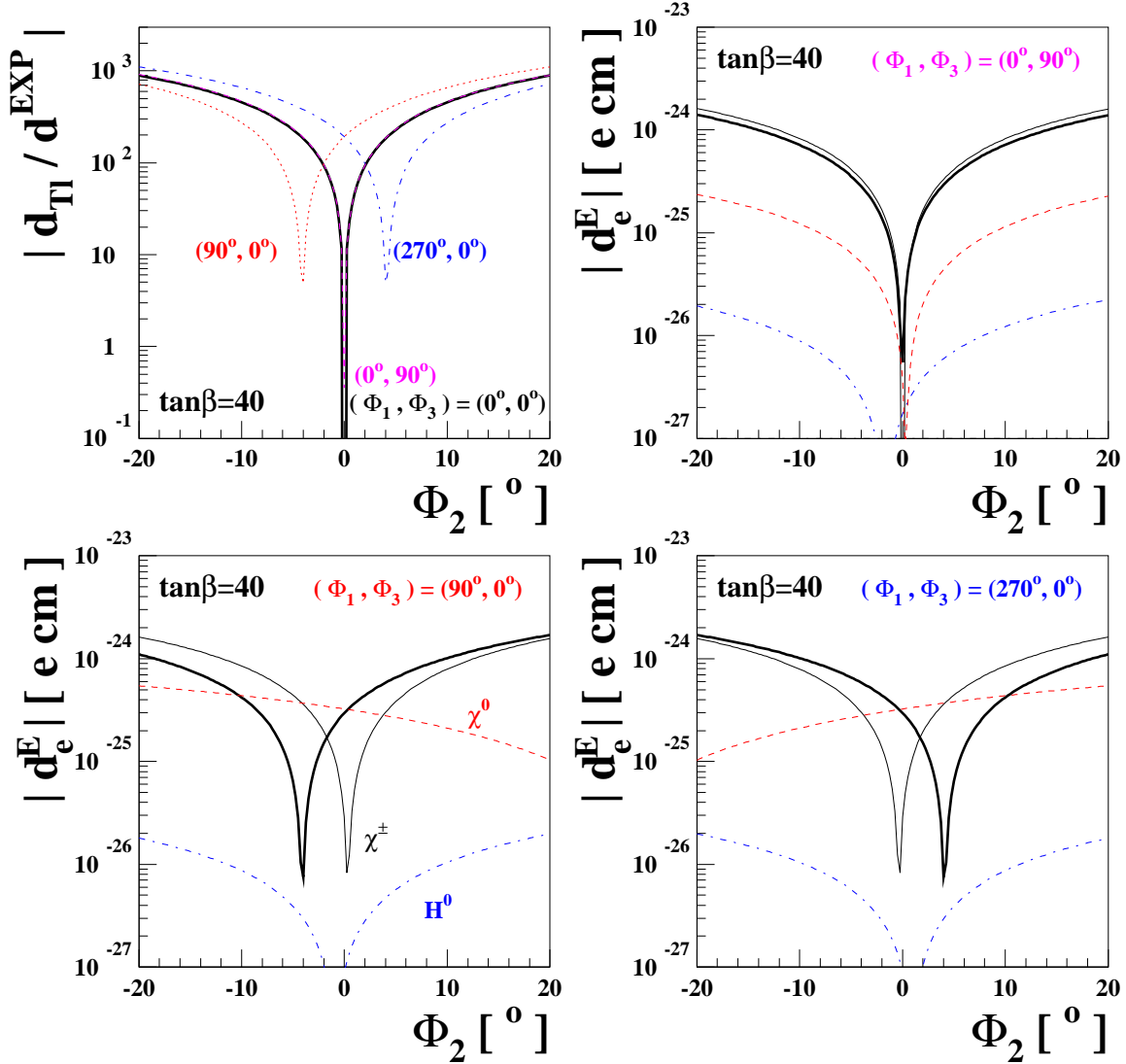


Figure 23: In the upper-left frame, we show the Thallium EDM in the MCPMFV scenario with  $\tan\beta = 40$  as a function of  $\Phi_2$  for several values of the CP-violating phases  $(\Phi_1, \Phi_3)$ :  $(0^\circ, 0^\circ)$  (solid),  $(0^\circ, 90^\circ)$  (dashed),  $(90^\circ, 0^\circ)$  (dotted), and  $(270^\circ, 0^\circ)$  (dash-dotted). The cases with  $(0^\circ, 0^\circ)$  and  $(0^\circ, 90^\circ)$  are hardly distinguishable from each other due to the dominance of the electron EDM,  $d_e^E$ . In the upper-right, lower-left, and lower-right frames, we show the electron EDM as a function of  $\Phi_2$  when  $(\Phi_1, \Phi_3) = (0^\circ, 90^\circ)$ ,  $(90^\circ, 0^\circ)$ , and  $(270^\circ, 90^\circ)$ , respectively. The lines are the same as in Fig. 17.



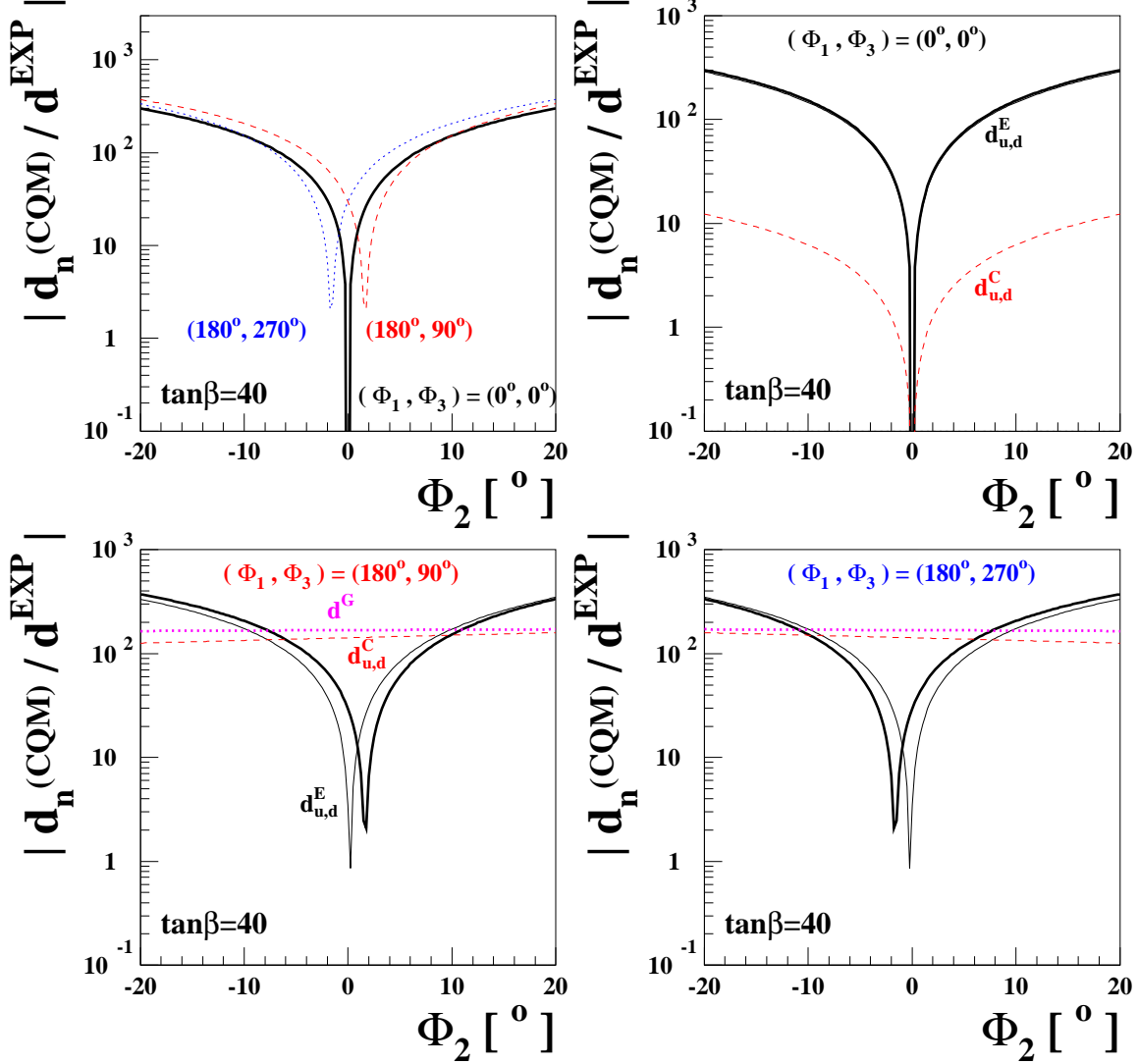


Figure 24: In the upper-left frame, we show the neutron EDM calculated in the chiral quark model in the MCPMFV scenario with  $\tan\beta = 40$  as a function of  $\Phi_2$  for several values of the CP-violating phases  $(\Phi_1, \Phi_3)$ :  $(0^\circ, 0^\circ)$  (solid),  $(180^\circ, 90^\circ)$  (dashed), and  $(180^\circ, 270^\circ)$  (dotted). In the upper-right, lower-left, and lower-right frames, we show the neutron EDM as a function of  $\Phi_2$  when  $(\Phi_1, \Phi_3) = (0^\circ, 0^\circ)$ ,  $(180^\circ, 90^\circ)$ , and  $(180^\circ, 270^\circ)$ , respectively, together with its constituent contributions from  $d_{u,d}^E$  (thin solid),  $d_{u,d}^C$  (thin dashed), and  $d^G$  (thin dotted). The thick solid lines are for the total EDM.

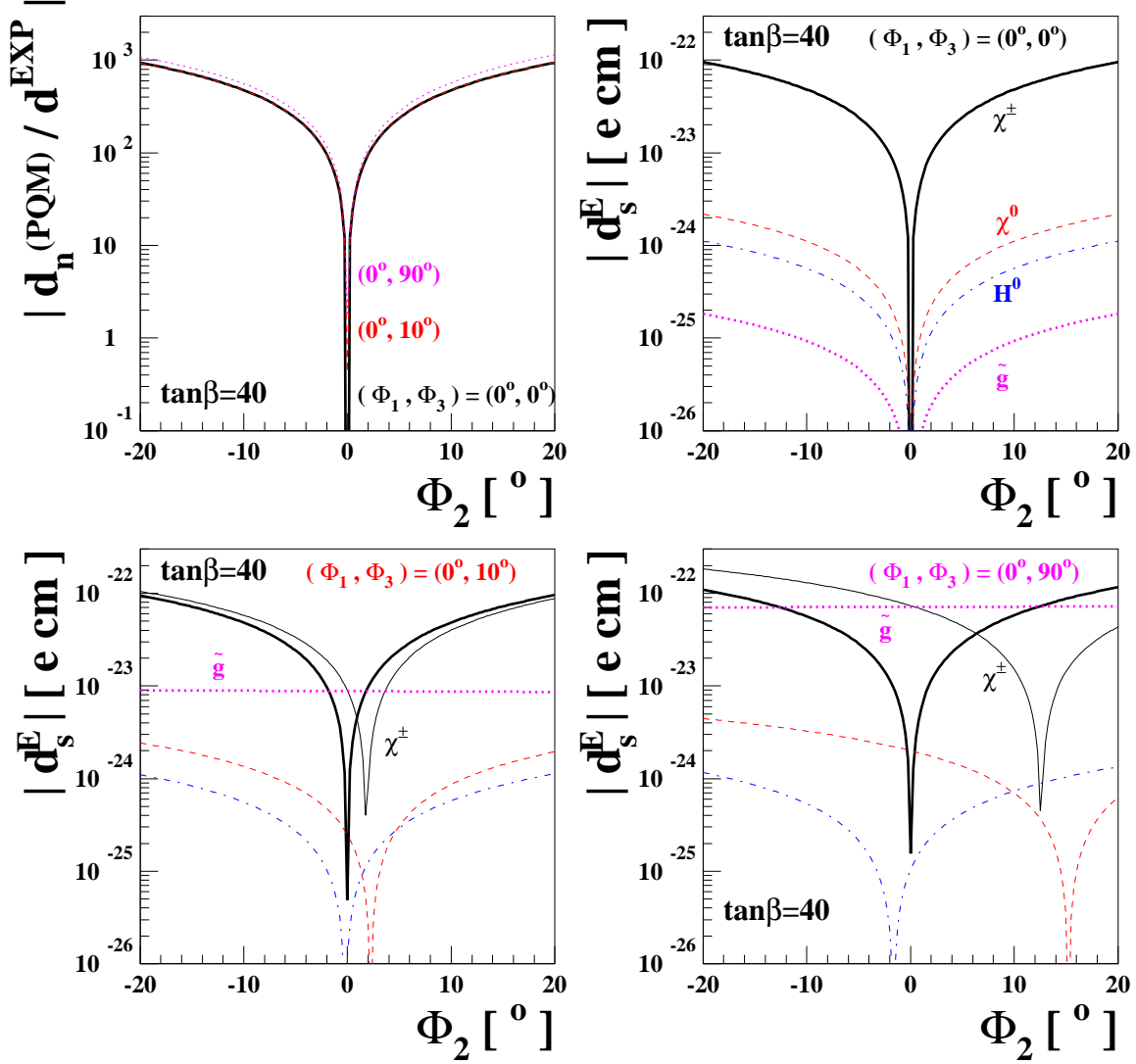


Figure 25: In the upper-left frame, we show the neutron EDM calculated in the PQM in the MCPMFV scenario with  $\tan\beta = 40$  as a function of  $\Phi_2$  for several values of the CP-violating phases  $(\Phi_1, \Phi_3)$ :  $(0^\circ, 0^\circ)$  (solid),  $(0^\circ, 10^\circ)$  (dashed), and  $(0^\circ, 90^\circ)$  (dotted). All cases are not distinguishable. In this model, the neutron EDM is dominated by the strange-quark EDM,  $d_s^E$ . In the upper-right, lower-left, and lower-right frames, we show the strange-quark EDM as a function of  $\Phi_2$  when  $(\Phi_1, \Phi_3) = (0^\circ, 0^\circ)$ ,  $(0^\circ, 10^\circ)$ , and  $(0^\circ, 90^\circ)$ , respectively. The thin lines are for the chargino- (solid), neutralino- (dashed), gluino- (dotted), and Higgs-mediated (dash-dotted) diagrams, respectively. The thick solid lines are for the total EDM.

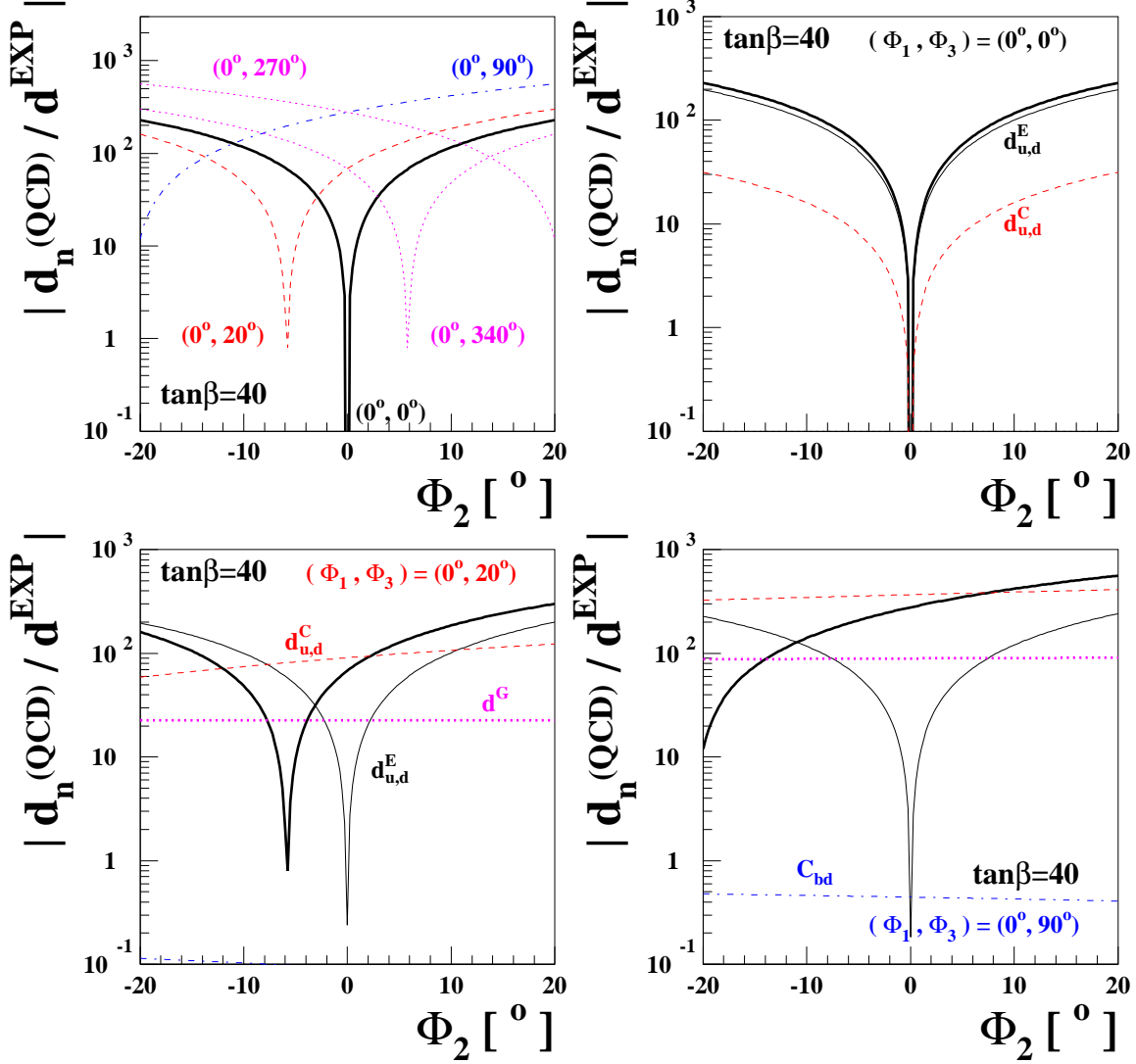


Figure 26: In the upper-left frame, we show the neutron EDM calculated using the QCD sum rule approach in the MCPMFV scenario with  $\tan\beta = 40$  as a function of  $\Phi_2$  for several values of the CP-violating phases  $(\Phi_1, \Phi_3)$ :  $(0^\circ, 0^\circ)$  (solid),  $(0^\circ, 20^\circ)$  (dashed),  $(0^\circ, 340^\circ)$  (dotted),  $(0^\circ, 270^\circ)$  (dotted), and  $(0^\circ, 90^\circ)$  (dash-dotted). In the upper-right, lower-left, and lower-right frames, we show the neutron EDM as a function of  $\Phi_2$  when  $(\Phi_1, \Phi_3) = (0^\circ, 0^\circ)$ ,  $(0^\circ, 20^\circ)$ , and  $(0^\circ, 90^\circ)$ , respectively. The lines are the same as in the lower frames of Fig. 19.

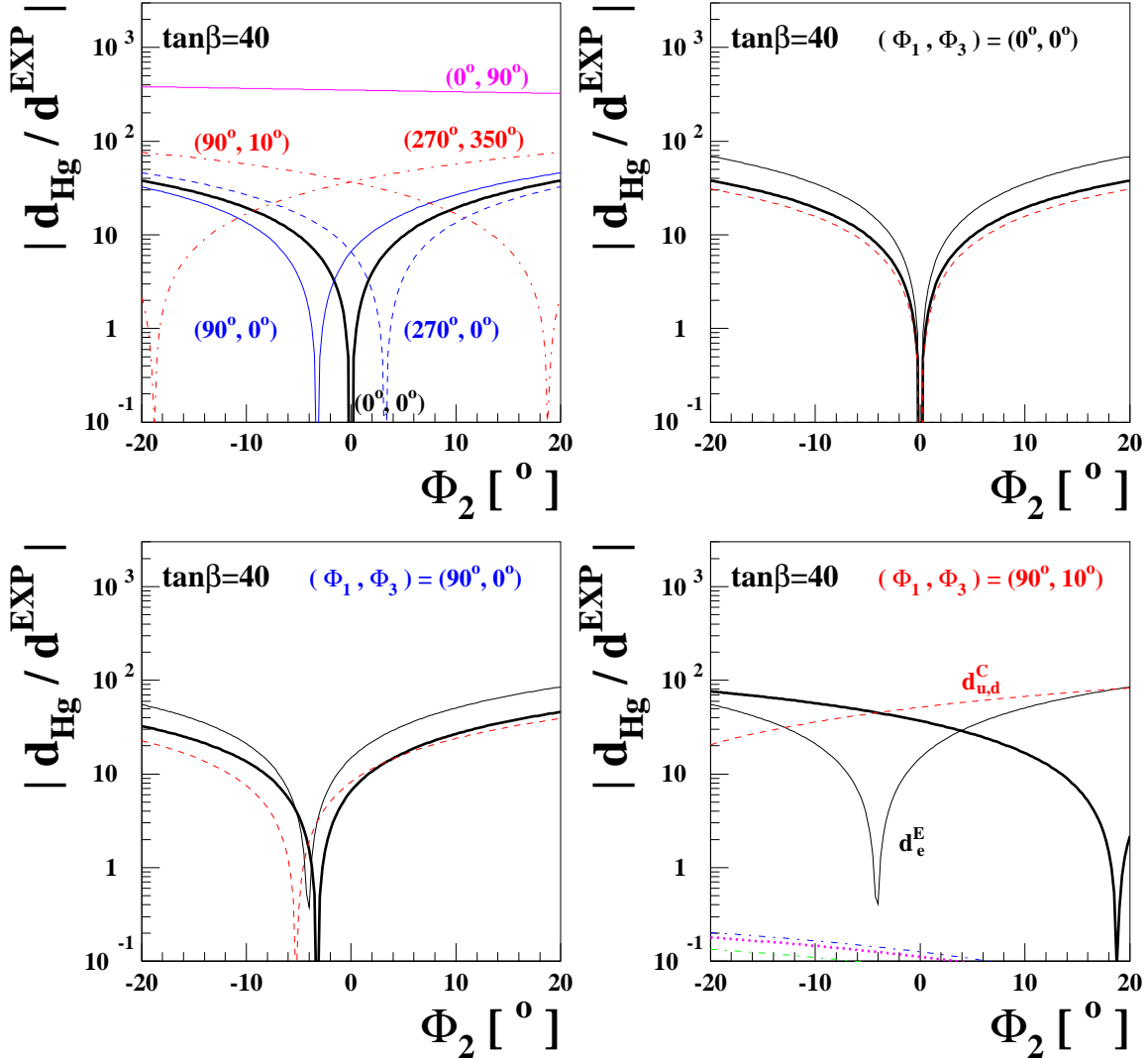


Figure 27: In the upper-left frame, we show the Mercury EDM calculated using the QCD sum rule approach in the MCPMFV scenario with  $\tan\beta = 40$  as a function of  $\Phi_2$  for several values of the CP-violating phases  $(\Phi_1, \Phi_3)$ :  $(0^\circ, 0^\circ)$  (solid),  $(90^\circ, 0^\circ)$  (solid),  $(270^\circ, 340^\circ)$  (dashed),  $(90^\circ, 10^\circ)$  (dash-dotted),  $(270^\circ, 350^\circ)$  (dash-dotted), and  $(0^\circ, 90^\circ)$  (solid). In the upper-right, lower-left, and lower-right frames, we show the Mercury EDM as a function of  $\Phi_2$  when  $(\Phi_1, \Phi_3) = (0^\circ, 0^\circ)$ ,  $(90^\circ, 0^\circ)$ , and  $(90^\circ, 10^\circ)$ , respectively. The lines are the same as in the lower-right frame of Fig. 16.

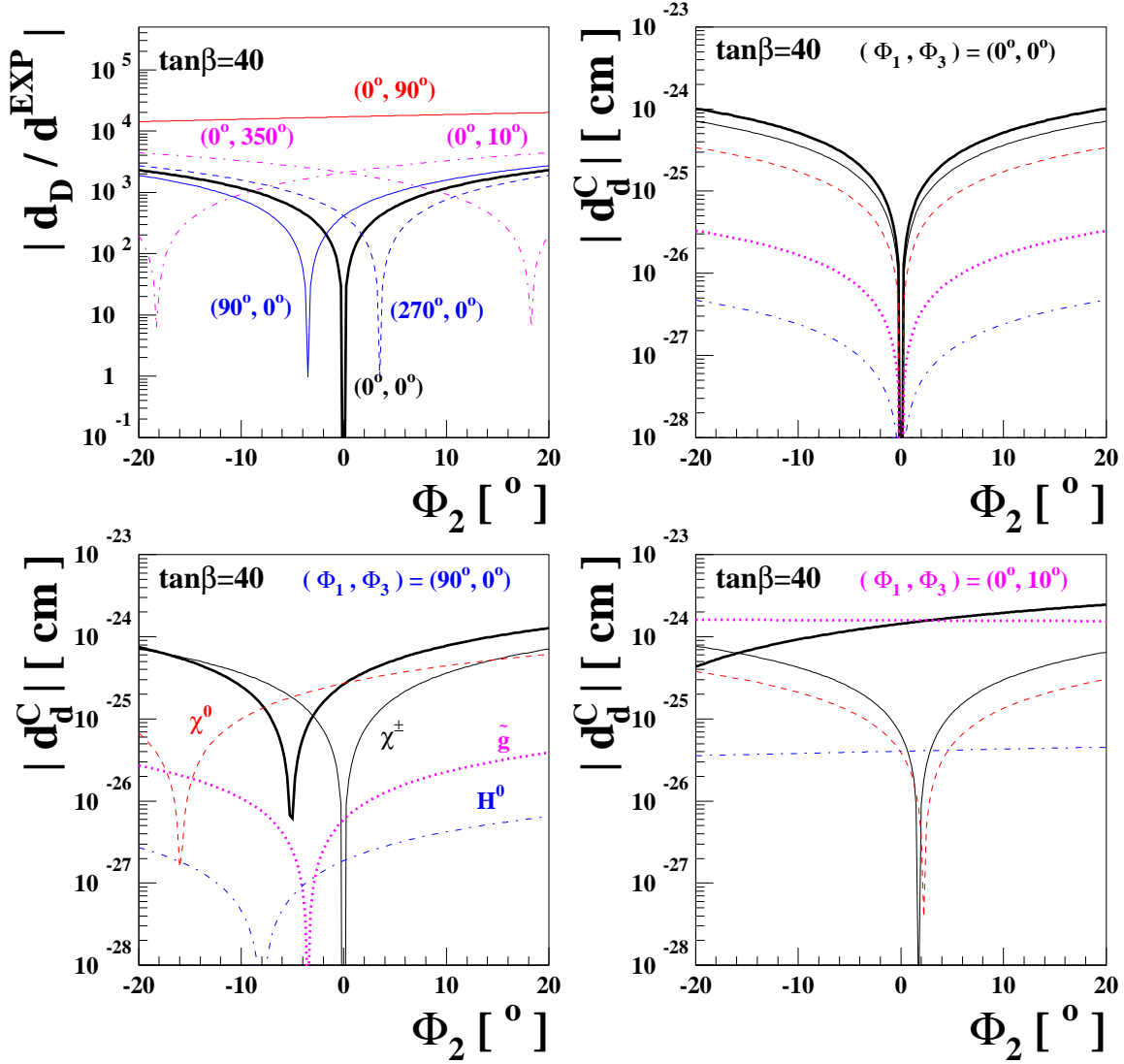


Figure 28: In the upper-left frame, we show the deuteron EDM calculated using the QCD sum rule techniques in the MCPMFV scenario with  $\tan\beta = 40$  as a function of  $\Phi_2$  for several values of the CP-violating phases  $(\Phi_1, \Phi_3)$ :  $(0^\circ, 0^\circ)$  (solid),  $(90^\circ, 0^\circ)$  (solid),  $(270^\circ, 0^\circ)$  (dashed),  $(0^\circ, 10^\circ)$  (dash-dotted),  $(0^\circ, 350^\circ)$  (dash-dotted), and  $(0^\circ, 90^\circ)$  (solid).  $d_D^{\text{EXP}} = 3 \times 10^{-27}$  is taken. The dominant contribution comes from the CEDM of the down quark,  $d_d^C$ . In the upper-right, lower-left, and lower-right frames, we show the CEDM of the down quark as functions of  $\Phi_2$  when  $(\Phi_1, \Phi_3) = (0^\circ, 0^\circ)$ ,  $(90^\circ, 0^\circ)$ , and  $(90^\circ, 10^\circ)$ , respectively. The lines are the same as in Fig. 25.